Studies on Global Bifurcation Structures and Effects of Changing Ion Channel Conductances on Pacemaker Rhythm in Cardiac Sinoatrial Node Cell Models

2011

PAN ZHENXING

Studies on Global Bifurcation Structures and Effects of Changing Ion Channel Conductances on Pacemaker Rhythm in Cardiac Sinoatrial Node Cell Models

2011
PAN ZHENXING
潘　　振興

Abstract

The sinoatrial node (cardiac pacemaker) cells generate rhythmic action potentials spontaneously to cause the cardiac activity, and the pacemaker rhythm (frequency of spontaneous action potential generation) in sinoatrial node cells decides the heart rate. Since various ion channels in cell membranes mainly control the action potential generation, their abnormalities disturb the pacemaker rhythm, and then the heart rate. As a result, a cardiac disease called a sinus arrhythmia may be caused. The arrhythmia is usually treated by drugs which have effects on ion channels. Thus, the study on the relation between ion channels and pacemaker rhythm is necessary for arrhythmia treatment. Besides physiological experiments (in vivo and in vitro experiments), numerical simulations and analyses (in silico experiments) of mathematical models are also useful for the study.

In our study, we utilize two typical sinoatrial node cell models: the YNI model and the Zhang model. Both the two models are Hodgkin-Huxley-type cell models, which describe the dynamic process of action potential generation by nonlinear ordinary differential equations with various parameters. The YNI model is a simple but rather classic one, and the Zhang model is a detailed one which considers the difference between periphery and center cells of sinoatrial node. We vary ion channel conductances as bifurcation parameters, to analyze the global bifurcation structures of the two models and the parameter sensitivities of pacemaker rhythm. Based on these analysis results, we investigate the effects of changing ion channel conductances on pacemaker rhythm.

Acknowledgments

First of all, I would like to express my sincere gratitude to former Professor Sadatoshi Kumagai at Division of Electrical, Electronic and Information Engineering, Graduate School of Engineering, Osaka University for providing me with the opportunity to study at Osaka University.

I would like to express my deepest gratitude to Professor Shinji Doi at Department of Electrical Engineering, Graduate School of Engineering, Kyoto University for his teaching, discussion, and encouragement throughout my entire study. Thanks to his constant guidance and support, I was able to complete this study. Under his mentorship, I have not only expanded my expert knowledge, but also improved my Japanese language skill.

I would like to express my sincere gratitude to Professor Shigemasa Takai and Associate Professor Toshiyuki Miyamoto at Division of Electrical, Electronic and Information Engineering, Graduate School of Engineering, Osaka University for their discussions and encouragements during my study. Their valuable advices always helped me improve my study, and their hearty supports enabled me to continue my study to the end.

I would like to express my sincere gratitude to Professor Tsuyoshi Funaki at Division of Electrical, Electronic and Information Engineering, Graduate School of Engineering, Osaka University for his careful review of this thesis. His suggestions and comments helped me improve this thesis. I would also like to express my sincere gratitude to the other members of thesis committee: Professor Toshifumi Ise and Professor Tetsuzo Tanino at Division of Electrical, Electronic and Information Engineering, Graduate School of Engineering, Osaka University, and Professor Hiroyuki Shiraga at Institute of Laser Engineering, Osaka University.

I would like to express my sincere gratitude to Professor Taishin Nomura at Division of Bioengineering, Graduate School of Engineering Science, Osaka University, who is the leader of the Global COE Program "In Silico Medicine" at Osaka Univer-

sity. He and his Global COE Program supported me throughout my entire study.

I am very grateful to the members of Takai Laboratory and former Kumagai Laboratory, in particular Mr. Iwata and Ms. Nakano for their helping.

I also wish to express my sincere gratitude to my uncle and his family, for their supports during my study in Japan. Without their supports, I would not have been possible to come to Japan and to start my study at Osaka University.

Finally, I thank everyone who helped and supported me during my study.

Contents

Chapter 1

Introduction

The heart repeats contraction and relaxation to pump blood to the whole body. Due to its importance in physiology and pathology, the heart has been studied by a vast amount of physiological experiments (i.e., in vivo and in vitro experiments) in different levels: molecule, cell, tissue, and then the whole heart. Based on the obtained experimental data, various mathematical models which describe cardiac structure and function of these levels have been developed. These mathematical models are not only able to represent various known physiological processes, but also able to predict some new discoveries leading to physiological experiments [1–7]. Therefore, besides physiological experiments, numerical simulations and analyses (i.e., in silico experiments) of mathematical models also help us in understanding physiology and pathology. With such a viewpoint, a "physiome project" aimed at "in silico medicine", which aids human medical care by numerical simulations and analyses, is proposed [8–10] and is now in progress worldwide, such as the IUPS physiome[1], the NSR physiome[2], the Europhysiome[3], and the Physiome.jp[4]. Compared to other organs' physiome projects, the cardiac physiome project is a well-developed one, although it is still in the early stage and needs further development [1, 11–14].

The cardiac activity (contraction and relaxation) is caused by cardiac cells' electrical excitations, which are initiated from sinoatrial node (SA node) and then propagated to atria, atrioventricular node (AV node), His bundle, Purkinje fibers, and ventricles [15]. The electrical excitation of a cardiac cell represents an action potential (AP) generation, and the action potential generation is mainly controlled by

[1]http://www.physiome.org.nz/
[2]http://www.physiome.org/
[3]http://www.europhysiome.org/
[4]http://www.physiome.jp/

various ion channels (pore-forming proteins) in the cell membrane [16]. Since the ion channels play a critical role in action potential generation, their abnormalities disturb the frequency of action potential generation or even stop the action potential generation in serious cases. As a result, a cardiac disease called an arrhythmia may be caused [17, 18]. Such diseases due to the abnormalities of ion channels are called channelopathies, e.g., arrhythmias and diabetes [19]. The channelopathies are usually treated by applying drugs which have effects on ion channels [18, 19].

Among various cardiac cells, the sinoatrial node (cardiac pacemaker) cells generate rhythmic action potentials spontaneously (pacemaker activity) to initiate the excitation conduction through the whole heart [20–22]. The pacemaker rhythm (frequency of spontaneous action potential generation) in sinoatrial node cells decides the heart rate. Therefore, the abnormalities of ion channels in sinoatrial node cells disturb the pacemaker rhythm, and then the heart rate. The corresponding arrhythmia is called a sinus arrhythmia. Thus, the study on how these ion channels' changes affect the pacemaker rhythm is necessary for sinus arrhythmia treatment. Here we carry out the study in silico, namely, we utilize sinoatrial node cell models, which describe the dynamic process of action potential generation of sinoatrial node cells, for the study.

Most cardiac cell models are Hodgkin-Huxley-type (HH-type) models, which are based on the Hodgkin-Huxley (HH) model of a squid giant axon (a nerve cell of squid) [23]. The HH model and also the HH-type models are dynamic models which are described by nonlinear ordinary differential equations (ODEs) with various parameters, on which their behaviors depend. Thus, the behavior may qualitatively change when varying parameters. Such a qualitative change of behavior is called a bifurcation [24, 25]. A nonlinear analysis which focuses on the bifurcation structures of dynamic models is called a bifurcation analysis [25]. The bifurcation analysis is an efficient method which can obtain the parameter dependance and sensitivity of behavior directly and globally [26–29], whereas the numerical simulation only can show one behavior as for specific initial conditions and specific parameter values, and should be executed plenty of times for different parameter values to obtain the parameter dependance and sensitivity. In our study, we analyze the bifurcation structures of sinoatrial node cell models and the variabilities of pacemaker rhythm. Although Kurata et al. also analyzed the bifurcation structures of their sinoatrial node cell model [30–33], their analysis were limited to only several ion channels. They performed both one- and two-parameter bifurcation analysis, however, they

did not analyze the variabilities of pacemaker rhythm in the latter case. In contrast, our analysis does not have these limitations.

So far, various sinoatrial node cell models (most are rabbit cell models) have been developed. In our study, we utilize two typical rabbit sinoatrial node cell models: the model by Yanagihara et al. (1980) [34] and the model by Zhang et al. (2000) [35, 36][5]. The two models hereinafter are referred to as Yanagihara-Noma-Irisawa (YNI) model and Zhang model, respectively. The YNI model is a simple but rather classic one, and the Zhang model is a detailed one which considers the regional difference of sinoatrial node (the difference between periphery and center cells of sinoatrial node). We analyze the global bifurcation structures of the two models where various ion channel conductances are varied as bifurcation parameters. The bifurcation analysis is divided into two stages: varying each ion channel conductance solely, whose results are shown in one-parameter bifurcation diagrams; varying two ion channel conductances simultaneously, whose results are shown in two-parameter bifurcation diagrams. Based on these bifurcation diagrams, we examine the variabilities of pacemaer rhythm, and then investigate the effects of changing each ion channel conductance on pacemaker rhythm. The pacemaker rhythm is sensitive to some ion channel conductance changes, whereas it is insensitive to others. It is thought that the ion channels corresponding to high sensitivities can be chosen to adjust pacemaker rhythm by certain drugs. Based on two-parameter bifurcation diagrams, we investigate the combined effects of changing two ion channel conductances simultaneously on pacemaker rhythm. A strong combined effect corresponds to the case that the pacemaker rhythm is sensitive to both ion channel conductance changes, whereas a weak one corresponds to the case that at least one ion channel conductance change affect the pacemaker rhythm little. In the former case, with reference to the two-parameter bifurcation diagram, one ion channel can be adjusted to correct the abnormal pacemaker rhythm caused by the other one. Since our in silico study aims at the prediction of how pacemaker rhythm varies with the changes of ion channels, and the suggestion of how to correct the abnormal pacemaker rhythm, the obtained results should be confirmed experimentally before clinical application.

This thesis is organized as follows: Chapter 2 introduces the cardiac structure and electrophysiology. The action potential generation in different cardiac cells and

[5]Since the model equations listed in the original paper by Zhang et al. [35] do not match the simulation results presented in the same paper, Garny et al. [36] have corrected the equations. The corrected model is utilized in our study.

the roles of various ion channels, ion pump, and ion exchanger in action potential generation are explained in detail. Then the sinoatrial node cells and their pacemaker activity are introduced. Chapter 3 first introduces the base model: the HH model of a squid giant axon, and then lists the developed HH-type cardiac cell models of sinoatrial node, atria, atrioventricular node, Purkinje fibers and ventricles. Next, the YNI model and the Zhang model of sinoatrial node cells are explained and compared. Chapter 4 briefly introduces the dynamical system and bifurcation analysis, then analyzes the global bifurcation structure of the HH model. Chapters 5 and 6 analyze the global bifurcation structures of the YNI model and the Zhang model, respectively. Based on the analysis results, the effects of conductance changes of various ion channels, and the coupling effect on pacemaker rhythm are investigated. Finally, Chapter 7 concludes this thesis.

Chapter 2

Cardiac Electrophysiology

The heart repeats contraction and relaxation to pump blood to the whole body. Such a cardiac activity is caused by cardiac cells' electrical excitations, which are initiated from sinoatrial node (cardiac pacemaker) and then propagated to atria, atrioventricular node, His bundle, Purkinje fibers, and ventricles. The electrical excitation of a cardiac cell represents an action potential generation, which is mainly controlled by various ion channels in cell membrane, and is also related to ion exchanger and ion pump in cell membrane, sarcoplasmic reticulum in cell cytoplasm. In this chapter, we first introduce the cardiac structure, then the electrical excitation (action potential generation) of various cardiac cells, and finally the pacemaker activity of cardiac pacemaker cells.

2.1 Cardiac Structure

The heart has a complicated structure and an amazing automaticity. It is made up of a vast amount of electrically excitable cells, whose electrical excitations cause the heart to repeat contraction and relaxation regularly. During their electrical excitations, these cardiac cells generate electrical signals (action potentials). Moreover, the heart is divided into several parts (several kinds of muscles): sinoatrial node, (left, right) atria, atrioventricular node, His bundle, Purkinje fibers, and (left, right) ventricles according to their different functions. Briefly, the atria and ventricles act as blood pumps, whereas the others (which is referred to as a cardiac conduction system) contribute to excitation conduction through the heart [37, 38]. With the help of the cardiac conduction system, the atria and ventricles are able to get electrically-excited to fulfill their pumping roles. Figure 2.1 shows schematic illustrations of the

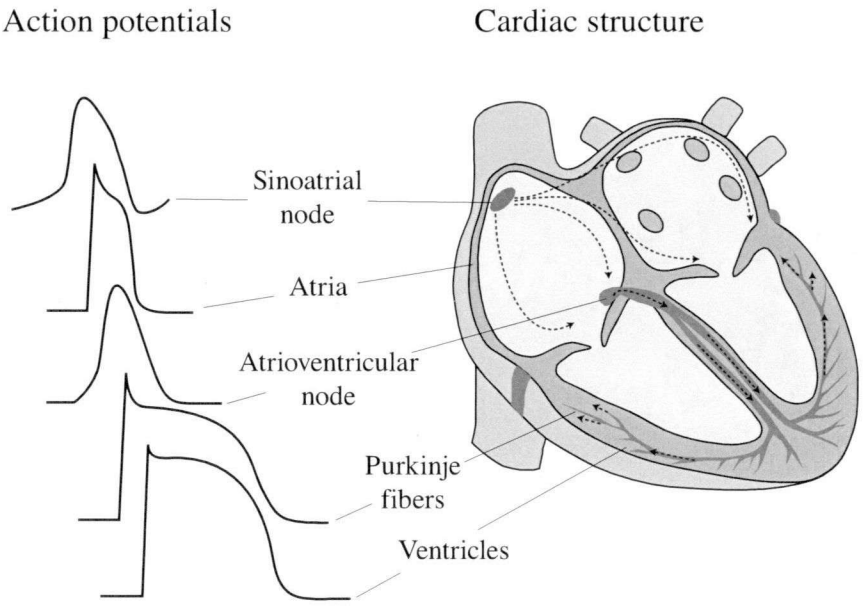

Figure 2.1: Schematic illustrations of the cardiac structure and the typical action potentials of different cardiac cells. The excitation conduction through the heart is denoted by arrowed dash lines.

cardiac structure and the typical action potentials of different cardiac cells. As shown in Fig. 2.1, the excitation conduction through the heart is in an order as follows:

- Sinoatrial node
  The sinoatrial node is located in the right atrium and near the entrance of the superior vena cava. The sinoatrial node cells generate rhythmic action potentials spontaneously (pacemaker activity) to initiate the excitation conduction through the whole heart. Thus the sinoatrial node is also referred to as a cardiac pacemaker. The pacemaker rhythm (frequency of spontaneous action potential generation) in sinoatrial node cells decides the heart rate.

- Atria
  The left and right atria are two chambers which contract/relax to let blood out/in them. The left atrium receives oxygenated blood from the lungs via the left and right pulmonary veins, then pumps the blood to the left ventricle. The right atrium receives deoxygenated blood from the whole body via the superior and inferior vena cavas, then pumps the blood to the right ventricle.

- Atrioventricular node

Table 2.1: Conduction velocities of different cardiac muscles and (intrinsic) pacemaker rhythms of their cells [37].

Cardiac muscle	Conduction velocity [m/sec]	Pacemaker rhythm [min^{-1}]
Sinoatrial node	< 0.01	60–100
Atria	1.0–1.2	None
Atrioventricular node	0.02–0.05	40–55*
His bundle	1.2–2.0	40–55*
Purkinje fibers	2.0–4.0	25–40*
Ventricles	0.3–1.0	None

* In isolated cells.

The atrioventricular node is located in the area between the atria and the ventricles, and is a bridge for excitation conduction from the atria to the ventricles. Moreover, the atrioventricular node has a very slow conduction velocity (Table 2.1), to provide sufficient time for completing atrial contraction prior to ventricular contraction. It is shown that, the isolated atrioventricular node cells are able to generate rhythmic action potentials spontaneously, that is, the atrioventricular node cells generate an intrinsic pacemaker activity. However, their intrinsic pacemaker rhythm is slower than that of sinoatrial node cells (Table 2.1). Thus the atrioventricular node cells in the heart follow the pacemaker rhythm of sinoatrial node cells and show no pacemaker activity.

- His bundle and Purkinje fibers
  The His bundle (which is also referred to as atrioventricular bundle) and Purkinje fibers are located in the inner ventricular walls, and have very high conduction velocities (Table 2.1). Thus they can propagate the electrical signals to the whole ventricles quite quickly. It is shown that, similar to the atrioventricular node cells, the cells of His bundle and Purkinje fibers also generate intrinsic pacemaker activity. However, their intrinsic pacemaker rhythms are also slower than that of sinoatrial node cells (Table 2.1). Thus the His bundle and Purkinje fibers in the heart show no pacemaker activity.

- Ventricles

The left and right ventricles are also two chambers. The left atrium pumps oxygenated blood (which is from the left atrium) to the whole body via the aorta, whereas the right atrium pumps deoxygenated blood (which is from the right atrium) to the lungs via the pulmonary arteries. Compared to the atria, the ventricles have thick walls, which are usually divided into three layers: endocardium, midmyocardium (whose cells are referred to as M cells), epicardium.

Table 2.1 compares the conduction velocities of these cardiac muscles and (intrinsic) pacemaker rhythms of their cells.

2.2 Electrical Excitation of Cardiac Cells

The cardiac cells are the fundamental components of the heart, and their electrical excitations (i.e., action potential generations) are essential to the cardiac activity. The action potential generation is a complicated dynamic process, which is mainly controlled by various ion channels in the cell membrane. Here we explain the mechanism of action potential generation in cardiac cells, and the roles of different ion channels and also some other cellular structures on the action potential generation.

2.2.1 Action Potential

In a biological cell (e.g., a cardiac cell), between the inside and the outside of cell membrane, a difference of ion concentrations generates an electrical potential difference, which is called a membrane potential (MP). In the cell membrane, there are various ion channels (pore-forming proteins) which open (activate) and close (inactivate) dynamically. When the ion channels open, specific ions (e.g., Na^+, K^+, Ca^{2+}, and Cl^-) flow through them passively. Thus the ion concentrations in the two sides of cell membrane vary. As a result, the membrane potential increases and decreases dynamically, to generate a spike-like action potential (Fig. 2.1).

In the heart, the sinoatrial node cells can generate rhythmic action potentials spontaneously, whereas the other cardiac cells cannot generate any action potentials until they are electrically stimulated (by their coupled cells which have already become electrically-excited) [39, 40]. That is, the cardiac cells except for sinoatrial node cells stay in their resting states until electrically stimulated. When a cardiac cell (except for a sinoatrial node cell) in its resting state, the total inflow and the total

outflow of ions via the opened ion channels reach a dynamic equilibrium. Thus the membrane potential keeps as a constant value, which is called a resting membrane potential (RMP).

For simplicity, let's first consider the dynamic equilibrium as for a certain ion. For example, when Na^+ flow through the opened sodium channels, they receive two forces: one is due to Na^+ concentration gradient, and the other is due to electrical potential gradient (i.e., membrane potential) between the two sides of cell membrane. The former force makes Na^+ flow following the concentration gradient, and the latter force makes Na^+ flow following the electrical potential gradient. As a result, Na^+ flow following their electrochemical gradient (related to both concentration and electrical potential gradients). If the force due to membrane potential just counterbalances the force due to Na^+ concentration gradient (that is, if the electrochemical gradient is just 0), the inflow and outflow of Na^+ through the cell membrane reach a dynamic equilibrium. Such a value of membrane potential is called an equilibrium potential or a reversal potential of Na^+. Therefore, if the membrane potential is smaller than the equilibrium potential of Na^+, the electrochemical potential at the inside of cell membrane is smaller than that at the outside, as a result Na^+ flow in cell membrane.

The following Nernst equation calculates the equilibrium potential of "ion" as for its concentration gradient between the two sides of cell membrane:

$$E_{\text{ion}} = \frac{\text{RT}}{z_{\text{ion}}\text{F}} \ln \frac{[\text{ion}]_{\text{o}}}{[\text{ion}]_{\text{i}}} \tag{2.1}$$

where E_{ion} [mV] (ion = Na^+, K^+, Ca^{2+}, or Cl^-) is the equilibrium potential of "ion", R (= 8.314 J/(K·mol)) is the gas constant, T [K] is the absolute temperature, z_{ion} is the valence of "ion", F (= 96,485 J/(V·mol)) is the Faraday constant, $[\text{ion}]_{\text{o}}$ and $[\text{ion}]_{\text{i}}$ [mM] are the extracellular and intracellular concentrations, respectively. Table 2.2 shows the typical values of ion concentrations and equilibrium potentials of Na^+, K^+, Ca^{2+}, and Cl^- in cardiac cells [19]. For Na^+, Ca^{2+}, and Cl^-, their extracellular concentrations are higher than intracellular concentrations, whereas for K^+, its extracellular concentration is lower than intracellular concentration.

Next, let's consider the dynamic equilibrium as for various ions. In general, when a cardiac cell (except for a sinoatrial node cell) in its resting state, only sodium, potassium and chlorine channels are open, then the total inflow and the total outflow of Na^+, K^+, and Cl^- through the cell membrane reach a dynamic equilibrium. Moreover, the cell membrane permeates Na^+, K^+, and Cl^- with very different permeability, which is determined by their channels. The following Goldman-Hodgkin-Katz

Table 2.2: Typical values of ion concentrations and equilibrium potentials of Na^+, K^+, Ca^{2+}, and Cl^- in cardiac cells [19].

Ion	Intracellular concentration	Extracellular concentration	Equilibrium potential*
Na^+	12 mM	135–145 mM	+66 mV
K^+	140 mM	3.5–5 mM	−93 mV
Ca^{2+}	10^{-4} mM	2.25–2.52 mM	+135 mV
Cl^-	2.5–50 mM	115 mM	−42 mV

* The equilibrium potentials are calculated for intermediate concentration values under 310 K.

(GHK) equation considers such a resting state of a cell and calculates the corresponding resting membrane potential:

$$E_m = \frac{RT}{F} \ln \frac{P_K[K^+]_o + P_{Na}[Na^+]_o + P_{Cl}[Cl^-]_i}{P_K[K^+]_i + P_{Na}[Na^+]_i + P_{Cl}[Cl^-]_o} \tag{2.2}$$

where E_m [mV] is the resting membrane potential, P_{ion} are the permeabilities of cell membrane to different ions. In general, the permeability to K^+ is quite higher than that to Na^+ or Cl^-. Thus the resting membrane potential appears to be near the equilibrium potential of K^+ (~ -90 mV).

The resting state of a cardiac cell (except for a sinoatrial node cell) represents a constant resting membrane potential, whereas the electrical excitation of a cardiac cell represents a dynamic action potential. The morphology of action potential varies with cardiac cells. Figure 2.2 compares the cardiac cell action potentials of different cardiac muscles [37]. In each panel, the abscissa denotes the time, and the ordinate denotes the membrane potential. The increase of membrane potential is referred to as a depolarization, whereas the decrease of membrane potential is referred to as a repolarization. According to its generation mechanism, an action potential is usually divided into 5 phases: phase 0–phase 4 (please note that not all action potentials have 5 phases fully). Each phase is related to certain ion channels, whose details will be explained in subsection 2.2.2. At first, let's see the action potentials with 5 phases, such as those of atria, Purkinje fibers, and ventricles (Fig. 2.2(b), (d), and (e)).

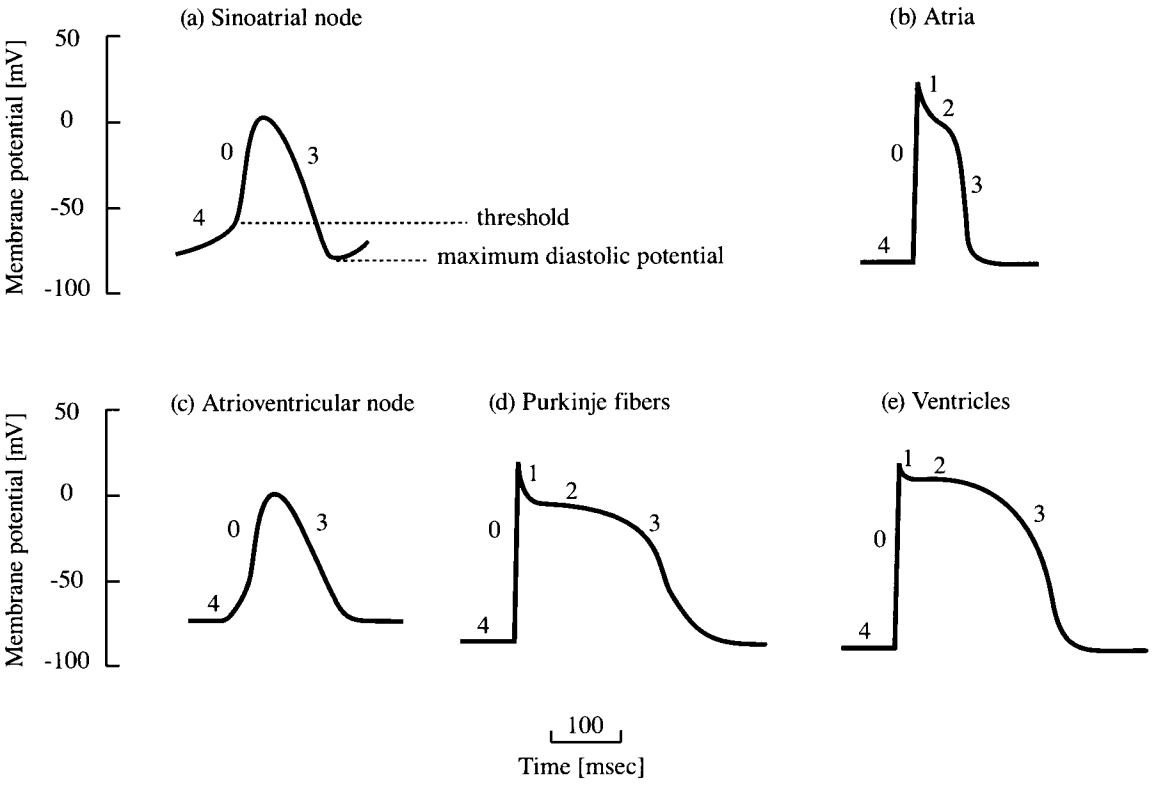

Figure 2.2: Comparison of the cardiac cell action potentials of different cardiac muscles [37].

- Phase 0

  An electrical stimulus (from its coupled cells) makes the cardiac cell increase membrane potential from the resting membrane potential. If the membrane potential reaches a threshold value (-70 to -60 mV), sodium channels begin to open to let Na^+ flow through them. Following their electrochemical gradient, Na^+ flow rapidly in cell membrane. As a result, the membrane potential increase rapidly to a positive value (a rapid depolarization). The sodium channels have a very fast inactivation, so they get closed quickly.

- Phase 1

  Potassium channels have several types. Here transient outward potassium channels begin to open to let K^+ flow through them. Following their electrochemical gradient, K^+ flow out cell membrane. As a result, the membrane potential decrease (an early repolarization). Then the transient outward potas-

sium channels get closed.

- Phase 2
  Here (outward) delayed rectifier potassium channels begin to open to let K^+ flow out cell membrane. Meanwhile, calcium channels also begin to open to let Ca^{2+} flow through them. Following their electrochemical gradient, Ca^{2+} flow in cell membrane. The Ca^{2+} inflow balances the K^+ outflow thereby preventing the decrease of membrane potential until the calcium channels get closed. Thus the phase 2 appears to be a plateau.

- Phase 3
  The (outward) delayed rectifier potassium channels still keep open to let K^+ flow out cell membrane. As a result, the membrane potential decrease to the resting membrane potential (a rapid repolarization).

- Phase 4
  The cardiac cell stays at its resting state, and its membrane potential retains resting membrane potential.

For the sinoatrial node and atrioventricular node, their action potentials only have phase 0, 3, and 4 (Fig. 2.2(a), (c)). It is mainly due to the lack or absent of sodium channels in their cells. For the action potential of sinoatrial node cells, its 3 phases are as follows:

- Phase 0
  Calcium channels begin to open to let Ca^{2+} flow in cell membrane. As a result, the membrane potential increases to a positive value (depolarization). Then the calcium channels get closed. Due to the lack or absent of sodium channels in a sinoatrial node cell, a rapid depolarization does not appear in its action potential.

- Phase 3
  Potassium channels begin to open to let K^+ flow out cell membrane. As a result, the membrane potential decrease to the most negative membrane potential, which is called a maximum diastolic potential (MDP). Then the potassium channels get closed.

- Phase 4
  The sinoatrial node cell has no resting state. Thus its membrane potential has

no resting membrane potential. The sinoatrial node cell increases its membrane potential spontaneously from the maximum diastolic potential to reach the threshold value for action potential generation. Such a (slow) depolarization is referred to as a diastolic depolarization, and the phase 4 is referred to as a diastolic depolarization phase. The phase 4 is also referred to as a pacemaker potential, since it makes the sinoatrial node cell able to generate action potential spontaneously. The details of pacemaker potential will be explained in subsection 2.3.1.

The action potential of atrioventricular node cells has similar phases as that of sinoatrial node cells, except that its phase 4 corresponds to a resting membrane potential.

2.2.2 Ion Channels, Ion Exchanger, and Ion Pump

The action potential generation of a cardiac cell is mainly controlled by various ion channels, and is also related to ion exchanger and ion pump in the cell membrane. These ion chanels, ion exchanger, and ion pump (all of them are transmembrane proteins) make the cell membrane able to permeate ions selectively since they only pass or transport specific ions (e.g., Na^+, K^+, and Ca^{2+}). The inflows of these ions generate inward currents, which cause the depolarization of membrane potential, whereas the outflows of these ions generate outward currents, which cause the repolarization of membrane potential. All of these inward/outward currents through the cell membrane are called membrane currents, which directly affect the membrane potential.

It is known that various ion channels contribute to the action potential generation. Each ion channel usually only passes a specific type of ion, but different ion channels may pass a same type of ion. In an ion channel, there exist several gates whose open and close are determined by membrane potential or some other factors (e.g., ligand). The ion channels whose gates are controlled by membrane potential are called voltage-gated or voltage-dependent ion channels. Most ion channels in cardiac cells are voltage-gated ones.

The following ion channels are the typical ones in cardiac cells.

Table 2.3: Comparison of characteristics of the T- and L-type calcium channels [37].

Characteristic	T-type calcium channel	L-type calcium channel
Activation potential	Low (~ -70 mV)	High (~ -40 mV)
Duration of activation	Short	Long
Channel conductance	Small (7–9 pS)	Large (15–25 pS)
Related phase of action potential	Phase 4 (SA node) Phase 0 (others)	Phase 0 (SA node, AV node) Phase 2 (others)

SA node: sinoatrial node; AV node: atrioventricular node.

Sodium Channel

The sodium channels in cardiac cells are voltage-gated channels (Na_v channels) and have a high voltage sensitivity. Their activation potentials are nearly between -70 and -60 mV. Namely, when the membrane potential reaches the activation potential, the sodium channels begin to open (activate). As a result, Na^+ flow in cell membrane rapidly, to generate an large inward current I_{Na}. The sodium channels have a fast inactivation, then they get closed quickly.

In the cells of atria, ventricles, and Purkinje fibers, there exist lots of sodium channels. These sodium channels contribute to the phase 0 (a rapid depolarization) of action potential since their large inward current I_{Na} makes the membrane potential increase quickly. In contrast to the above three types of cells, the sinoatrial node and atrioventricular node cells appear to be have little/no sodium channels. Therefore, there exist no rapid depolarizations in their action potentials.

Calcium Channel

The calcium channels in cardiac cells are voltage-gated channels (Ca_v channels) and have two types (T- and L-type). The T-type calcium channels correspond to a "T"ransient activation, whereas the L-type calcium channels correspond to a "L"ong-lasting activation. The characteristics of the T- and L-type calcium channels are compared in Table 2.3.

Both the T- and L-type calcium channels generate inward currents ($I_{Ca,T}$, $I_{Ca,L}$), which cause the membrane potential to increase. However, due to their different characteristics, the two types of calcium channels contribute to different phases of action potential. The T-type calcium channels have a low activation potential. Thus

they can activate at an early stage of action potential generation. In sinoatrial node cells, the T-type calcium channels contribute to the phase 4 of action potential (i.e., pacemaker potential). And in other cardiac cells, they contribute to the phase 0 of action potential, although their contribution appears to be small (compared to the sodium channels). The L-type calcium channels have a relative high activation potential and last for a long time of activation. Thus they contribute to the phase 0 of action potential in sinoatrial node and atrioventricular node cells, or phase 2 of action potential in other cardiac cells.

Potassium Channel

There are several types of potassium channels in cardiac cells. They are mainly classified into outward potassium channels and inward rectifier potassium channels (K_{ir} channels). The outward potassium channels are voltage-gated channels (K_v channels) and activate at a positive membrane potential after depolarization. They generate outward currents to cause the repolarization of membrane potential. The K_{ir} channels are voltage-independent ones, and are present in the cardiac cells except for sinoatrial node and atrioventricular node cells. Different form other ion channels, the K_{ir} channels remain open at very negative membrane potentials (e.g., the resting membrane potential or the equilibrium potential E_K of K^+). As a result, the K_{ir} channels play a role in stabilizing the resting membrane potential near E_K: via these opened K_{ir} channels, K^+ flow out/in the cell membrane if the membrane potential is bigger/smaller than E_K, thereby generating outward/inward current to return the membrane potential to E_K. It is found that, the K_{ir} channels generate inward current more than outward current. Thus they are called "inward" rectifier potassium channels. Table 2.4 lists these potassium channels and their contributions to action potential generation of cardiac cells.

Hyperpolarization-activated Cyclic Nucleotide-gated Channel

In sinoatrial node cells, there exists a special type of ion channel: hyperpolarization-activated cyclic nucleotide-gated (HCN) channel. The HCN channels are able to activate at a low negative membrane potential and are permeable to both Na^+ and K^+ (a high permeability to Na^+, whereas a low permeability to K^+). The corresponding "h"yperpolarization-activated current I_h, which is also referred to as a "f"unny current I_f, appears to be an inward current in most time. It is known that the HCN

Table 2.4: Various types of potassium channels and their contributed phases of cardiac cell action potential [37].

Potassium channel	Current	Action potential
Transient outward potassium channel	I_{to}	Phase 1
Rapid (outward) delayed rectifier potassium channel	$I_{K,r}$	Phase 2
Slow (outward) delayed rectifier potassium channel	$I_{K,s}$	Phase 3
Inward rectifier potassium channel	I_{K1}	Phase 4

channels contribute to the phase 4 of action potential (pacemaker potential), which is essential to spontaneous action potential generation in sinoatrial node cells [42].

Via various ion channels, specific ions are able to flow in/out cell membrane. In general, Na^+ and Ca^{2+} flow in cell membrane, whereas K^+ flow out cell membrane. If such ion fluxes continue, the intracellular and extracellular ion concentrations would be destroyed, and finally no action potential can be generated. In order to generate rhythmic action potentials successfully, the maintenance of ion concentrations in the two sides of cell membrane becomes necessary. Such a maintenance is carried out by sodium-potassium pumps and sodium-calcium exchangers, which transport specific ions in/out cell membrane.

Sodium-potassium Pump

The sodium-potassium pumps transport 3 Na^+ to outside and 2 K^+ to inside of cell membrane at once. Thus the corresponding current I_p appears to be an outward current. Since both Na^+ and K^+ are transported against their electrochemical gradients, the chemical energy from ATP hydrolysis is necessary.

Sodium-calcium Exchanger

The sodium-calcium exchangers are bidirectional exchangers, and they exchange 3 Na^+ with 1 Ca^{2+} at once. When the membrane potential is very negative (e.g., near the resting membrane potential), the exchangers transport 1 Ca^{2+} to outside and 3 Na^+ to inside of cell membrane. When the membrane potential is positive, these exchangers work in the opposite direction, that is, 3 Na^+ leaves and 1 Ca^{2+} enters the cell membrane. It is known that the sodium-calcium exchangers contribute to the phase 4 of action potential in sinoatrial node cells, since they generate an inward

current I_{NaCa} during that phase.

During the action potential generation, various ion channels, sodium-potassium pump, and sodium-calcium exchanger in the cell membrane generate inward/outward membrane currents, to cause the depolarization/repolarization of membrane potential. All these transmembrane proteins contribute to the action potential generation directly. Meanwhile, there exists a sarcoplasmic reticulum (SR) (a store of Ca^{2+}) in the cell cytoplasm. The SR releases/uptakes Ca^{2+} to/from the cell cytoplasm. As a result, the intracellular Ca^{2+} concentration and then the membrane potential varies. Thus, the SR has an indirect contribution to the action potential generation.

2.3 Pacemaker Activity of Sinoatrial Node Cells

In the heart, the sinoatrial node cells generate rhythmic action potentials spontaneously (pacemaker activity) to fulfill the role of cardiac pacemaker. They are surround by atrial cells, although there exists no distinct border between the two kinds of cells. From the center to the periphery of sinoatrial node, the sinoatrial node cells show a gradual increase in cell size and amount of cellular element, and are becoming more and more like atrial cells. The center cells (also referred to as typical sinoatrial node cells) are small and nearly empty, whereas the periphery cells are large and contains many more myofilaments. Table 2.5 shows the sizes of typical sinoatrial node cells as for various animals. These cell sizes are much smaller than those of atrial cells (15–20 μm in diameter and $\sim$ 100 μm in length).

Figure 2.3 shows a schematic illustration of a sinoatrial node cell. In the cell membrane, there are various ion channels of Na^+, K^+, Ca^{2+}, sodium-potassium pump, and sodium-calcium exchanger, through which ions flow in and out the cell membrane. As a result, various inward and outward membrane currents are generated. The explanations of these membrane currents are shown in Table 2.6. In the cyto-

Table 2.5: Sizes of typical sinoatrial node cells (sinoatrial node center cells) as for various animals [41].

Size	Human	Rabbit	Dog	Cat	Monkey	Pig	Guinea pig
Diameter [μm]	5–10	< 8	5–10	< 10	~ 7	4–8	< 8
Length [μm]	—	25–30	—	—	—	40	20–30

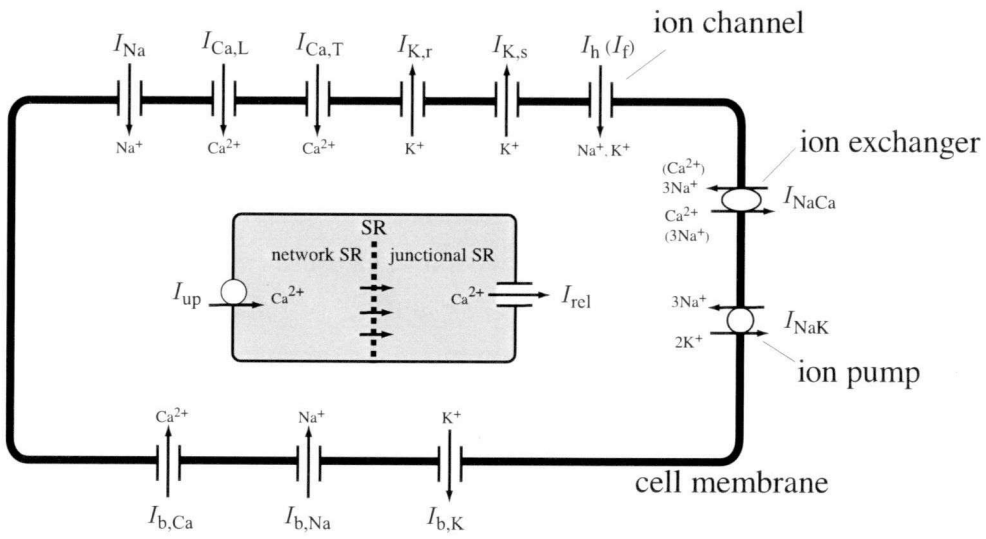

Figure 2.3: Schematic illustration of a sinoatrial node cell. There are various ion channels, ion exchange, ion pump in cell membrane, and a sarcoplasmic reticulum (SR) in cell cytoplasm.

plasm, there is a sarcoplasmic reticulum (SR), which has two domains: junctional SR and network SR. The junctional SR releases Ca^{2+} to the cell cytoplasm via a channel, whereas the network SR uptakes Ca^{2+} from the cell cytoplasm via a pump.

2.3.1 Pacemaker Potential

As described in subsection 2.2.1, due to the pacemaker potential in phase 4, the sinoatrial node cells are able to generate rhythmic action potentials spontaneously. Thus, the pacemaker potential is the key factor of the pacemaker activity of sinoatrial node cells.

Different from the atrial cells and ventricular cells, the sinoatrial node cells have no K_{ir} channels. Therefore, their membrane potentials would not fall into a very negative value (near the equilibrium potential of K^+). Their most negative membrane potentials (i.e., maximum diastolic potentials) are larger than those (i.e., resting membrane potentials) of atrial and ventricular cells. For the sinoatrial node cells, such a not very negative membrane potential makes the depolarization start easily.

The absent of K_{ir} channels provides a favorable condition for pacemaker potential generation. Next, specific membrane currents contribute to the pacemaker potential

Table 2.6: Typical membrane currents in sinoatrial node cells.

Membrane current	Ion	Direction	Explanation
I_{Na}	Na^+	Inward	Sodium current
$I_{Ca,L}$	Ca^{2+}	Inward	L-type calcium current
$I_{Ca,T}$	Ca^{2+}	Inward	T-type calcium current
$I_{K,r}$	K^+	Outward	Rapid delayed rectifier potassium current
$I_{K,s}$	K^+	Outward	Slow delayed rectifier potassium current
I_h (I_f)	Na^+, K^+	Inward/outward	Hyperpolarization-activated current
$I_{b,Na}$	Na^+	Inward	Background sodium current
$I_{b,Ca}$	Ca^{2+}	Inward	Background calcium current
$I_{b,K}$	K^+	Outward	Background potassium current
I_p	Na^+, K^+	Outward	Sodium-potassium pump current
I_{NaCa}	Na^+, Ca^{2+}	Inward/outward	Sodium-calcium exchanger current

generation directly. It is found that several inward membrane currents contribute to the pacemaker potential generation. The most important one is thought to be the hyperpolarization-activated current I_h (I_f) which corresponds to the hyperpolarization-activated cyclic nucleotide-gated (HCN) channels. The I_h is a small inward current which increases the membrane potential from the maximum diastolic potential slowly. Therefore, I_h is also called a pacemaker current [42]. The sodium-calcium exchanger current I_{NaCa} and the T-type calcium current $I_{Ca,T}$ also contribute to the pacemaker potential generation. Moreover, during the pacemaker potential generation, the SR releases Ca^{2+} to the cell cytoplasm, to increase the intercellular Ca^{2+} concentration, and then the membrane potential.

2.3.2 Pacemaker Rhythm

The sinoatrial node cells generate rhythmic action potentials spontaneously to initiate the excitation conduction through the heart. One cycle of the excitation conduction from the sinoatrial node to the ventricles corresponds to one heart beat. Therefore, the pacemaker rhythm (frequency of spontaneous action potential generation) in sinoatrial node cells decides the heart rate. Since the ion channels mainly control the action potential generation, their abnormalities disturb the pacemaker rhythm and then the heart rate. As a result, sinus arrhythmia such as sinus tachy-

cardia may be caused [17,18]. The arrhythmias are usually treated by applying drugs which have effects on certain ion channels. Thus, the study on how the abnormalities of ion channels affect the pacemaker rhythm is necessary for the arrhythmia treatment. Here we utilize HH-type sinoatrial node cell models (which describe the dynamic process of action potential generation in sinoatrial node cells) for the study.

Chapter 3

Hodgkin-Huxley-type Cardiac Cell Models

So far, the action potentials and ion channels of various cardiac cells have been well studied by performing plenty of physiological experiments. Especially, the voltage clamp technique[1] and the patch clamp technique[2] make us able to understand the action potential generation mechanism and the roles of various ion channels deeply. Based on the experimental data, cardiac cell models (which describe the dynamic processes of action potential generation in different cardiac cells) have been developed. Most of these cardiac cell models are Hodgkin-Huxley-type (HH-type) models which are based on the famous Hodgkin-Huxley (HH) model of a squid giant axon [23]. In this chapter, we first introduce the HH model, and then list the developed cardiac cell models of sinoatrial node, atria, atrioventricular node, Purkinje fibers, and ventricles, respectively. Then the YNI model and the Zhang model of sinoatrial node cells are introduced and compared.

3.1 Base Model: Hodgkin-Huxley (HH) Model

The HH model describes the action potential generation of a squid giant axon [23]. It considers an equivalent circuit of the squid giant axon as shown in Fig. 3.1. The cell membrane corresponds to a capacitor, and the Na^+ channel, K^+ channel, leak channel correspond to three resistors. The coupling current from coupled cells corresponds to

[1] A technique for recording the total ion currents across the cell membrane under a controlled membrane potential [23, 43].

[2] A technique for recording the ion current of a single channel dynamically [44].

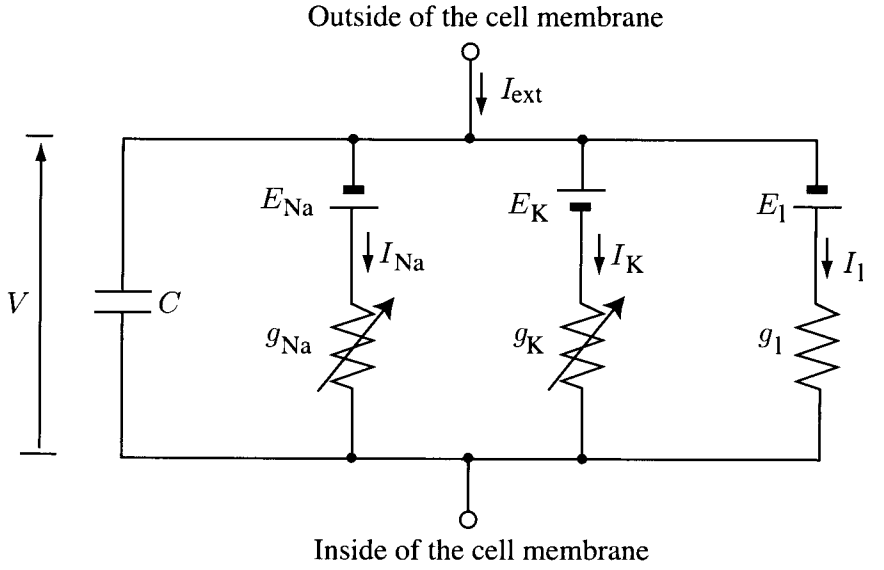

Figure 3.1: Equivalent circuit of a squid giant axon considered in the HH model.

an external current I_{ext}. The HH model is described by nonlinear ordinary differential equations (ODEs) with four variables: V, m, n, and h.

The follows show the detailed equations of the HH model:

$$\begin{aligned}
\frac{dV}{dt} &= -\frac{1}{C}(I_{\text{total}} - I_{\text{ext}}) = -\frac{1}{C}(I_{\text{Na}} + I_{\text{K}} + I_{\text{l}} - I_{\text{ext}}) \\
&= -\frac{1}{C}\left[\bar{g}_{\text{Na}} m^3 h(V - E_{\text{Na}}) + \bar{g}_{\text{K}} n^4 (V - E_{\text{K}}) + \bar{g}_{\text{l}}(V - E_{\text{l}}) - I_{\text{ext}}\right], \quad (3.1) \\
\frac{dx}{dt} &= \frac{x^{\infty}(V) - x}{\tau_x(V)}, \ (x = m, n, h); \quad (3.2) \\
\tau_x(V) &= \frac{1}{\alpha_x(V) + \beta_x(V)}, \quad x^{\infty}(V) = \frac{\alpha_x(V)}{\alpha_x(V) + \beta_x(V)}; \\
\alpha_m(V) &= \frac{0.1(25 - V)}{\exp\left[(25 - V)/10\right] - 1}, \quad \beta_m(V) = 4\exp\left(-\frac{V}{18}\right); \\
\alpha_n(V) &= \frac{0.01(10 - V)}{\exp\left[(10 - V)/10\right] - 1}, \quad \beta_n(V) = 0.125\exp\left(-\frac{V}{80}\right); \\
\alpha_h(V) &= 0.07\exp\left(-\frac{V}{20}\right), \quad \beta_h(V) = \frac{1}{\exp\left[(30 - V)/10\right] + 1}; \\
\bar{g}_{\text{Na}} &= 120, \quad \bar{g}_{\text{K}} = 36, \quad \bar{g}_{\text{l}} = 0.3\,\text{mS/cm}^2; \\
E_{\text{Na}} &= 115, \quad E_{\text{K}} = -12, \quad E_{\text{l}} = 10.599\,\text{mV};
\end{aligned}$$

where the explanations of these notations are as follows:

- V [mV]: membrane potential.
- t [msec]: time.
- C (= 1 μF/cm^2): membrane capacitance per unit area.
- I_{total} [μA/cm^2]: total membrane current per unit area.
- I_{ext} [μA/cm^2]: external current (coupling current) per unit area.
- I_{ion} (ion = Na, K, and l) [μA/cm^2]: ion channel currents per unit area.
- $\bar{g}_{\text{ion}}$ [mS/cm^2]: maximum conductances of ion channels per unit area.
- E_{ion} [mV]: equilibrium potentials of ions.
- x (= m, n, and h): gating variables (dimensionless, ranging between 0 and 1) denoting the states of ion channels' gates. 0 corresponds to a fully closed state, whereas 1 corresponds to a fully opened state.
- g_{Na} ($\equiv \bar{g}_{\text{Na}} m^3 h$), g_{K} ($\equiv \bar{g}_{\text{K}} n^4$) [mS/cm^2]: dynamic variable conductances of ion channels per unit area.
- $x^{\infty}(V)$: steady-state values of gating variables.
- $\tau_x(V)$ [msec]: time constants of gating variables.
- $\alpha_x(V)$, $\beta_x(V)$ [msec^{-1}]: rate constants of the transition between opened and closed states of gates.

3.2 Various Cardiac Cell Models

Based on the HH model, various HH-type cardiac cell models have been developed. With the development of measurement technique and accumulation of experimental data, these cardiac cell models become detailed and complicated [1, 45]. In general, a new model is developed by incorporating new experimental findings into existing models or by correcting some improper formulations of existing models. Such an existing model is called a parent model of the new model. Tables 3.1–3.5 list the developed cardiac cell models of sinoatrial node, atria, atrioventricular node, Purkinje fibers, and ventricles, respectively [45–47].

Table 3.1: Sinoatrial node cell models

Animal	Model (parent model if any)	NV	NCC	WPEC	WSR
Rabbit	Yanagihara et al. (1980) (YNI) [34]	7	5	no	no
	Irisawa and Noma (1982) [48] (YNI [34])	?	?	?	?
	Bristow and Clark (1982) [49] (McAllister et al. (1975) [72])	7	5	no	no
	Noble and Noble (1984) [50] (DiFrancesco and Noble (1985) [73])	15	8	yes	no
	Noble et al. (1989) [51] (Noble and Noble (1984) [50])	14	7	yes	no
	Wilders et al. (1991) [52] (Noble and Noble (1984) [50])	15	8	yes	yes
	Demir et al. (1994) [53]	27	6	yes	yes
	Dokos et al. (1996) [54] (Wilders et al. (1991) [52])	18	7	yes	yes
	Zhang et al. (2000) [35]	12 (center) 15 (periphery)	11	yes	no
	Kurata et al. (2002) [30]	27 (center) 30 (periphery)	11	yes	yes
	Sarai et al. (2003) [55]	50	11	yes	yes
	Lovell et al. (2004) [56]*	29	11	yes	yes
	Maltsev and Lakatta (2009) [57] (Kurata et al. (2002) [30])	29	5	yes	yes
Bullfrog	Rasmusson et al. (1990) [58]	14	6	yes	yes
Mouse	Mangoni et al. (2006) [59] (Zhang et al. (2000) [35])	22	13	yes	no
	Kharche et al. (2011) [60]	38	15	yes	yes

NV: number of variables; NCC: number of channel currents;

WPEC: whether the model considers the pump and exchanger currents;

WSR: whether the model considers the sarcoplasmic reticulum (SR);

* The model considers the opening and closing of ion channels as Markov processes.

Table 3.2: Atrial cell models

Animal	Model (parent model if any)	NV	NCC	WPEC	WSR
Rabbit	Hilgemann and Noble (1987) [61] (DiFrancesco and Noble (1985) [73])	15	6	yes	yes
	Earm and Noble (1990) [62] (Hilgemann and Noble (1987) [61])	16	7	yes	yes
	Lindblad et al. (1996) [63]	28	11	yes	yes
Human	Nygren et al. (1998) [64] (Lindblad et al. (1996) [63])	29	9	yes	yes
	Courtemanche et al. (1998) [65] (Luo and Rudy (1994) [80])	21	9	yes	yes
	Simitev and Biktashev (2006) [66]	3	1	no	no
Bullfrog	Rasmusson et al. (1990) [67] (Rasmusson et al. (1990) [58])	16	8	yes	yes
Canine	Ramirez et al. (2000) [68] (Courtemanche et al. (1998) [65])	26	10	yes	yes
	Cherry et al. (2007) [69] (Fenton and Karma (1998) [77])	4	3	no	no

Table 3.3: Atrioventricular node cell models

Animal	Model (parent model if any)	NV	NCC	WPEC	WSR
Rabbit	Liu et al. (1993) [70] (YNI [34])	7	5	no	no

Table 3.4: Purkinje fiber cell models

Animal	Model (parent model if any)	NV	NCC	WPEC	WSR
General	Noble (1962) [71]	4	3	no	no
	McAllister et al. (1975) (MNT) [72] (Noble (1962) [71])	10	9	no	no
	DiFrancesco and Noble (1985) [73] (MNT [72])	16	8	yes	yes
Canine	Stewart et al. (2009) [74]	21	10	yes	yes
Human	Sampson et al. (2010) [75]	82	11	yes	yes

Table 3.5: Ventricular cell models

Animal	Model (parent model if any)	NV	NCC	WPEC	WSR
General	Beeler and Reuter (1977) [76] (MNT [72])	8	4	no	no
	Fenton and Karma (1998) [77]	3	3	no	no
Guinea pig	Luo and Rudy (1991) (LR1) [78] (Beeler et al. (1977) [76])	8	6	no	no
	Nordin (1993) [79]	14	9	yes	yes
	Luo and Rudy (1994) (LRd) [80] (LR1 [78])	21	13	yes	yes
	Jafri et al. (1998) [81] (LRd [80])	30	10	yes	yes
	Matsuoka et al. (2003) [82]	45	11	yes	yes
Human	Priebe and Beuckelmann (1998) [83] (LRd [80])	17	8	yes	yes
	Bernus et al. (2002) [84]† (Priebe et al. (1998) [83])	6	7	yes	no
	Ten Tusscher et al. (2004) (TNNP) [85]† (LR1 [78])	17	7	yes	yes
	Ten Tusscher and Panfilov (2006) [86] (TNNP [85])	19	9	yes	yes
	Ten Tusscher and Panfilov (2006) [87] (TNNP [85])	9	9	yes	no
	Iyer et al. (2004) [88]*†	67	8	yes	yes
	Bueno et al. (2008) [89] (Fenton et al. (1998) [77])	4	3	no	no
Canine	Winslow et al. (1999) [90] (Jafri et al. (1998) [81])	33	9	yes	yes
	Fox et al. (2002) [91] (Winslow et al. (1999) [90])	13	10	yes	yes
	Cabo and Boyden (2003) [92]† (LRd [80])	16	13	yes	yes
	Hund and Rudy (2004) [93]† (LRd [80])	29	13	yes	yes
	Greenstein and Winslow (2002) [94]† (Winslow et al. (1999) [90])	42	9	yes	yes
Rabbit	Puglisi and Bers (2001) [95] (LRd [80])	20	11	yes	yes
	Shannon et al. (2004) [96]* (Puglisi and Bers (2001) [95])	45	9	yes	yes
	Mahajan et al. (2008) [97] (Shannon et al. (2004) [96])	27	7	yes	yes
bullfrog	Pandit et al. (2001) [98]† (Demir et al. (1994) [53])	26	6	yes	yes
Mouse	Bondarenko et al. (2004) [99]*	44	12	yes	yes

* The model considers the opening and closing of ion channels as Markov processes.

† The model considers the difference of epicardial cell, midmyocardial cell (M cell), endocardia cell of ventricular muscle.

3.3 Two Typical Sinoatrial Node Cell Models: YNI Model and Zhang Model

As listed in Table 3.1, starting with the YNI model [34], various sinoatrial node cell models have been developed. Most of them are rabbit cell models. Among these rabbit cell models, Irisawa and Noma [48] made an extension of the YNI model by incorporating some new experimental data. Noble and Noble [50] developed a new sinoatrial node cell model from a Purkinje fiber model [73], which firstly incorporated the sodium-calcium exchanger and sodium-potassium pump. Then the model of Noble and Noble [51] was extended by Wilders et al. [52], and the model of Wilders et al. [52] was again extended by Dokos et al. [54]. Zhang et al. [35] considered the regional difference of sinoatrial node and proposed two types of cell models (peripheral and central cell models). The recent models have become very complicated such as those proposed by Kurata et al. [30], by Sarai et al. [55], by Lovell et al. [56], and by Maltsec and Lakatta [57].

In our study, we utilize the YNI model and the Zhang model of rabbit sinoatrial node cells. The YNI model is a rather classical model, which is able to represent the essential features of action potential generation in spite of its simplicity. The Zhang model is a detailed model which considers regional difference of the sinoatrial node. That is, its parameter values vary between periphery cell and center cell of sinoatrial node. The Zhang model is able to represent the essential features of action potential for both periphery and center cells.

Both the YNI model and Zhang model are HH-type models. They describe the dynamic process of action potential generation by nonlinear ODEs, similar as those shown in Eqs. (3.1) and (3.2). However, the membrane currents vary with models. Figure 3.2 shows the schematic illustrations of the two models. The explanation of their membrane currents are listed in Table 3.6.

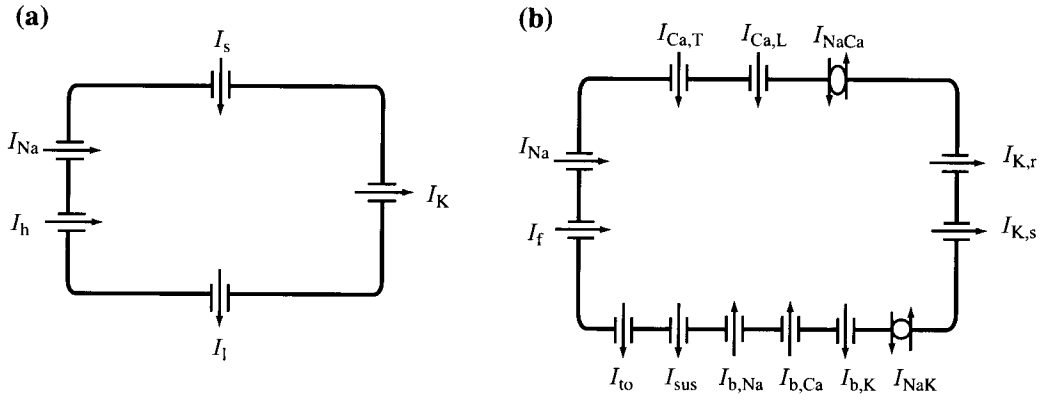

Figure 3.2: Schematic illustrations of sinoatrial node cells considered in (a) YNI model, (b) Zhang model.

The YNI model and the Zhang model have the same sodium current I_{Na} and hyperpolarization-activated current I_{h} (I_{f}). For other membrane currents, they have the following relations [45, 50, 101]:

$$I_{\mathrm{s}} = I_{\mathrm{Ca,L}} + I_{\mathrm{Ca,T}} + I_{\mathrm{NaCa}}, \tag{3.3}$$

$$I_{\mathrm{K}} = I_{\mathrm{K,r}} + I_{\mathrm{K,s}}, \tag{3.4}$$

where the left-hand side corresponds to the YNI model, and the right-hand side corresponds to the Zhang model. Moreover, both the two models do not consider the Ca^{2+} cycle of SR. The equations of the two models will be explained in Chapter 5 and Chapter 6, respectively.

Table 3.6: Membrane currents considered in the YNI model and the Zhang model.

Model	Membrane current	
YNI model	I_{Na}	Sodium current
	I_s	Slow inward current
	I_K	Potassium current
	I_h	Hyperpolarization-activated current
	I_l	Leak current
Zhang model	I_{Na}	Sodium current
	$I_{Ca,L}$	L-type calcium current
	$I_{Ca,T}$	T-type calcium current
	$I_{K,r}$	Rapid delayed rectifier potassium current
	$I_{K,s}$	Slow delayed rectifier potassium current
	I_{to}	Transient 4-aminopyridine-sensitive current
	I_{sus}	Sustained 4-aminopyridine-sensitive current
	I_f	Hyperpolarization-activated current
	$I_{b,Na}$	Background sodium current
	$I_{b,Ca}$	Background calcium current
	$I_{b,K}$	Background potassium current
	I_p	Sodium-potassium pump current
	I_{NaCa}	Sodium-calcium exchanger current

Chapter 4

Dynamical System and Bifurcation Analysis

Dynamical systems describe dynamic processes in mathematics, e.g., the HH model describes the action potential generations by nonlinear ODEs. In general, the dynamical systems are classified into two types: discrete- and continuous-time ones. The discrete-time dynamical systems are usually descried by difference equations, and the continuous-time dynamical systems are usually described by differential equations. In this chapter, we briefly introduce the dynamical systems, and then introduce a powerful nonlinear analysis - bifurcation analysis for such systems. Compared to numerical simulations, the bifurcation analysis has a quite high efficiency in investigating dynamical systems' behaviors. Here we perform the bifurcation analysis of the HH model, which represents a typical dynamical system. The bifurcation structure of the HH model help us in understanding the HH-type cardiac cell models.

4.1 Dynamical System

Each dynamical system considers two basic elements: one is states of the system at certain time, another is a law of state transition with time. The dynamical systems are classified into discrete- and continuous-time ones, which are commonly described by difference equations and differential equations, respectively. Hereinafter we only consider the continuous-time dynamical systems, as which the HH model and the HH-type cardiac cell models are developed.

A continuous-time dynamical system can be described by differential equations

such as

$$\frac{d}{dt}\boldsymbol{x}(t) = \boldsymbol{f}\left(\boldsymbol{x}(t)\right),\ \boldsymbol{x}(t) \in \mathcal{R}^N,\ t \in \mathcal{R}, \tag{4.1}$$

where the N-dimensional real vector $\boldsymbol{x}(t)$ is referred to as a state point which denotes the state of system at time t, and the vector-valued function $\boldsymbol{f}$ is referred to as a vector field since it assigns a vector $\boldsymbol{f}(\boldsymbol{x}(t))$ to each $\boldsymbol{x}(t)$. The law of state transition with time is determined implicitly by the function $\boldsymbol{f}$.

The follows are some important definitions about dynamical systems.

- A state space or a phase space: a set of all state points.
- An initial state point: a state point $\boldsymbol{x}(0)$ at $t = 0$.
- An orbit or a trajectory: an ordered set of state points determined by Eq. (4.1) as for a $\boldsymbol{x}(0)$.
- A periodic orbit: for an orbit, if there exists a $T > 0$ such that $\boldsymbol{x}(t) = \boldsymbol{x}(t+T)$ for any t, the orbit is referred to as a periodic orbit. The minimal T is referred to as the periodic orbit's period.
- An equilibrium point or a fixed point: a state point $\boldsymbol{x}^*$ such that $\boldsymbol{f}(\boldsymbol{x}^*) = 0$.
- Stability (stable or unstable): for an equilibrium point or a periodic orbit, if its nearby orbits approach it as time increase, it is referred to as a stable one, otherwise, it is referred to as an unstable one.

4.2 Bifurcation Analysis

A dynamical system may show several behaviors. When the dynamical system reach its steady state after a long time, it may stay at a stable equilibrium point, may repeat a stable periodic orbit, also may fall into a complicated behavior. Moreover, a dynamical system usually incorporates various parameters in its equations. Thus, its behavior depends on these parameters (parameter dependance). When these parameters are varied, the behavior may change qualitatively, namely, the number or stability of equilibrium points or periodic orbits may change. Such a qualitative change of behavior is called a bifurcation [24, 25].

The follows are some typical bifurcations and the behavior changes at these bifurcations.

- Hopf bifurcation: stability of an equilibrium point changes, and a (stable or unstable) periodic orbit is bifurcated. If the bifurcated periodic orbit is stable, the Hopf bifurcation is referred to as a supercritical one, whereas if the bifurcated periodic orbit is unstable, the Hopf bifurcation is referred to as a subcritical one.

- Saddle-node bifurcation: a pair of equilibrium points are generated or disappear.

- Double-cycle bifurcation: it is the saddle-node bifurcation of periodic orbits. A pair of periodic orbits are generated or disappear.

- Period-doubling bifurcation: stability of a periodic orbit changes, and another periodic orbit with a double period is generated.

- Homoclinic bifurcation: a periodic orbit collides with an equilibrium point. Near the homoclinic bifurcation, the period of periodic orbit becomes very long.

A nonlinear analysis which analyzes the bifurcation structures of dynamical systems is referred to as a bifurcation analysis [24]. When performing bifurcation analysis of a dynamical system, we vary certain parameters (which is referred to as bifurcation parameters), then examine whether bifurcations occur or not (i.e., whether the number and stability of equilibrium point, periodic orbit change or not). Based on the obtained bifurcation structures, we investigate the parameter dependence and sensitivity of the dynamical system's behavior. The bifurcation analysis has a high efficiency since it tracks equilibrium points or periodic orbits one by one algebraically. However, the numerical simulation only can show the system's behavior as for specific initial conditions and specific parameter values. Thus, it should be executed plenty of times to investigate the parameter dependence and sensitivity.

In our study, a bifurcation analysis software AUTO [100] is used for analysis. We perform the bifurcation analysis in two stages: one-parameter bifurcation analysis which varies one bifurcation parameter solely, and two parameter bifurcation analysis which varies two bifurcation parameters simultaneously. Their analysis results are presented as one- and two-parameter bifurcation diagrams, respectively. In the following section, we perform the bifurcation analysis of the HH model.

4.3 Global Bifurcation Structure of the HH Model

The HH model represents a continuous-time dynamical system, which is described by nonlinear ODEs with four variables and various parameters (please refer to section 3.1 for details). Here we use the bifurcation analysis software AUTO to analyze the global bifurcation structure of the HH model, and investigate the parameter dependance and sensitivity of the HH model's behavior.

4.3.1 One-parameter Bifurcation Analysis

In this subsection, we vary the external current I_{ext} as a bifurcation parameter to analyze the global bifurcation structure of the HH model. Figure 4.1 shows the one-parameter bifurcation diagram of the HH model as for I_{ext}. The abscissas denote the bifurcation parameter I_{ext}, and the ordinates denote the membrane potential V. The solid and broken curves show the values of V of stable and unstable equilibrium points for each value of I_{ext}, respectively. The • and ○ circles show the maximum values of V of stable and unstable periodic orbits for each value of I_{ext}, respectively. A stable periodic orbit means that the membrane potential repeats a variation (increase, decrease) periodically. Thus it corresponds to the case of rhythmic action potentials can be generated. A stable equilibrium point means that the membrane potential asymptotically converges to the stable equilibrium point. Thus it corresponds to the case of no rhythmic action potential can be generated. Moreover, the maximum values of stable periodic orbits correspond to the amplitudes of action potentials. The bifurcation points of Hopf, double-cycle, and period-doubling bifurcations are denoted by HB, DC, and PD (with a number), respectively.

The one-parameter bifurcation diagram of Fig. 4.1(a) can be divided into two parts: one is curves which correspond to equilibrium points, and the other is circles which correspond to periodic orbits. These equilibrium points or periodic orbits are tracked one by one when I_{ext} is varied slightly. Here let's start from $I_{\text{ext}} = 0$, which corresponds to a stable equilibrium point (solid curve). We increase I_{ext} and track the equilibrium point. Then a Hopf bifurcation point HB1 appears, where the stability of equilibrium point changes form stable to unstable, and an unstable periodic orbit is bifurcated. We continue to increase I_{ext} and track the equilibrium point form HB1. Then another Hopf bifurcation HB2 appears, where the stability of equilibrium point returns to stable again, and a stable periodic orbit is bifurcated. Similarly, let's start form the Hopf bifurcation point HB1 to track these periodic orbits. After

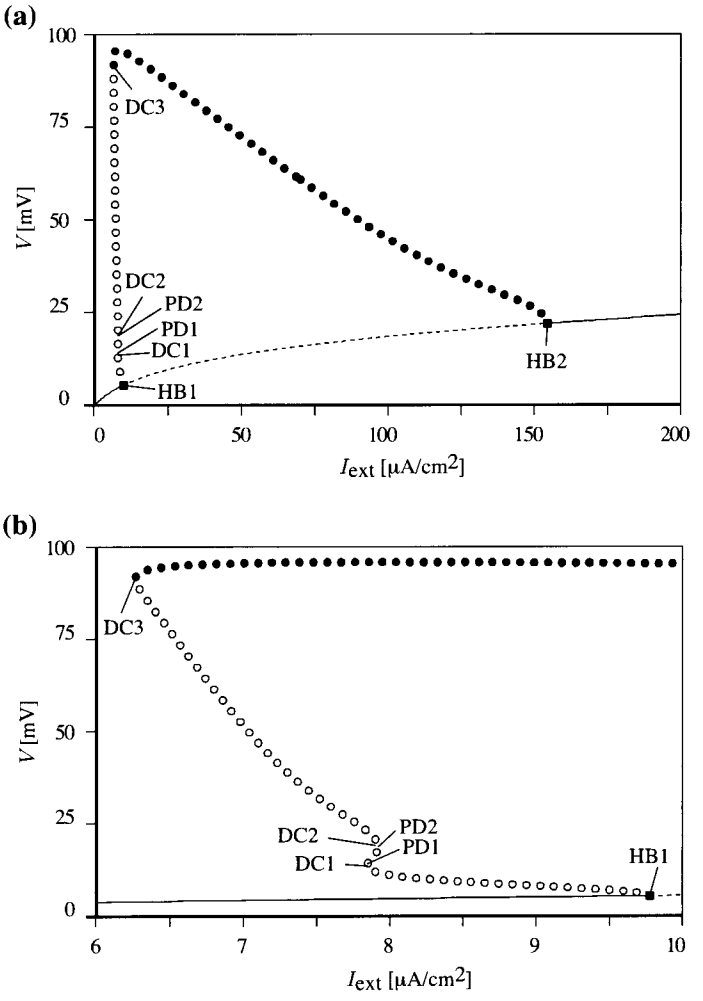

Figure 4.1: (a) One-parameter bifurcation diagram of the HH model as for the external current I_{ext}, (b) magnification of (a). The solid and broken curves show the values of V of stable and unstable equilibrium points for each value of I_{ext}, respectively. The • and ○ circles show the maximum values of V of stable and unstable periodic orbits for each value of I_{ext}, respectively. The bifurcation points of Hopf, double-cycle, and period-doubling bifurcations are denoted by HB, DC, and PD (with a number), respectively.

three double-cycle bifurcation points DC1–DC3 and two period-doubling bifurcation points PD1, PD2, the stability of periodic orbit changes to stable. At last, the stable periodic orbit connects to the one bifurcated from the Hopf bifurcation point HB2.

Based on the one-parameter bifurcation diagram of Fig. 4.1, the effect of changing

I_{ext} on action potential generation can be obtained directly. For each value of I_{ext} between HB1 and HB2, since there exists a stable periodic orbit, rhythmic action potentials can be generated. For each value of I_{ext} in the left side of DC3 or in the right side of HB2, since there exists a stable equilibrium point, no rhythmic action potentials can be generated. For each value of I_{ext} between DC3 and HB1, since there exist both a stable equilibrium point and a stable periodic orbit, whether rhythmic action potentials can be generated or not depends on the initial conditions. The above results show that rhythmic action potentials can be generated under proper values of I_{ext} (not too small and not too large), which means a proper external stimulus is necessary for action potential generation, although the amplitude of action potential decreases with the increase of I_{ext}.

4.3.2 Two-parameter Bifurcation Analysis

In the above subsection, we only varied one bifurcation parameter I_{ext} and computed the corresponding one-parameter bifurcation diagram, in which various bifurcation points appeared. Here we vary another bifurcation parameter to examine how these bifurcation points will move. We introduce new parameters V_{x1} and V_{x2} ($x = m, n$, and h) to shift the voltage dependency of $x^{\infty}(V)$ and $\tau_x(V)$, respectively. That is, we rewrite $x^{\infty}(V)$, $\tau_x(V)$ as $x^{\infty}(V - V_{x1})$, $\tau_x(V - V_{x2})$, respectively. We vary V_{x1} or V_{x2} as another bifurcation parameter to analyze the bifurcation structure of the HH model. The analysis results are shown in two-parameter bifurcation diagrams, in which the loci of various bifurcations (bifurcation curves) are plotted. Figure 4.2 shows these two-parameter bifurcation diagrams.

At first, let's compare the two-parameter bifurcation diagrams in panels (a) and (b), whose ordinates V_{m1} and V_{m2} correspond to a same gating variable m. Panel (a) shows the two-parameter bifurcation diagram as for I_{ext} and V_{m1}. The line of $V_{m1} = 0$ (broken line) corresponds to the case of one-parameter bifurcation diagram as for I_{ext} in Fig. 4.1. That is, when V_{m1} is fixed to 0 and only I_{ext} is varied, the "one-parameter" bifurcation diagram as for I_{ext} of Fig. 4.1 is obtained. The values of I_{ext} at the intersection points between the line $V_{m1} = 0$ and the Hopf bifurcation curve HB1, 2 in Fig. 4.2(a) are the same as those at the Hopf bifurcation points HB1, HB2 in Fig. 4.1(a). Here we focus on the area where the line $V_{m1} = 0$ across the Hopf bifurcation curve HB1, 2: the top edge of the curve HB1, 2. Therefore, if V_{m1} is increased from 0 a little, such as $V_{m1} = 2$ (a very small increase compared to the membrane potential's variation range during action potential generation), there

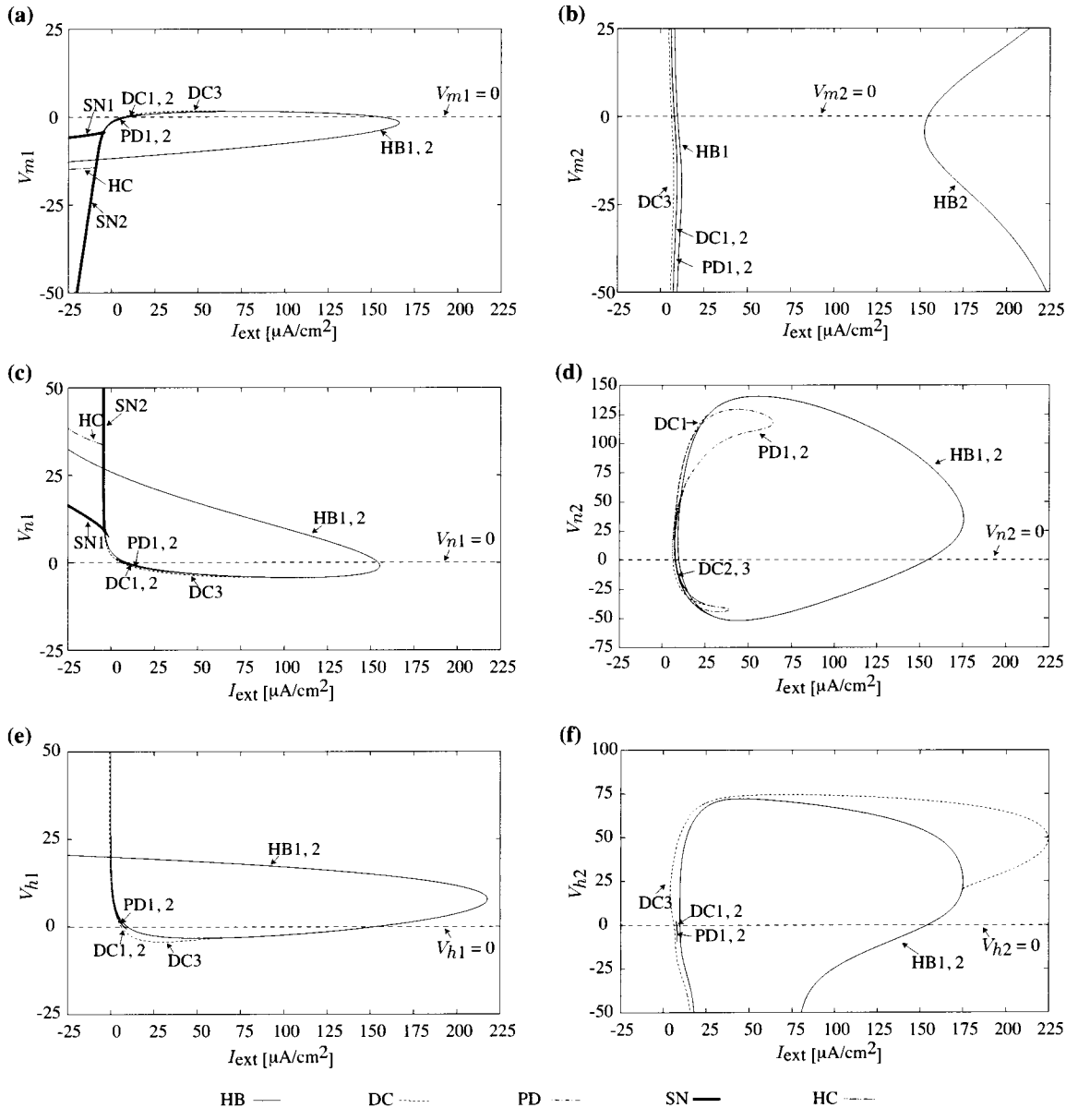

Figure 4.2: Two-parameter bifurcation diagrams of the HH model. Abscissas denote the bifurcation parameter I_{ext} for all panels, ordinates denote the other bifurcation parameters: (a) V_{m1}, (b) V_{m2}, (c) V_{n1}, (d) V_{n2}, (e) V_{h1}, and (f) V_{h2}. The bifurcation curves of Hopf, saddle-node, double-cycle, and period-doubling bifurcations are denoted by HB, SN, DC, and PD (with a number), respectively.

exists no intersection point between the line of $V_{m1} = 2$ and the Hopf bifurcation curve HB1, 2. Thus, in the case of $V_{m1} = 2$, no matter how I_{ext} is varied, Hopf

bifurcation point never appears, and no periodic orbit would be bifurcated. Such a result shows that the HH model's behavior is sensitive to the change of parameter V_{m1}.

Panel (b) shows the two-parameter bifurcation diagram as for I_{ext} and V_{m2}. Here we also focus on the area where the line $V_{m2} = 0$ across the Hopf bifurcation curves HB1, HB2: near the middle part of the curves HB1, HB2. Therefore, if V_{m1} is increased from 0 a little, such as $V_{m2} = 2$, intersection points between the line of $V_{m2} = 2$ and the Hopf bifurcation curves HB1, HB2 vary little. Thus, in the case of $V_{m2} = 2$, when I_{ext} is varied, there exist Hopf bifurcation points, from which periodic orbits are bifurcated. Such a result shows that the HH model's behavior is insensitive to the change of parameter V_{m2}. Comparing the parameter sensitivities in panels (a) and (b), although V_{m1} and V_{m2} correspond to a same gating variable m, their changes have different effects on the HH model's behavior: V_{m1} corresponds to a strong one, whereas V_{m2} corresponds to a weak one. Such different effects also exist between V_{n1} and V_{n2}, V_{h1} and V_{h2}. Therefore, we can say that the HH model's behavior has high sensitivities to shifting the voltage dependance of $x^{\infty}(V)$ ($x = m$, n, and h), whereas it has low sensitivities to shifting the voltage dependance of $\tau_x(V)$.

Next, let's see the other bifurcation (e.g., period-doubling and double-cycle bifurcations) curves besides the Hopf bifurcation curves. Figure 4.3(a) and (b) shows the period-doubling and double-cycle bifurcation curves of Fig. 4.2(d), respectively. Figure 4.3(c) shows the magnification of Fig. 4.2(d) near $V_{n2} = 0$, in which PD1 and PD2 locate very near DC1 and DC2, respectively. However, as shown in Fig. 4.3(a) and (b), when V_{n2} is increased or decreased much more, such as 100 or -40, PD1 and PD2 leave far from DC1 and DC2, respectively. But for other two-parameter bifurcation diagrams in Fig. 4.2, PD1 and PD2 would not leave DC1 and DC2 much. For example, Figure 4.4(a) shows a magnification of Fig. 4.2(f), in which PD1 and PD2 always locate near DC1 and DC2, respectively, although there exist small differences between PD1, 2 and DC1, 2 as shown in Fig. 4.4(b) and (c).

Here we investigate the period-doubling bifurcation curve PD1, 2 in Fig. 4.2(d) in detail. When $V_{n2} = 0$, the period-doubling bifurcation points PD1, PD2 and Hopf bifurcation point HB1 locate in a small range of I_{ext} (which is also shown in the one-parameter bifurcation diagram of Fig. 4.1). However, when V_{n2} is varied, PD1 and PD2 leave far from HB1, and go to the right side of HB1. Thus, the positional relation of period-doubling bifurcation point and Hopf bifurcation point changes. Figrue 4.5 shows the one-parameter bifurcation diagram as for I_{ext} when

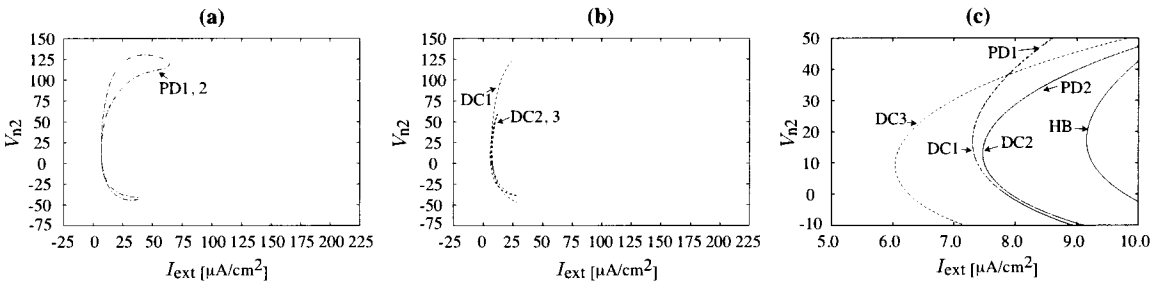

Figure 4.3: (a) Period-doubling bifurcation curves PD1, 2, (b) double-cycle bifurcation curves DC1 and DC2, 3, and (c) magnification of Fig.4.2(d).

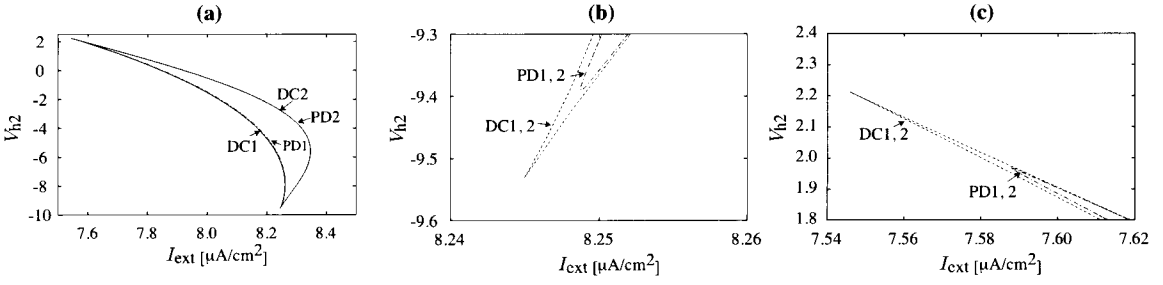

Figure 4.4: Magnifications of period-doubling bifurcation curves PD1, 2 and double-cycle bifurcation curves DC1, 2 of Fig. 4.2(f) with different scales.

$V_{n2} = -40$. The label TR denotes a torus bifurcation point, at which the stability of periodic orbit changes. Different from Fig. 4.1, DC2 and DC3 disappear and PD2 moves to the right side of HB1. As a result, for the values of I_{ext} between HB1 and PD2, there exist no stable equilibrium point or stable periodic orbit, which suggests some complicated behaviors of the HH model. Thus, we investigate the HH model's behavior as for the value of I_{ext} between HB1 and PD2 by numerical simulations. Figure 4.6 shows the corresponding one-parameter bifurcation diagram. For each value of I_{ext} between 15 and 35, we apply the fourth-order Runge-Kutta method to solve the ODEs, and then plot the local maximum and minimum values of V in the steady states after a long time. It shows that, for the values of I_{ext} between PD2 and HB1, complicated variations of membrane potential appear. Figure 4.7 shows two waveforms of membrane potential when $I_{\text{ext}} = 21$ and 30, both of which show abnormal action potential generation.

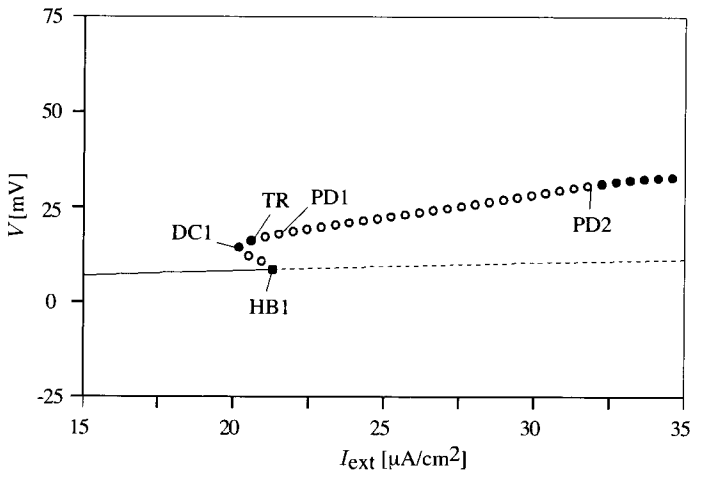

Figure 4.5: One-parameter bifurcation diagram of the HH model as for I_{ext} when $V_{n2} = -40$ obtained by AUTO.

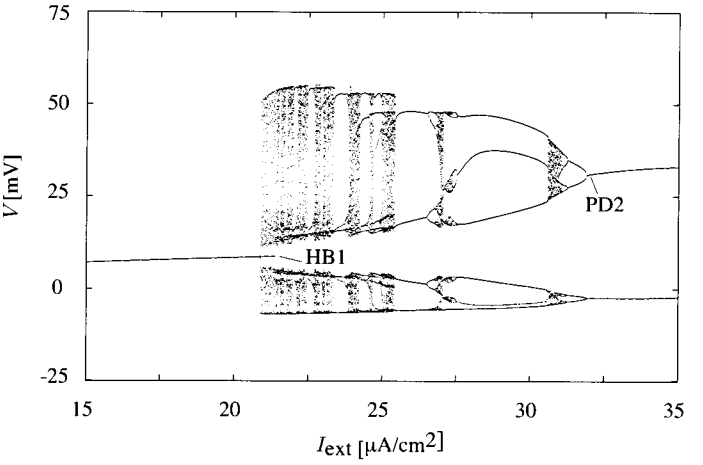

Figure 4.6: One-parameter bifurcation diagram of the HH model as for I_{ext} when $V_{n2} = -40$ obtained by numerical simulations.

We analyzed the global bifurcation structure of the HH model, and investigated the parameter dependence and sensitivity of the HH model's behavior. The behavior was sensitive to the change of V_{x1} ($x = m$, n, and h), whereas it was insensitive to the change of V_{x2}. Moreover, very complicated behaviors appeared as for certain parameter values. These results clearly show the effects of changing external current or gating variables' voltage dependencies on action potential generation. It was shown

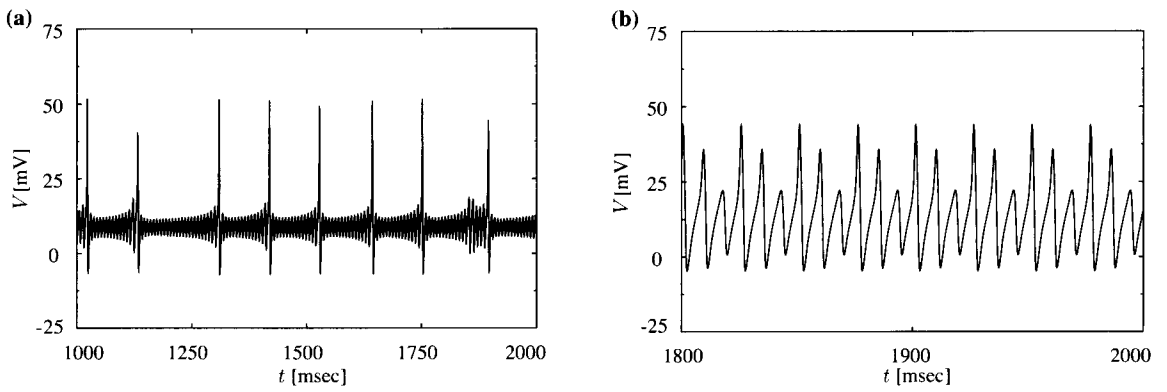

Figure 4.7: Examples of complicated behaviors of the HH model. (a) $V_{n2} = -40$, $I_{\text{ext}} = 21$, (b) $V_{n2} = -40$, $I_{\text{ext}} = 30$.

that the bifurcation analysis has a high efficiency in investigating the parameter dependance and sensitivity of the HH model. In the next two chapters, we utilize this efficient bifurcation analysis to analyze the HH-type sinoatrial node cell models.

Chapter 5

Analysis of the YNI Model

The YNI model of rabbit sinoatrial node cells is described by the HH-type equations with seven variables: membrane potential V [mV], dimensionless gating variables m, h, d, f, p, and q. The temporal variation of membrane potential V is described by

$$\begin{aligned}\frac{dV}{dt} &= -\frac{1}{C}(I_{\text{total}} - I_{\text{ext}}) \\ &= -\frac{1}{C}(I_{\text{Na}} + I_{\text{s}} + I_{\text{K}} + I_{\text{h}} + I_{\text{l}} - I_{\text{ext}}),\end{aligned} \tag{5.1}$$

where C (=1 μF/cm^2) and I_{ext} [μA/cm^2] denote the membrane capacitance and the external current per unit area, respectively. I_{total} [μA/cm^2] is the total membrane current per unit area, which contains five ion channel currents I_{Na}, I_{s}, I_{K}, I_{h}, and I_{l} [μA/cm^2]. The five ion channel currents are described as follows:

- Sodium current

$$I_{\text{Na}} = c_{\text{Na}}\bar{g}_{\text{Na}}m^3h(V - 30),\ \bar{g}_{\text{Na}} = 0.5; \tag{5.2}$$

- Slow inward current

$$I_{\text{s}} = c_{\text{s}}\bar{g}_{\text{s}}(0.95d + 0.05)(0.95f + 0.05)\left[\exp\left(\frac{V - 30}{15}\right) - 1\right],\ \bar{g}_{\text{s}} = 12.5; \tag{5.3}$$

- Potassium current

$$I_{\text{K}} = c_{\text{K}}\bar{g}_{\text{K}}p\frac{\exp\left[0.0277\,(V + 90)\right] - 1}{\exp\left[0.0277\,(V + 40)\right]},\ \bar{g}_{\text{K}} = 0.7; \tag{5.4}$$

- Hyperpolarization-activated current

$$I_{\text{h}} = c_{\text{h}}\bar{g}_{\text{h}}q(V + 45),\ \bar{g}_{\text{h}} = 0.4; \tag{5.5}$$

- Leak current

$$I_{\mathrm{l}} = c_{\mathrm{l}}\bar{g}_{\mathrm{l}}\left[1 - \exp\left(-\frac{V+60}{20}\right)\right],\ \bar{g}_{\mathrm{l}} = 0.8; \tag{5.6}$$

where $\bar{g}_{\mathrm{ion}}$ (ion = Na, s, K, h, and l) [mS/cm^2] are the maximum conductances of ion channels per unit area. The parameters c_{ion} are newly introduced dimensionless coefficients for denoting conductance changes of ion channels, and their standard values are 1.0. The gating variables m, h, d, f, p, and q (dimensionless, ranging between 0 and 1) denote the states of ion channels' gates.

Temporal variations of the gating variables are described as follows:

$$\frac{dx}{dt} = \frac{x^{\infty}(V) - x}{\tau_x(V)},\ (x = m,\ h,\ d,\ f,\ p,\ q), \tag{5.7}$$

where $x^{\infty}(V)$ and $\tau_x(V)$ [msec] are the steady-state values and time constants of gating variables. The details are as follows:

$$\tau_x(V) = \frac{1}{\alpha_x(V) + \beta_x(V)},\quad x^{\infty}(V) = \frac{\alpha_x(V)}{\alpha_x(V) + \beta_x(V)};$$

$$\alpha_m(V) = \frac{V+37}{1 - \exp\left[-(V+37)/10\right]},\quad \beta_m(V) = 40\exp\left(-\frac{V+62}{17.8}\right);$$

$$\alpha_h(V) = 1.209 \times 10^{-3}\exp\left(-\frac{V+20}{6.534}\right),\quad \beta_h(V) = \frac{1}{1 + \exp\left[-(V+30)/10\right]};$$

$$\alpha_d(V) = \frac{1.045 \times 10^{-2}(V+35)}{1 - \exp\left[-(V+35)/2.5\right]} + \frac{3.125 \times 10^{-2}V}{1 - \exp\left(-V/4.8\right)},$$

$$\beta_d(V) = \frac{-4.21 \times 10^{-3}(V-5)}{1 - \exp\left[(V-5)/2.5\right]};$$

$$\alpha_f(V) = \frac{-3.55 \times 10^{-4}(V+20)}{1 - \exp\left[(V+20)/5.633\right]},\quad \beta_f(V) = \frac{9.44 \times 10^{-4}(V+60)}{1 + \exp\left[-(V+29.5)/4.16\right]};$$

$$\alpha_p(V) = \frac{9 \times 10^{-3}}{1 + \exp\left[-(V+3.8)/9.71\right]} + 6 \times 10^{-4},\quad \beta_p(V) = \frac{-2.25 \times 10^{-4}(V+40)}{1 - \exp\left[(V+40)/13.3\right]};$$

$$\alpha_q(V) = \frac{-3.4 \times 10^{-4}(V+100)}{1 - \exp\left[(V+100)/4.4\right]} + 4.95 \times 10^{-5},$$

$$\beta_q(V) = \frac{5 \times 10^{-4}(V+40)}{1 - \exp\left[-(V+40)/6\right]} + 8.45 \times 10^{-5}.$$

Figure 5.1(a) and (b) shows temporal variations of membrane potential and various membrane currents in normal condition ($I_{\mathrm{ext}} = 0.0\ \mu\mathrm{A/cm}^2$, $c_{\mathrm{ion}} = 1.0$), respectively. The normal period of action potential generation is about 380 msec in the YNI model. Since the sinoatrial node plays the role of cardiac pacemaker, its cells generate rhythmic action potentials spontaneously without electrical stimuli ($I_{\mathrm{ext}} = 0.0$

μA/cm^2). In Fig. 5.1(b), the inward and outward currents are denoted by negative and positive values, respectively. The inward currents cause the membrane potential to increase (depolarization) and the ourward currents cause the membrane potential to decrease (repolarization), respectively. In the five membrane currents, the slow inward current $I_{\rm s}$ has the largest amplitude, whereas the hyperpolarization-activated current $I_{\rm h}$ has the least one in the normal action potential generation process.

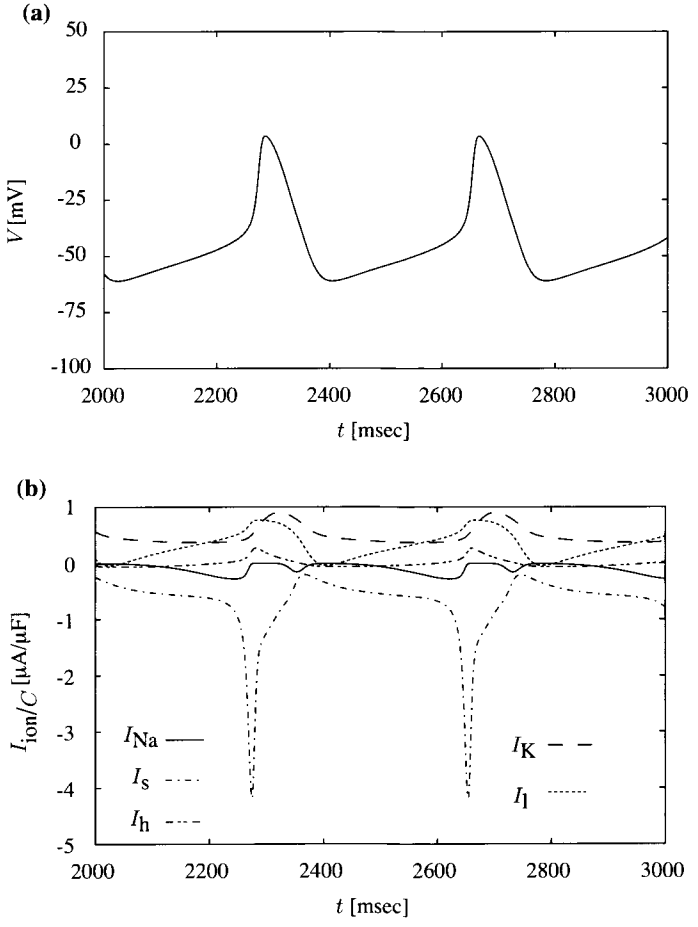

Figure 5.1: Temporal variations of (a) membrane potential V and (b) membrane currents $I_{\rm ion}$ (ion=Na, s, h, K, and l) in normal condition ($I_{\rm ext}$ = 0.0 μA/cm^2, $c_{\rm ion}$ = 1.0). In the panel (b), the inward currents and outward currents are denoted by negative and positive values, respectively.

5.1 Effects of Changing Ion Channel Conductances on Pacemaker Rhythm

In this section, we analyze the YNI model without the external current ($I_{\rm ext} = 0.0$ μA/cm^2), which corresponds to the case of a single sinoatrial node cell. The global structure of the YNI model is analyzed by using the bifurcation analysis software AUTO, where the conductance coefficients $c_{\rm ion}$ are varied as bifurcation parameters[1]. Based on these analysis results, the effects of changing ion channel conductances on pacemaker rhythm in a single cell are investigated.

5.1.1 One-parameter Bifurcation Analysis

Sodium Current $I_{\rm Na}$

Figure 5.2(a) shows the one-parameter bifurcation diagram of the YNI model as for the sodium current $I_{\rm Na}$. The abscissa denotes the bifurcation parameter $c_{\rm Na}$, and the ordinate denotes the membrane potential V. The solid and broken curves show the values of V of stable and unstable equilibrium points as for each value of $c_{\rm Na}$, respectively. The • and ○ circles show the maximum values of V of stable and unstable periodic orbits as for each value of $c_{\rm Na}$, respectively. The bifurcation points of Hopf, saddle-node, double-cycle, period-doubling, and homoclinic bifurcations are denoted by HB, SN, DC, PD, and HC (with a number), respectively.

For each value of $c_{\rm Na}$ between the two Hopf bifurcation points HB1 and HB2, a (stable or unstable) periodic orbit exists. Periods of several periodic orbits are also shown in the one-parameter bifurcation diagram. In normal condition ($c_{\rm Na} = 1.0$), a stable periodic orbit whose period is about 380 msec exists, whose corresponding waveform of action potential is shown in Fig. 5.2(e). The period of periodic orbit decreases when $c_{\rm Na}$ is increased. Figure 5.2(d) and (f) shows two typical waveforms of action potentials, whose periods are long and short, respectively. When changing $c_{\rm Na}$, although the period of periodic orbit varies much, the amplitude varies little. It shows that, the conductance change has a strong effect on the pacemaker rhythm, but it has a weak effect on the intensity of action potential generation.

Figure 5.2(b) shows the periods of periodic orbits appeared in (a). The period

[1]Under physiological conditions, the conductances of ion channels would not be negative or too large. However, in order to show the global bifurcation structure of the model, we compute for negative or very large conductance coefficients if necessary.

varies little when c_{Na} is increased from 1.0 (normal value), whereas it is big when c_{Na} is decreased from 1.0. Especially when c_{Na} takes a value near 0.25, the period changes very sensitively to c_{Na}. This sensitivity is mainly caused by the homoclinic bifurcation HC1 (and also the two saddle-node bifurcations SN1 and SN2). These results show that the parameter sensitivity of pacemaker rhythm in the case of a small value of c_{Na} is stronger than that in the case of a large value of c_{Na}.

In both the left side of HB2 and the right side of HB1, only stable equilibrium points exist. Since c_{Na} is too small or too large, it is difficult to generate rhythmic action potentials continuously. The typical waveforms of action potentials in the two cases are shown in Fig. 5.2(c) and (g), respectively. Both of the membrane potentials asymptotically converge to the stable equilibrium points, where the values of equilibrium points are different in the two cases.

Since only unstable periodic orbits and unstable equilibrium points were detected by AUTO for the values of c_{Na} between PD2 and DC1 in Fig. 5.2(a), we also computed the one-parameter bifurcation diagram by numerical simulations for $3.6 \leq c_{\mathrm{Na}} \leq 4.0$ (Fig. 5.3(a)). In this diagram, both the local maximum and minimum values of the membrane potential V for each value of c_{Na} were plotted. When c_{Na} is increased from the period-doubling bifurcation point PD2 to the double-cycle bifurcation point DC1, many complicated variations of membrane potential are generated sensitively to c_{Na}. The waveforms of action potentials when $c_{\mathrm{Na}} = 3.7$ and 3.8 are shown in Fig. 5.3(b) and (c), respectively. Both waveforms show abnormalities in action potential generation.

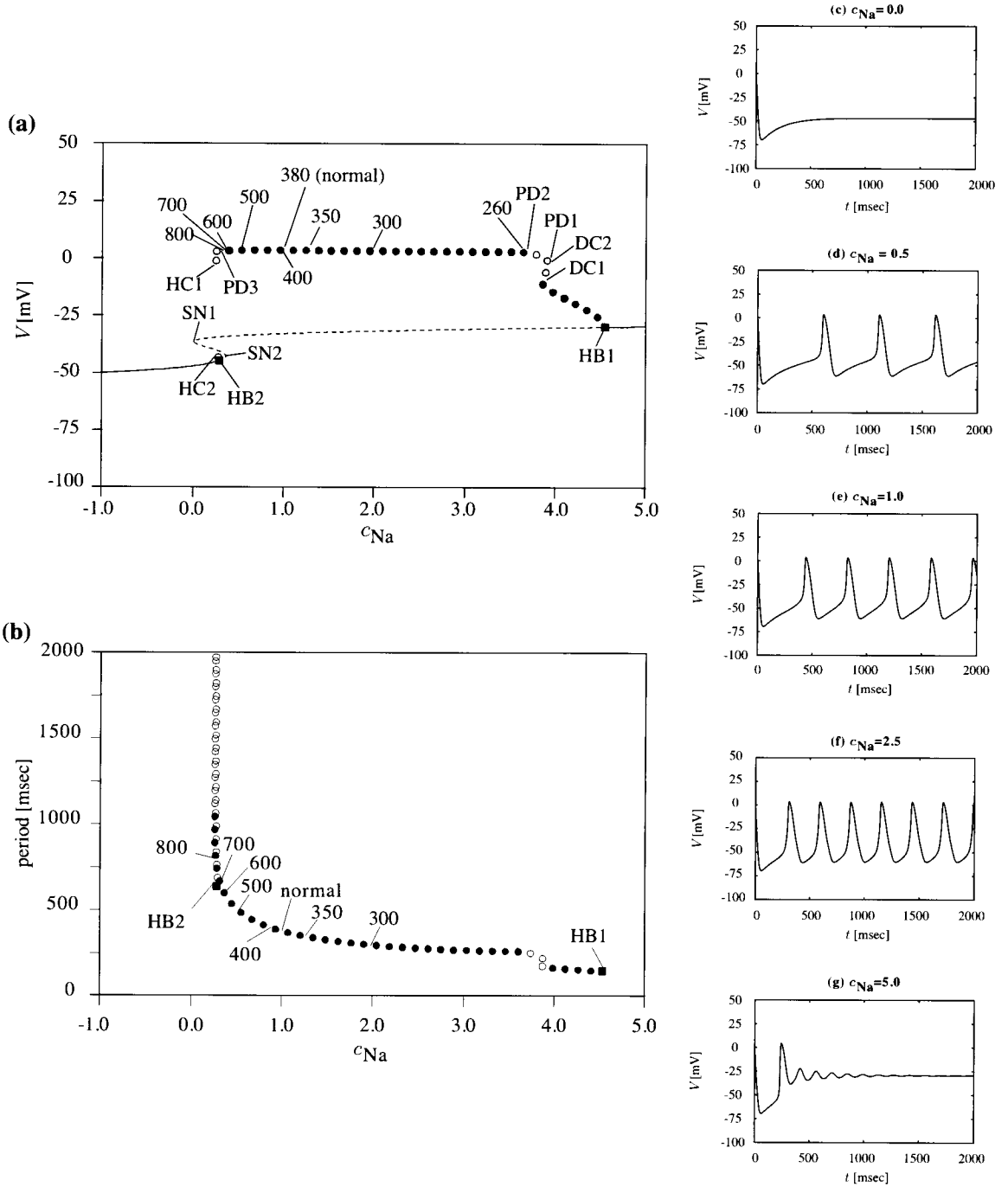

Figure 5.2: (a) One-parameter bifurcation diagram of the YNI model as for the sodium current I_{Na} obtained by AUTO. The bifurcation points of Hopf, saddle-node, double-cycle, period-doubling, and homoclinic bifurcations are denoted by HB, SN, DC, PD, and HC (with a number), respectively. (b) Periods of periodic orbits appeared in (a). (c)–(g) Typical waveforms of action potentials for various values of c_{Na}.

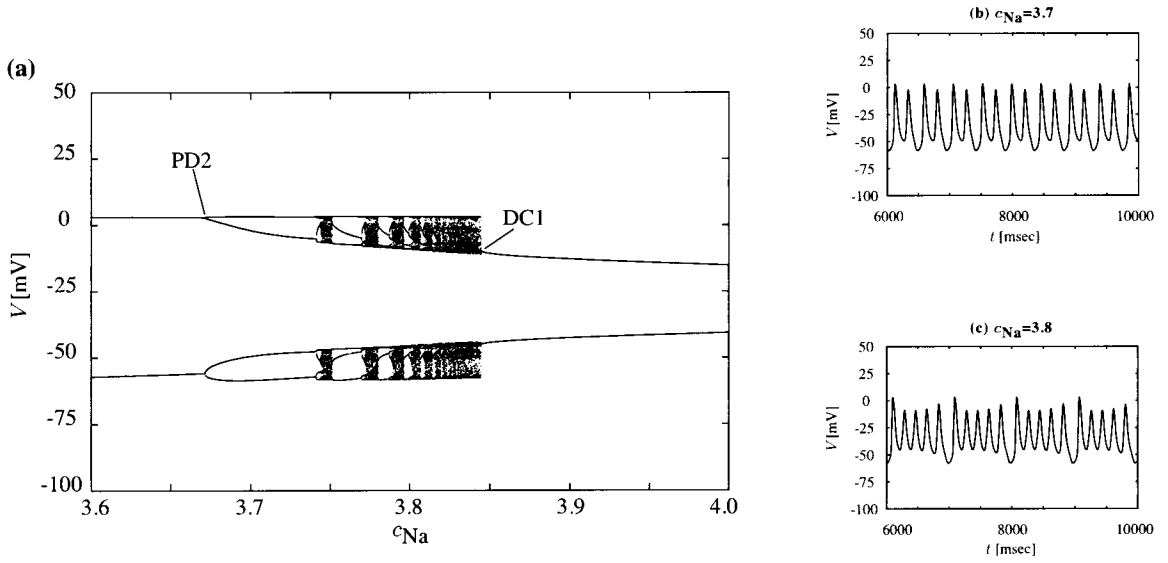

Figure 5.3: (a) One-parameter bifurcation diagram of the YNI model as for the sodium current I_{Na} obtained by numerical simulations, in which both the local maximum and minimum values of the membrane potential V for each value of c_{Na} are plotted. (b) and (c) Abnormal waveforms of action potentials for two values of c_{Na}.

Slow Inward Current I_s

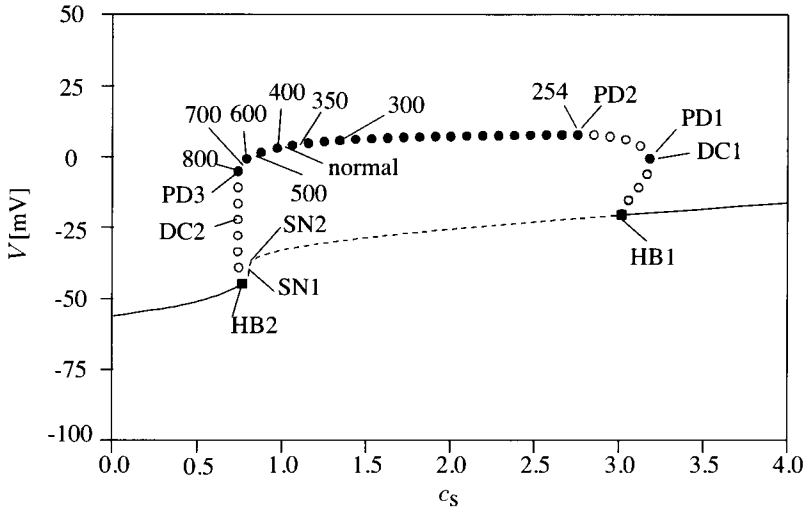

Figure 5.4: One-parameter bifurcation diagram of the YNI model as for the slow inward current I_s obtained by AUTO.

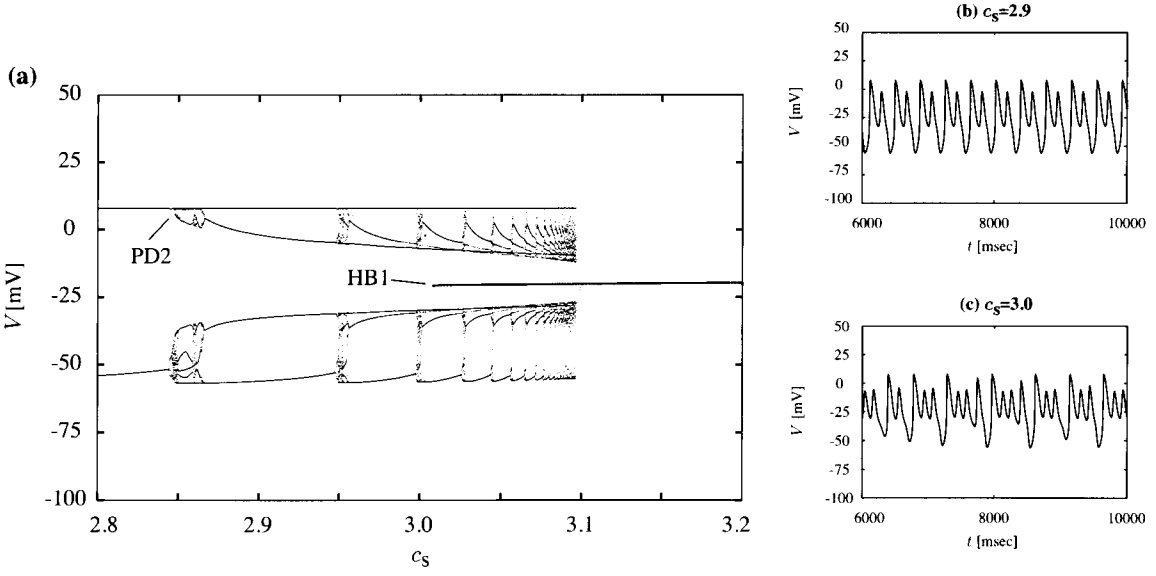

Figure 5.5: One-parameter bifurcation diagram of the YNI model as for the slow inward current I_s obtained by numerical simulations. (b) and (c) Abnormal waveforms of action potentials for two values of c_s.

The one-parameter bifurcation diagram of the YNI model as for the slow inward current I_s is shown in Fig. 5.4. In this diagram, there exist two (subcritical) Hopf bifurcation points HB1 and HB2, from which (unstable) period orbits are bifurcated. For each value of c_s between HB1 and HB2, a (stable or unstable) periodic orbit exists, and for the normal value ($c_s = 1.0$), a stable periodic orbit with a period of 380 msec exists. Similar to the case of c_{Na}, when c_s is increased, the period of periodic orbit decreases, whereas the amplitude of periodic orbit varies little. It shows that the conductance change mainly affects the pacemaker rhythm, but not the intensity of action potential generation. Moreover, the period of periodic orbit changes more sensitively to c_s when c_s is increased from 1.0 (normal value) than when c_s is decreased from 1.0. It shows that the parameter sensitivities of pacemaker rhythm are different between long period and short period.

Moreover, for each value of c_s between the Hopf bifurcation point HB1 and the period-doubling bifurcation point PD2, there exists no stable equilibrium point or stable periodic orbit. Therefore, we computed the corresponding one-parameter bifurcation diagram by numerical simulations, which is shown in Fig. 5.5(a). Also the two typical waveforms of action potentials of (b), (c) show abnormal action potential generation.

Potassium Current I_K

Figure 5.6 shows the one-parameter bifurcation diagram of the YNI model as for the potassium current I_K. For the values of c_K between the two Hopf bifurcation points HB1 and HB2, there exist stable periodic orbits with different periods. Different from the cases of c_{Na} and c_s, the period of periodic orbit increases when c_K is increased. This is due to the fact that I_K is an outward current, whereas I_{Na} and I_s are inward currents. Moreover, the variation of period is big when c_K is increased from 1.0 (normal value), whereas it is little when c_K is decreased from 1.0. Although the variations (increase or decrease) of pacemaker rhythm are opposite between the case of increasing c_K and the case of increasing c_{Na} or c_s, the parameter sensitivities of pacemaker rhythm in some ways are similar: a high parameter sensitivity in the case of long periods and a low one in the case of short periods.

Hyperpolarization-activated Current I_h

The one-parameter bifurcation diagram of the YNI model as for the hyperpolarization-activated current I_h is computed. There also exist two Hopf bifurcation points HB1

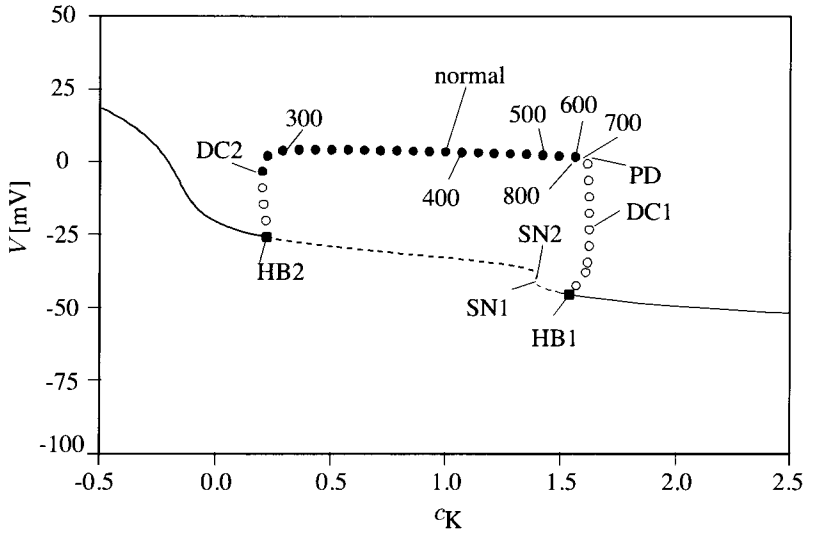

Figure 5.6: One-parameter bifurcation diagram of the YNI model as for the potassium current I_K.

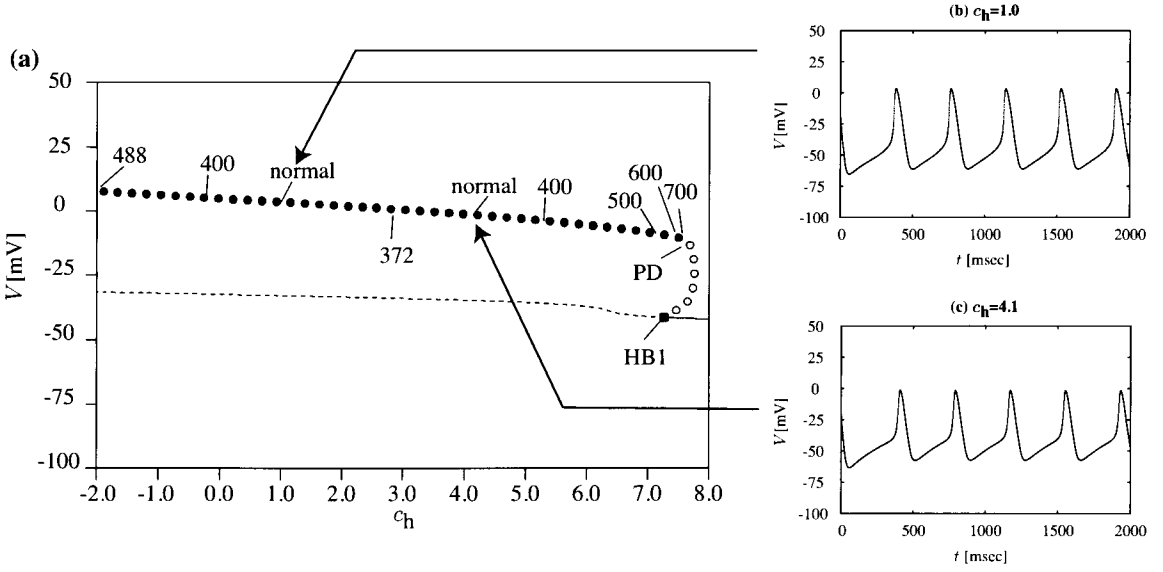

Figure 5.7: (a) One-parameter bifurcation diagram of the YNI model as for the hyperpolarization-activated current I_h. (b) and (c) Waveforms of action potential with the normal period (380 msec).

and HB2, where HB2 corresponds to a very negative value of $c_h = -71.0$. Thus, HB2 does not appear in the one-parameter bifurcation diagram of Fig. 5.7(a). For the

value of c_h in the left side of HB1, various periodic orbits exist. In the cases of I_{Na}, I_s, and I_K, the period of periodic orbit increases or decreases monotonically when increasing their conductance coefficients. However, in the case of I_h, the period of periodic orbit decreases and then increases when c_h is increased. Such a variation is related to the fact that I_h is a bidirectional current (Fig. 5.1). Figure 5.7(b) and (c) shows two waveforms of action potentials which have the normal period (380 msec), but have different amplitudes. Except for the value of c_h near PD, the period changes insensitively to the variation of c_h, which shows a low parameter sensitivity of pacemaker rhythm.

Leak Current I_l

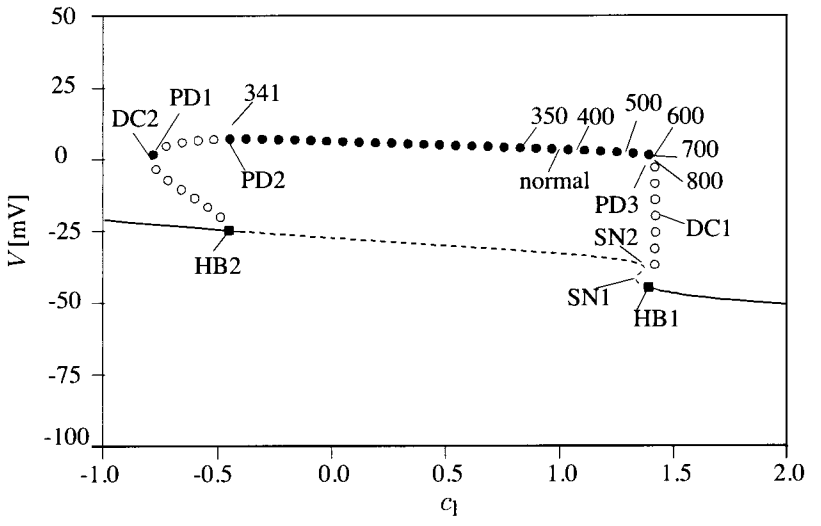

Figure 5.8: One-parameter bifurcation diagram of the YNI model as for the leak current I_l.

Figure 5.8 shows the one-parameter bifurcation diagram of the YNI model as for the leak current I_l. The diagram shows that the period of periodic orbit increases when increasing c_l, and also shows a strong parameter sensitivity especially for the values of c_l near the period-doubling point PD3. Although it is a leak current, I_l seems to be important in maintaining the pacemaker rhythm.

So far, we have analyzed the effects of conductance changes on pacemaker rhythm for I_{ion} (ion = Na, s, K, h, and l). Here we compare their effects. Figure 5.9 plots the periods of stable periodic orbits when each c_{ion} is varied near the normal value

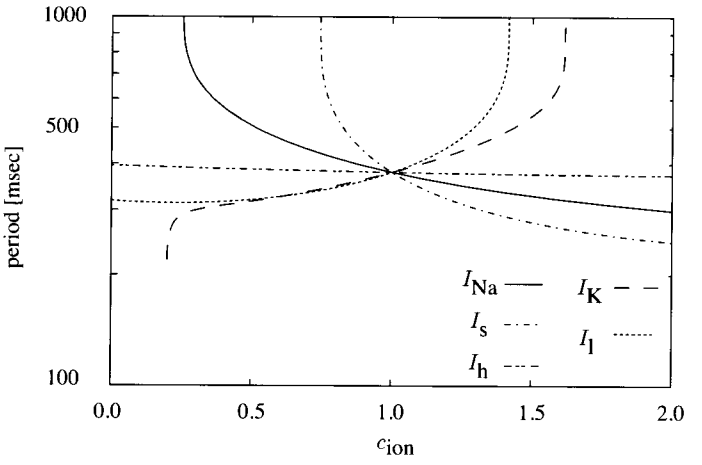

Figure 5.9: The periods of stable periodic orbits are plotted when each conductance coefficient c_{ion} (ion = Na, s, h, K, and l) is varied, for comparison of the variabilities of pacemaker rhythm for different membrane currents.

1.0. As for I_{h}, the variation of c_{h} does not change the period much, which means the conductance change has a weak effect on pacemaker rhythm. For other four ion currents, the period changes with the variation of each conductance coefficient, particularly in the range of long periods. Moreover, for the inward currents I_{Na} and I_{s}, the period decreases when c_{Na} or c_{s} is increased. For the outward currents I_{K} and I_{l}, the period increases when c_{K} or c_{l} is increased. These results show that the conductance changes of the above four currents have strong effects on pacemaker rhythm.

5.1.2 Two-parameter Bifurcation Analysis

In the above subsection, we have analyzed the parameter sensitivity of pacemaker rhythm as for each ion channel current solely. In this subsection, we analyze the parameter sensitivity as for two ion channel currents simultaneously. The bifurcation curves and contour lines of various periods when two conductance coefficients are varied, are plotted in two-parameter bifurcation diagram to examine the pacemaker rhythm.

Sodium Current I_{Na} and Potassium Current I_{K}

The two-parameter bifurcation diagram as for the sodium current I_{Na} and the potassium current I_{K} is shown in Fig. 5.10(a). The abscissa and ordinate denote the two bifurcation parameters c_{Na} and c_{K}, respectively. The curve labeled with "normal" denotes the contour line of the normal period (380 msec), and the point labeled with "BT" denotes the Bogdanov-Takens bifurcation point, where three bifurcation curves of HB, SN and HC meet together. The double-cycle bifurcation curve DC3 meets the Hopf bifurcation curve HB1 at the nHB point which is called a neutral or degenerate Hopf bifurcation point. When c_{K} is fixed to 1.0 and c_{Na} is varied, the result corresponds to the "one-parameter" bifurcation diagram of Fig. 5.2(a).

The Hopf bifurcation curves HB1 and HB2 separate Fig. 5.10(a) into three areas. In area 2, various periodic orbits exist, where rhythmic action potentials can be generated. The period becomes short when c_{Na} is increased, and it becomes long when c_{K} is increased. The density of contour line of long period is high, and that of short period is low (Note that near the Hopf bifurcation curve HB2, the contour lines with long period and other bifurcation curves such as HC1 and HC2 gather together). This difference shows that the parameter sensitivity in the case of long periods is stronger than that of short periods. Figure 5.10(c) and (e) shows two abnormal (too-long and too-short periods) waveforms of action potentials when c_{Na} takes a small and a large values (c_{K} is fixed to 1.0), respectively. If we want to get the normal period 380 msec in such abnormal cases of c_{Na}, the value of c_{K} should be adjusted as shown in Fig. 5.10(d) and (f), respectively. Namely, when the two ion channel currents have a strong interrelation, we can correct the pacemaker rhythm caused by one abnormal ion channel, by adjusting the other one according to the "normal" contour line.

In area 1 and area 3, rhythmic action potentials cannot be generated successfully.

Figure 5.10(g) and (h) shows the typical waveforms of action potentials in area 1 and area 3, respectively. Both of the membrane potentials converge to the equilibrium points eventually and cannot generate rhythmic action potentials.

Moreover, Figure 5.10(b) shows the periods of (stable or unstable) periodic orbits as a function of c_{Na} along the Hopf bifurcation curves HB1 and HB2 of Fig. 5.10(a). The solid and broken curves correspond to stable and unstable periodic orbits (will be bifurcated from the Hopf bifurcation), respectively, and the stability changes at the neutral (degenerate) Hopf bifurcation point nHB. It shows that the period of periodic orbit varies drastically near the Bogdanov-Takens bifurcation point BT, and the parameter sensitivity of pacemaker rhythm becomes very high.

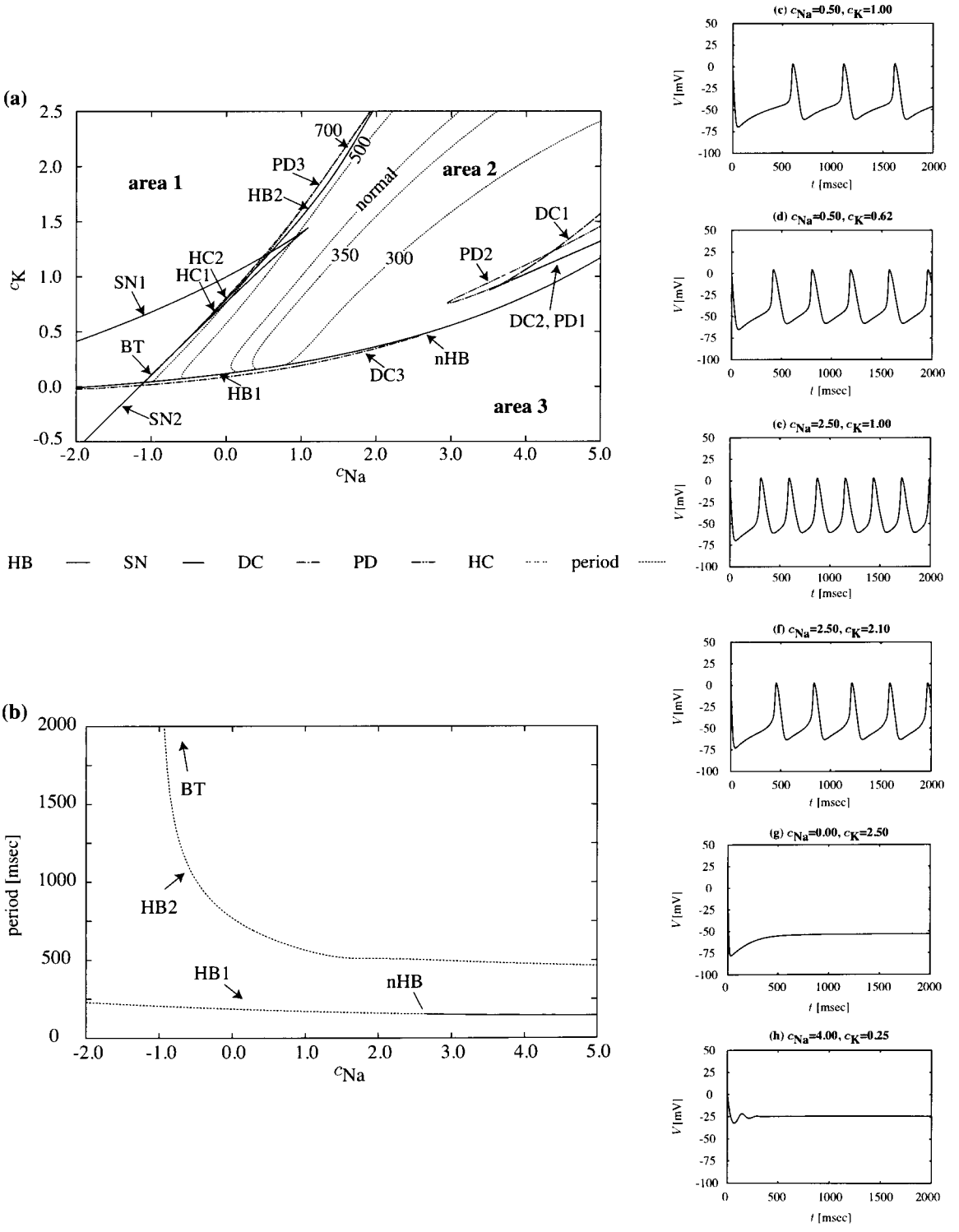

Figure 5.10: (a) Two-parameter bifurcation diagram as for the sodium current I_{Na} and the potassium current I_{K}. (b) Periods of periodic orbits along the Hopf bifurcation curves HB1 and HB2 of (a). (c)–(h) Typical waveforms of membrane potentials for various values of c_{Na} and c_{K}.

Slow Inward Current I_s and Potassium Current I_K

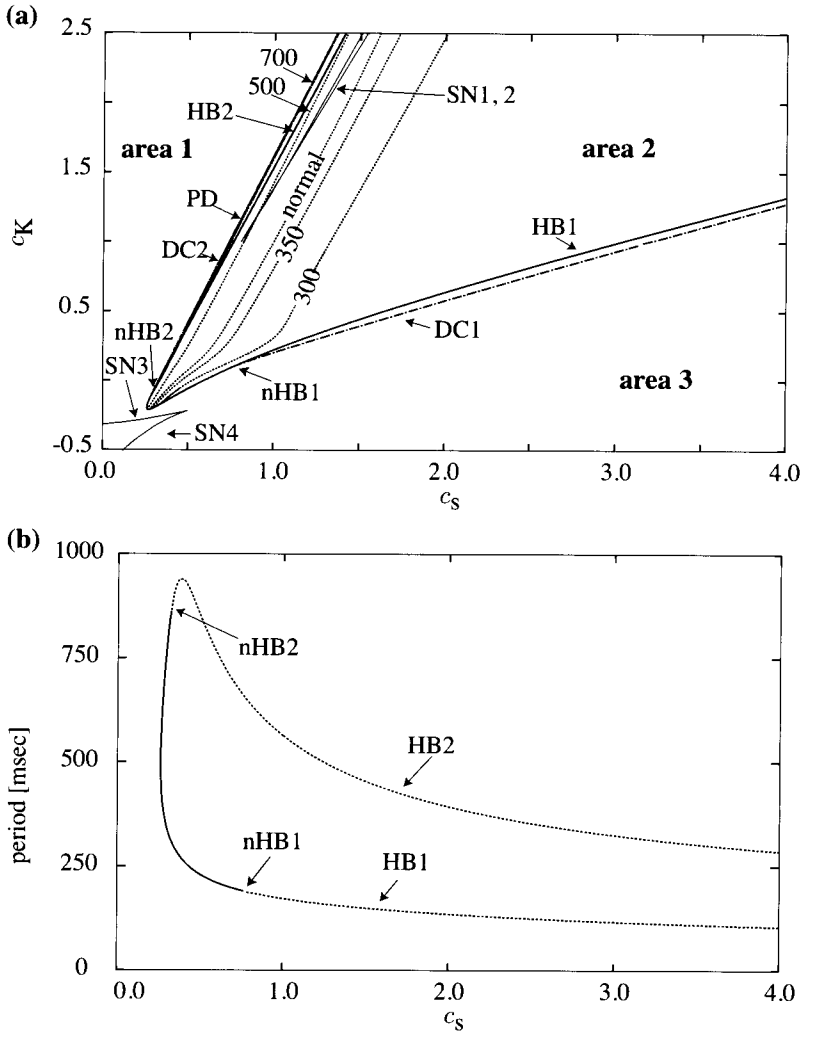

Figure 5.11: (a) Two-parameter bifurcation diagram as for the slow inward current I_s and the potassium current I_K. (b) Periods of periodic orbits along the Hopf bifurcation curves HB1 and HB2 of (a).

The two-parameter bifurcation diagram as for the slow inward current I_s and the potassium current I_K is shown in Fig. 5.11(a). The result of Fig. 5.11(a) is very similar to that of Fig. 5.10(a). That is, the rhythmic action potentials can be generated in area 2 (which is surrounded by the Hopf bifurcation curves HB1 and HB2), whereas those cannot be generated in area 1 or area 3. For periodic orbits (pacemaker activities) in area 2, the adjustment of c_K (c_s) can recover the abnormal

periods caused by c_s (c_K) to the normal period referring to the "normal" contour line.

The variation of period along the Hopf bifurcation curves HB1 and HB2 of Fig. 5.11(a) is shown in (b). Between the neutral Hopf bifurcation points nHB1 and nHB2, stable periodic orbits are bifurcated from the Hopf bifurcation. It is obvious that for small values of both c_s and c_K, the period of periodic orbit at Hopf bifurcation varies drastically, and the parameter sensitivities of pacemaker rhythm are very high (please compare the loci of two points nHB1 and nHB2 between panels (a) and (b)).

Slow Inward Current I_s and Sodium Current I_{Na}

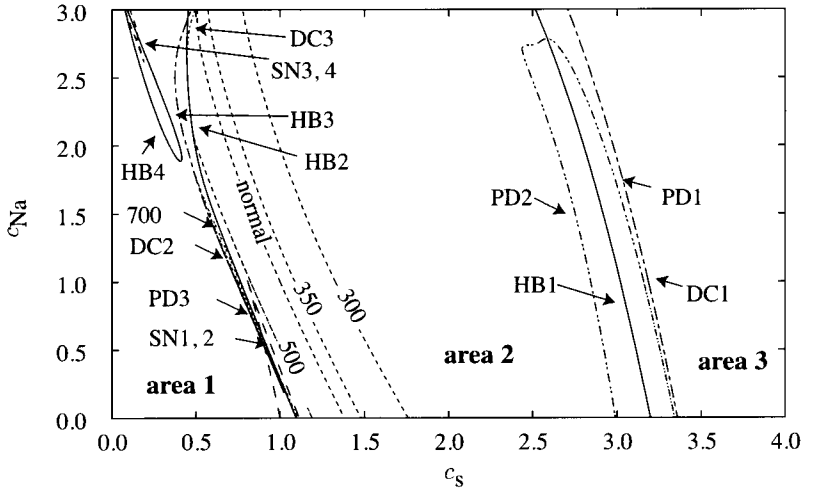

Figure 5.12: Two-parameter bifurcation diagram as for the slow inward current I_s and the sodium current I_{Na}.

The two-parameter bifurcation diagram as for the slow inward current I_s and the sodium current I_{Na} is shown in Fig. 5.12. This diagram also is separated into three areas by the Hopf bifurcation curves HB1 and HB2. In area 2, the period of periodic orbit becomes short when increasing either c_s or c_{Na}, since both I_s and I_{Na} are inward currents. In other words, the two inward currents complement each other to maintain the pacemaker rhythm. An abnormal pacemaker rhythm caused by a large c_s can be adjusted by using a small c_{Na}. Moreover, it is shown that the pacemaker rhythm changes more sensitively to c_s than to c_{Na}, since these bifurcation curves and contour lines of periods are nearly vertical.

Sodium Current I_{Na} and Hyperpolarization-activated Current I_{h}

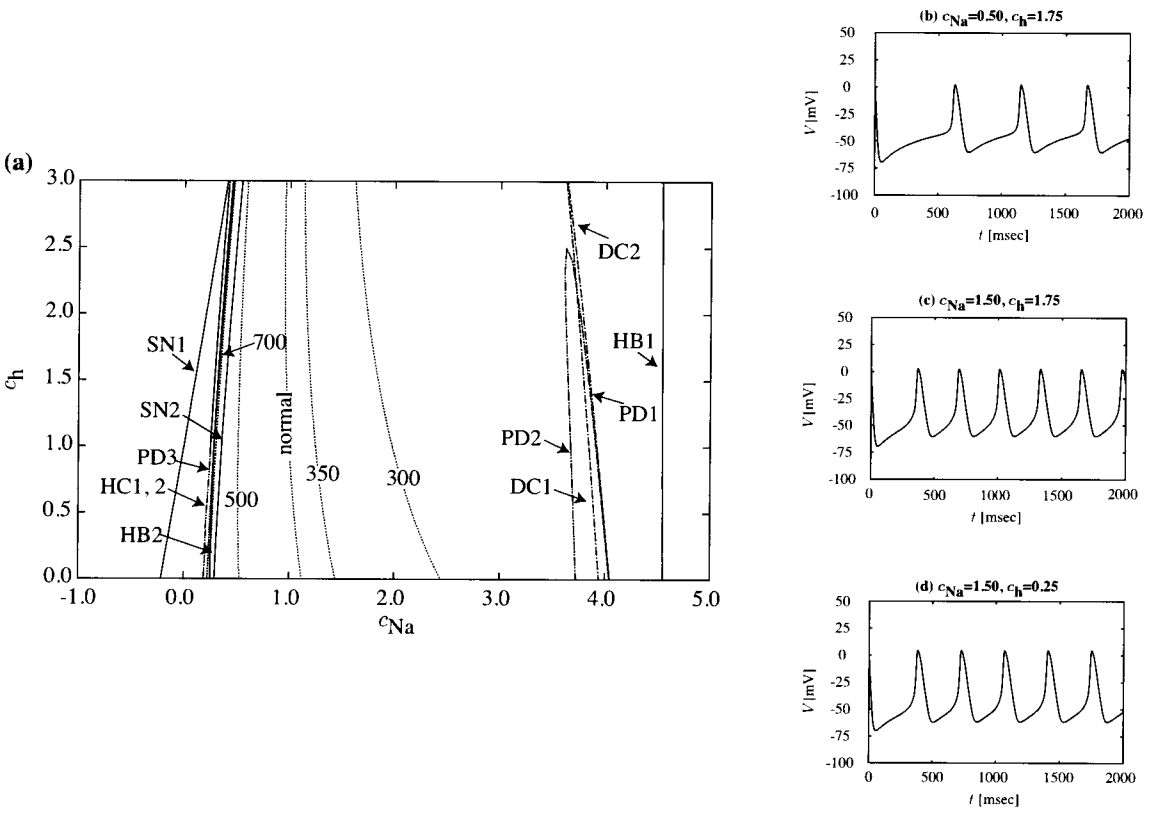

Figure 5.13: (a) Two-parameter bifurcation diagram as for the sodium current I_{Na} and the hyperpolarization-activated current I_{h}. (b)–(d) Typical waveforms of membrane potentials for various values of c_{Na} and c_{h}.

Figure 5.13(a) is the two-parameter bifurcation diagram where c_{Na} and c_{h} are bifurcation parameters. Both the bifurcation curves and contour lines are almost vertical, which means that the change of c_{h} affects the pacemaker rhythm little whereas the change of c_{Na} affects it much, although the effect of c_{h} becomes relatively larger when c_{Na} is large. From the waveforms shown in Fig. 5.13(b), (c), and (d), we can also see that the pacemaker rhythm changes greatly when c_{Na} is varied, but it changes little when c_{h} is varied. We have also examined other two-parameter bifurcation diagrams as for the parameters: c_{h} and c_{s}, c_{h} and c_{K}, c_{h} and c_{l}, which are not shown in this thesis. All results are similar to Fig. 5.13: I_{h} has little effect on the period of periodic orbit (pacemaker rhythm), and the corresponding ion channel plays a minor role in rhythmic action potential generation.

5.2 Effect of Changing External Current on Pacemaker Rhythm

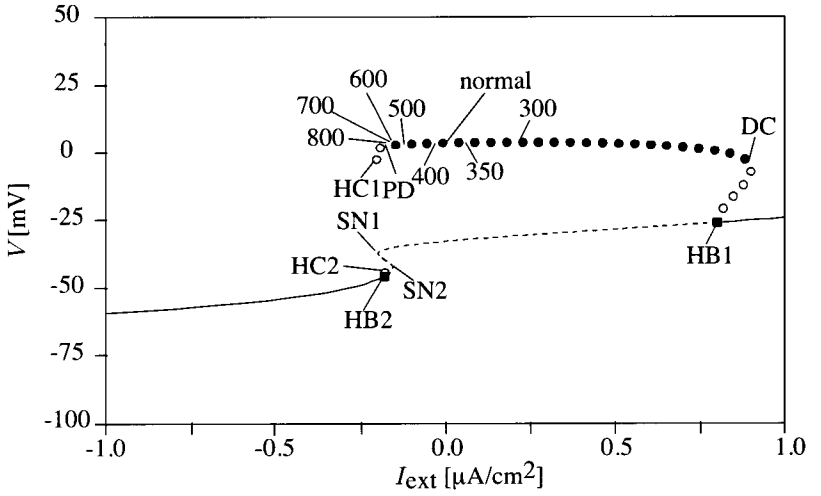

Figure 5.14: One-parameter bifurcation diagram of the YNI model as for the external current I_{ext}.

In above section, we have only investigated the pacemaker rhythm of a single cell (without the external current I_{ext}). Here we vary the external current I_{ext} to investigate the coupling effect on pacemaker rhythm approximately.

At first, we examine the one-parameter bifurcation diagram as for the external current I_{ext} (Fig. 5.14). The bifurcation structure of the YNI model shown in Fig. 5.14 is very similar to that shown in Fig. 5.2(a), since the positive current I_{ext} can be thought to be an inward current, which plays a similar role to I_{Na} in action potential generation. The period of periodic orbit between HB1 and HB2 decreases when I_{ext} is increased. It shows that the external stimuli (positive currents) accelerate action potential generation in cardiac pacemaker cells.

Next, the relations between each ion channel current and the external current are illustrated in the two-parameter bifurcation diagrams in Figs. 5.15 and 5.16. There are strong interrelations between I_{Na} and I_{ext}, I_{s} and I_{ext}, I_{K} and I_{ext}, whereas there is a weak interrelation between I_{h} and I_{ext}. For the inward currents I_{Na} and I_{s}, the Hopf bifurcation points HB1 and HB2 shift to left when I_{ext} is increased, which means that a small I_{Na} or I_{s} can generate rhythmic action potentials successfully

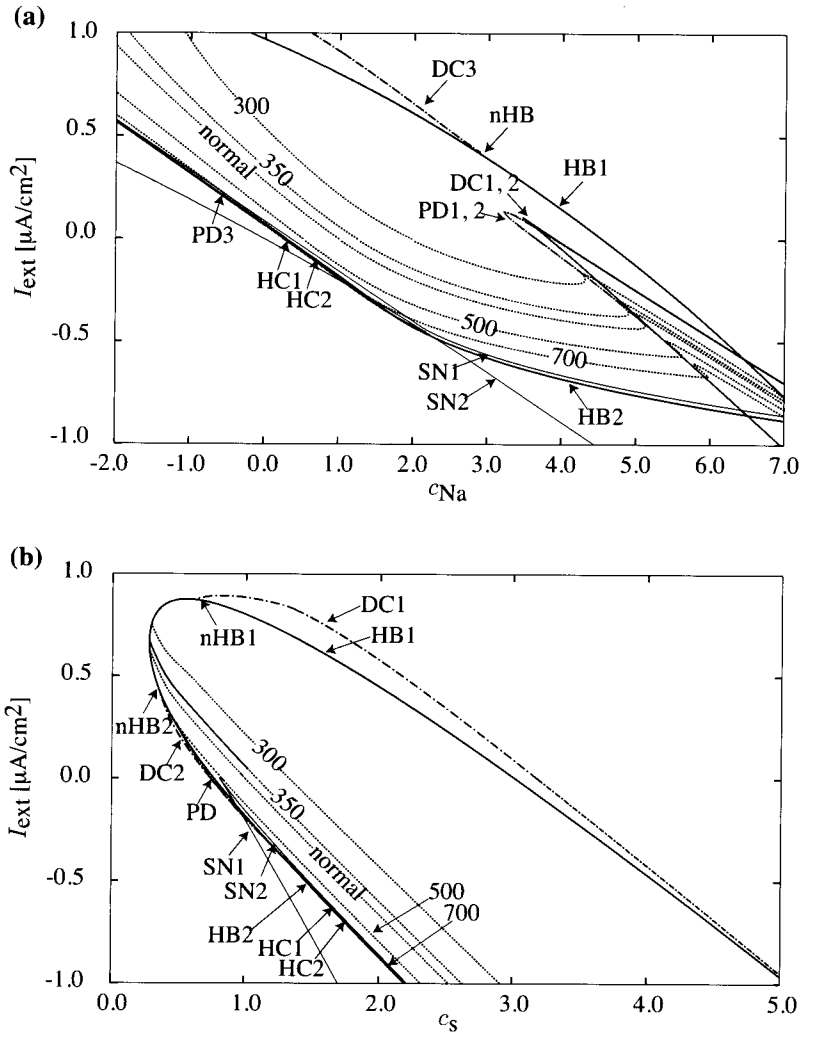

Figure 5.15: Two-parameter bifurcation diagram as for the the ion channel current I_{ion} (ion = Na and s) and the external current I_{ext}.

with the help of I_{ext} in these cases. However, the effects of I_{ext} on pacemaker rhythm are different for the above two inward currents. When I_{ext} takes a value near 1.0 μA/cm^2, rhythmic action potentials can be generated by adjusting c_{Na}, whereas it cannot be done by adjusting c_{s}.

For the outward current I_{K}, when I_{ext} is increased, the Hopf bifurcation points HB1 and HB2 shift to right (the opposite direction to those of the inward currents), and the two points HB1 and HB2 deviate each other. For I_{h}, both the bifurcation curves and contour lines are almost horizontal, which shows that the conductance

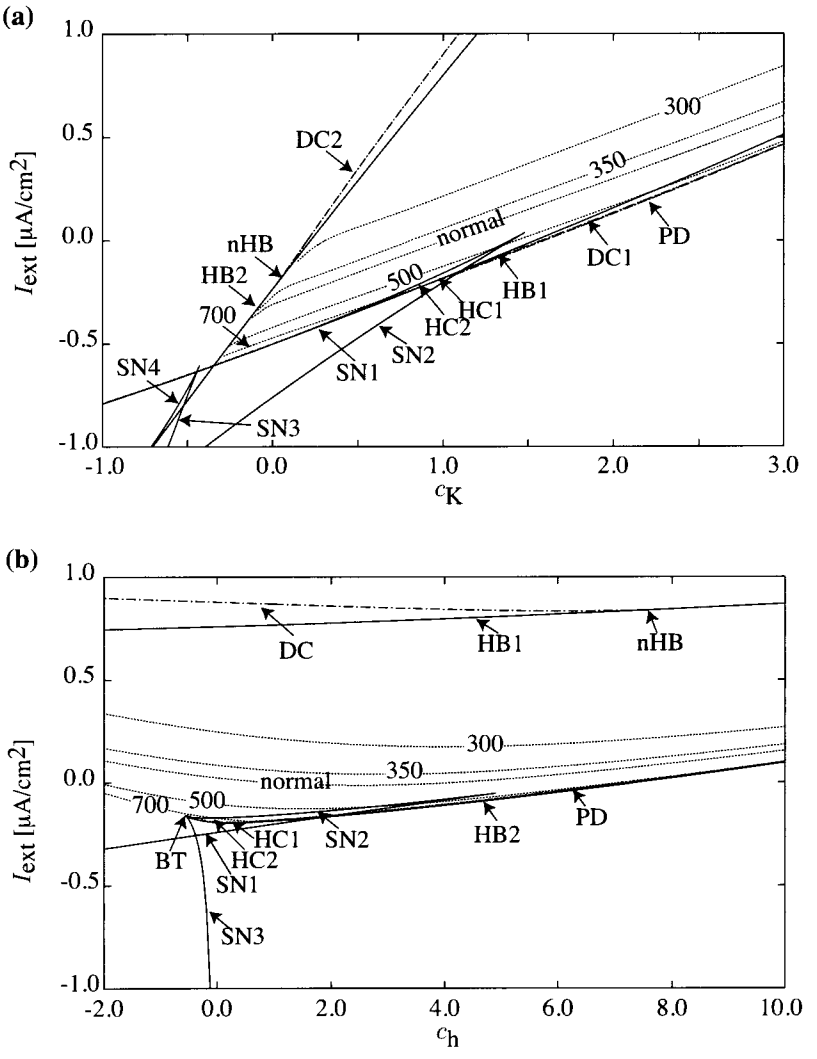

Figure 5.16: Two-parameter bifurcation diagram as for the ion channel current I_{ion} (ion = K and h) and the external current I_{ext}.

change of I_{h} has little effect on pacemaker rhythm. From the above results, we know that the ion channels of I_{Na}, I_{s} and I_{K} play important roles in action potential generation, whereas the ion channel of I_{h} plays a minor role in the action potential generation for both a single cell and coupled cells.

So far, we have analyzed the bifurcation structure of the YNI model, and have investigated the variabilities of pacemaker rhythm. However, there are several limitations on the YNI model since it is an early and simple model. The YNI model does not consider some cellular structures such as sodium-potassium pump and sodium-

calcium exchanger. The sodium current I_{Na}, which corresponds to the sodium channel, changes with the region of sinoatrial node largely. The sodium channel is only present in the periphery cells of sinoatrial node [35, 36]. Thus, it is necessary to analyze the effect of regional difference on pacemaker rhythm [32]. The slow inward current I_{s} plays an important role in action potential generation, but it is a sum of the calcium current I_{Ca} and the sodium-calcium exchange current I_{NaCa} [73]. Moreover, I_{Ca} can be divided into two types of currents: L-type and T-type calcium currents ($I_{\mathrm{Ca,L}}$ and $I_{\mathrm{Ca,T}}$). The potassium current I_{K} can also be divided into rapid and slow delayed rectifying potassium currents ($I_{\mathrm{K,r}}$ and $I_{\mathrm{K,s}}$) [101]. Therefore, in the next chapter, we analyze a detailed sinoatrial node cell model of the Zhang model, and compare the results of the two models.

Chapter 6

Analysis of the Zhang Model

The Zhang model of rabbit sinoatrial node cells is described by the HH-type equations with fifteen variables: membrane potential V [mV], dimensionless gating variables m, h_1, h_2, d_{L}, f_{L}, d_{T}, f_{T}, $p_{\mathrm{a,f}}$, $p_{\mathrm{a,s}}$, p_{i}, x_{s}, q, r, and y. The temporal variation of membrane potential V is described by

$$\begin{aligned}\frac{dV}{dt} &= -\frac{1}{C}(I_{\mathrm{total}} - I_{\mathrm{ext}}) \\ &= -\frac{1}{C}(I_{\mathrm{Na}} + I_{\mathrm{Ca,L}} + I_{\mathrm{Ca,T}} + I_{\mathrm{K,r}} + I_{\mathrm{K,s}} + I_{\mathrm{to}} + I_{\mathrm{sus}} + I_{\mathrm{f}} \\ &\quad + I_{\mathrm{b,Na}} + I_{\mathrm{b,Ca}} + I_{\mathrm{b,K}} + I_{\mathrm{NaCa}} + I_{\mathrm{p}} - I_{\mathrm{ext}}),\end{aligned} \tag{6.1}$$

where C [pF] and I_{ext} [pA] denote the membrane capacitance and the external current, respectively. I_{total} [pA] is the total membrane current, which contains eleven ion channel currents: I_{Na}, $I_{\mathrm{Ca,L}}$, $I_{\mathrm{Ca,T}}$, $I_{\mathrm{K,r}}$, $I_{\mathrm{K,s}}$, I_{to}, I_{sus}, I_{f}, $I_{\mathrm{b,Na}}$, $I_{\mathrm{b,Ca}}$, and $I_{\mathrm{b,K}}$, one ion exchanger current I_{NaCa}, and one ion pump current I_{p}. The thirteen membrane currents are described as follows:

- Sodium current

$$I_{\mathrm{Na}} = c_{\mathrm{Na}}\bar{g}_{\mathrm{Na}} m^3 h [\mathrm{Na}^+]_{\mathrm{o}} \frac{\mathrm{F}^2}{\mathrm{RT}} \frac{\exp\left[\left(\left(V - E_{\mathrm{Na}}\right)\mathrm{F}\right)/\mathrm{RT}\right]}{\exp\left(V\mathrm{F}/\mathrm{RT}\right)} V; \tag{6.2}$$

- L-type calcium current

$$I_{\mathrm{Ca,L}} = c_{\mathrm{Ca,L}}\bar{g}_{\mathrm{Ca,L}} \left[d_{\mathrm{L}} f_{\mathrm{L}} + \frac{0.006}{\exp\left[-\left(V + 14.1\right)/6\right]} \right] \left(V - E_{\mathrm{Ca,L}}\right); \tag{6.3}$$

- T-type calcium current

$$I_{\mathrm{Ca,T}} = c_{\mathrm{Ca,T}}\bar{g}_{\mathrm{Ca,T}} d_{\mathrm{T}} f_{\mathrm{T}} \left(V - E_{\mathrm{Ca,T}}\right); \tag{6.4}$$

- Rapid delayed rectifier potassium current

$$I_{\mathrm{K,r}} = c_{\mathrm{K,r}} \bar{g}_{\mathrm{K,r}} p_a p_{\mathrm{i}} \left(V - E_{\mathrm{K}}\right); \tag{6.5}$$

- Slow delayed rectifier potassium current

$$I_{\mathrm{K,s}} = c_{\mathrm{K,s}} \bar{g}_{\mathrm{K,s}} x_s^2 \left(V - E_{\mathrm{K,s}}\right); \tag{6.6}$$

- Transient 4-aminopyridine-sensitive current

$$I_{\mathrm{to}} = c_{\mathrm{to}} \bar{g}_{\mathrm{to}} q r \left(V - E_{\mathrm{K}}\right); \tag{6.7}$$

- Sustained 4-aminopyridine-sensitive current

$$I_{\mathrm{sus}} = c_{\mathrm{sus}} \bar{g}_{\mathrm{sus}} r \left(V - E_{\mathrm{K}}\right); \tag{6.8}$$

- Hyperpolarization-activated current

$$I_{\mathrm{f}} = I_{\mathrm{f,Na}} + I_{\mathrm{f,K}} = c_{\mathrm{f}} \bar{g}_{\mathrm{f}} y \left[\left(V - E_{\mathrm{Na}}\right) + \left(V - E_{\mathrm{K}}\right)\right]; \tag{6.9}$$

- Background sodium current

$$I_{\mathrm{b,Na}} = c_{\mathrm{b,Na}} \bar{g}_{\mathrm{b,Na}} \left(V - E_{\mathrm{Na}}\right); \tag{6.10}$$

- Background calcium current

$$I_{\mathrm{b,Ca}} = c_{\mathrm{b,Ca}} \bar{g}_{\mathrm{b,Ca}} \left(V - E_{\mathrm{Ca}}\right); \tag{6.11}$$

- Background potassium current

$$I_{\mathrm{b,K}} = c_{\mathrm{b,K}} \bar{g}_{\mathrm{b,K}} \left(V - E_{\mathrm{K}}\right); \tag{6.12}$$

- Sodium-potassium pump current

$$I_{\mathrm{p}} = \bar{I}_{\mathrm{p}} \left(\frac{[\mathrm{Na}^+]_{\mathrm{i}}}{K_{\mathrm{m,Na}} + [\mathrm{Na}^+]_{\mathrm{i}}}\right)^3 \left(\frac{[\mathrm{K}^+]_{\mathrm{o}}}{K_{\mathrm{m,K}} + [\mathrm{K}^+]_{\mathrm{o}}}\right)^2 \frac{1.6}{1.5 + \exp\left[-(V+60)/40\right]}; \tag{6.13}$$

- Sodium-calcium exchanger current

$$I_{\mathrm{NaCa}} = k_{\mathrm{NaCa}} \left[\frac{[\mathrm{Na}^+]_{\mathrm{i}}^3 [\mathrm{Ca}^{2+}]_{\mathrm{o}} \exp\left(0.0374 V \gamma_{\mathrm{NaCa}}\right)}{1 + d_{\mathrm{NaCa}} \left([\mathrm{Ca}^{2+}]_{\mathrm{i}} [\mathrm{Na}^+]_{\mathrm{o}}^3 + [\mathrm{Ca}^{2+}]_{\mathrm{o}} [\mathrm{Na}^+]_{\mathrm{i}}^3\right)}\right.$$
$$\left. - \frac{[\mathrm{Na}^+]_{\mathrm{o}}^3 [\mathrm{Ca}^{2+}]_{\mathrm{i}} \exp\left[0.0374 V \left(\gamma_{\mathrm{NaCa}} - 1\right)\right]}{1 + d_{\mathrm{NaCa}} \left([\mathrm{Ca}^{2+}]_{\mathrm{i}} [\mathrm{Na}^+]_{\mathrm{o}}^3 + [\mathrm{Ca}^{2+}]_{\mathrm{o}} [\mathrm{Na}^+]_{\mathrm{i}}^3\right)}\right]; \tag{6.14}$$

$$
\begin{aligned}
&[\mathrm{Na}^+]_\mathrm{o} = 140,\ [\mathrm{Na}^+]_\mathrm{i} = 8\,\mathrm{mM},\ E_\mathrm{Na} = \frac{\mathrm{RT}}{\mathrm{F}} \ln \frac{[\mathrm{Na}^+]_\mathrm{o}}{[\mathrm{Na}^+]_\mathrm{i}};\\
&[\mathrm{Ca}^{2+}]_\mathrm{o} = 2,\ [\mathrm{Ca}^{2+}]_\mathrm{o} = 0.0001\,\mathrm{mM},\ E_\mathrm{Ca} = \frac{\mathrm{RT}}{2\mathrm{F}} \ln \frac{[\mathrm{Ca}^{2+}]_\mathrm{o}}{[\mathrm{Ca}^{2+}]_\mathrm{i}};\\
&[\mathrm{K}^+]_\mathrm{o} = 5.4,\ [\mathrm{K}^+]_\mathrm{o} = 140\,\mathrm{mM},\ E_\mathrm{K} = \frac{\mathrm{RT}}{\mathrm{F}} \ln \frac{[\mathrm{K}^+]_\mathrm{o}}{[\mathrm{K}^+]_\mathrm{i}},\\
&E_\mathrm{K,s} = \frac{\mathrm{RT}}{\mathrm{F}} \ln \left(\frac{[\mathrm{K}^+]_\mathrm{o} + 0.03[\mathrm{Na}^+]_\mathrm{o}}{[\mathrm{K}^+]_\mathrm{i} + 0.03[\mathrm{Na}^+]_\mathrm{i}} \right);\\
&d_\mathrm{NaCa} = 0.0001, \quad \gamma_\mathrm{NaCa} = 0.5;\\
&K_\mathrm{m,Na} = 5.64, \quad K_\mathrm{m,K} = 0.621;
\end{aligned}
$$

where $\bar{g}_\mathrm{ion}$ (ion = Na, Ca,L, Ca,T, K,r, K,s, to, sus, f, b,Na, b,Ca, and b,K) [mS] are the maximum conductances of ion channels. The parameters c_ion are newly introduced dimensionless coefficients for denoting conductance changes of ion channels, and their standard values are 1.0. The gating variables m, h_1, h_2, d_L, f_L, d_T, f_T, $p_\mathrm{a,f}$, $p_\mathrm{a,s}$, p_i, x_s, q, r, and y (dimensionless, ranging between 0 and 1) denote the states of ion channels' gates.

Temporal variations of these gating variables are described by

$$
\begin{aligned}
&\frac{dx}{dt} = \frac{x^\infty(V) - x}{\tau_x(V)},\\
&(x = m,\ h_1,\ h_2,\ d_\mathrm{L},\ f_\mathrm{L},\ d_\mathrm{T},\ f_\mathrm{T},\ p_\mathrm{a,f},\ p_\mathrm{a,s},\ p_\mathrm{i},\ x_\mathrm{s},\ q,\ r,\ y),
\end{aligned}
\tag{6.15}
$$

where $x^\infty(V)$ and $\tau_x(V)$ [msec] are the steady-state values and time constants of gating variables. The details are as follows:

$$
\begin{aligned}
\tau_m(V) &= \frac{0.6247 \times 10^{-3}}{0.832 \exp\left[-0.335\,(V + 56.7)\right] + 0.627 \exp\left[0.082\,(V + 65.01)\right]} + 4 \times 10^{-5},\\
m^\infty(V) &= \left[\frac{1}{1 + \exp\left[-\,(V + 30.32)\,/5.46\right]} \right]^{1/3};\\
h &= (1 - F_\mathrm{Na}(V))\,h_1 + F_\mathrm{Na}(V) h_2,\\
F_\mathrm{Na}(V) &= \frac{9.52 \times 10^{-2} \times \exp\left[-6.3 \times 10^{-2}\,(V + 34.4)\right]}{1 + 1.66 \exp\left[-0.225\,(V + 63.7)\right]} + 8.69 \times 10^{-2},\\
\tau_{h_1}(V) &= \frac{3.717 \times 10^{-6} \times \exp\left[-0.2815\,(V + 17.11)\right]}{1 + 3.732 \times 10^{-3} \exp\left[-0.3426\,(V + 37.36)\right]} + 5.977 \times 10^{-4},\\
\tau_{h_2}(V) &= \frac{3.186 \times 10^{-8} \times \exp\left[-0.6219\,(V + 18.8)\right]}{1 + 7.189 \times 10^{-5} \exp\left[-0.6683\,(V + 34.07)\right]} + 3.556 \times 10^{-3},\\
h_1^\infty(V) &= h_2^\infty(V) = \frac{1}{1 + \exp\left[(V + 66.1)\,/6.4\right]};
\end{aligned}
$$

$$\alpha_{d_{\mathrm{L}}}(V) = \frac{-14.19\,(V+35)}{\exp\left[-(V+35)/2.5\right]-1} + \frac{-42.45V}{\exp(-0.208V)-1},$$

$$\beta_{d_{\mathrm{L}}}(V) = \frac{5.71\,(V-5)}{\exp\left[0.4\,(V-5)\right]-1},$$

$$\tau_{d_{\mathrm{L}}}(V) = \frac{1}{\alpha_{d_{\mathrm{L}}}(V)+\beta_{d_{\mathrm{L}}}(V)}, \quad d_{\mathrm{L}}^{\infty}(V) = \frac{1}{1+\exp\left[-(V+23.1)/6\right]};$$

$$\alpha_{f_{\mathrm{L}}}(V) = \frac{3.75(V+28)}{\exp\left[(V+28)/4\right]-1}, \quad \beta_{f_{\mathrm{L}}}(V) = \frac{30}{1+\exp\left[-(V+28)/4\right]},$$

$$\tau_{f_{\mathrm{L}}}(V) = \frac{1.2-0.2F_{\mathrm{cell}}}{\alpha_{f_{\mathrm{L}}}(V)+\beta_{f_{\mathrm{L}}}(V)}, \quad f_{\mathrm{L}}^{\infty}(V) = \frac{1}{1+\exp\left[(V+45)/5\right]};$$

$$\alpha_{d_{\mathrm{T}}}(V) = 1,068\exp\left(\frac{V+26.3}{30}\right), \quad \beta_{d_{\mathrm{T}}}(V) = 1,068\exp\left(-\frac{V+26.3}{30}\right),$$

$$\tau_{d_{\mathrm{T}}}(V) = \frac{1}{\alpha_{d_{\mathrm{T}}}(V)+\beta_{d_{\mathrm{T}}}(V)}, \quad d_{\mathrm{T}}^{\infty}(V) = \frac{1}{1+\exp\left[-(V+37)/6.8\right]};$$

$$\alpha_{f_{\mathrm{T}}}(V) = 15.3\exp\left(-\frac{V+71.7}{83.3}\right), \quad \beta_{f_{\mathrm{T}}}(V) = 15.3\exp\left(\frac{V+71.7}{83.3}\right),$$

$$\tau_{f_{\mathrm{T}}}(V) = \frac{1}{\alpha_{f_{\mathrm{T}}}(V)+\beta_{f_{\mathrm{T}}}(V)}, \quad f_{\mathrm{T}}^{\infty}(V) = \frac{1}{1+\exp\left[(V+71)/9\right]};$$

$$p_a = 0.6p_{a,f} + 0.4p_{a,s},$$

$$\tau_{p_{a,f}}(V) = \frac{1}{37.2\exp\left[(V-9)/15.9\right]+0.96\exp\left[-(V-9)/22.5\right]},$$

$$\tau_{p_{a,s}}(V) = \frac{1}{4.2\exp\left[(V-9)/17\right]+0.15\exp\left[-(V-9)/21.6\right]},$$

$$p_{a,f}^{\infty}(V) = p_{a,s}^{\infty}(V) = \frac{1}{1+\exp\left[-(V+14.2)/10.6\right]};$$

$$\tau_{p_{\mathrm{i}}} = 0.002, \quad p_i^{\infty}(V) = \frac{1}{1+\exp\left[(V+18.6)/10.1\right]};$$

$$\alpha_{x_s}(V) = \frac{14}{1+\exp\left[-(V-40)/9\right]}, \quad \beta_{x_s}(V) = \exp\left(-\frac{V}{45}\right),$$

$$\tau_{x_s}(V) = \frac{1}{\alpha_{x_s}(V)+\beta_{x_s}(V)}, \quad x_s^{\infty}(V) = \frac{\alpha_{x_s}(V)}{\alpha_{x_s}(V)+\beta_{x_s}(V)};$$

$$\tau_{q1}(V) = 0.5686\exp\left[-0.08161\,(V+39+10F_{\mathrm{cell}})\right],$$

$$\tau_{q2}(V) = 0.7174\exp\left[(0.2719-0.1719F_{\mathrm{cell}})\,(V+40.93+10F_{\mathrm{cell}})\right],$$

$$\tau_q(V) = 10.103\times10^{-3} + \frac{65.17\times10^{-3}}{\tau_{q1}(V)+\tau_{q1}(V)}, \quad q^{\infty}(V) = \frac{1}{1+\exp\left[(V+59.37)/13.1\right]};$$

$$\tau_r(V) = 2.9775\times10^{-3} + \frac{19.595\times10^{-3}}{1.037\exp\left[0.09012\,(V+30.61)\right]+0.369\exp\left[-0.119\,(V+23.84)\right]},$$

$$r^{\infty}(V) = \frac{1}{1+\exp\left[-(V-10.93)/19.7\right]};$$

$$\alpha_y(V) = \exp\left(-\frac{V+78.91}{26.63}\right), \quad \beta_y(V) = \exp\left(\frac{V+75.13}{21.25}\right),$$

$$\tau_y(V) = \frac{1}{\alpha_y(V)+\beta_y(V)}, \quad y^{\infty}(V) = \frac{\alpha_y(V)}{\alpha_y(V)+\beta_y(V)};$$

$$F_{\text{cell}} = \frac{1.07(3d_{\text{cell}} - 0.1)}{3\left[1 + 0.7745\exp\left[-\left(3d_{\text{cell}} - 2.05\right)/0.295\right]\right]},$$
$$d_{\text{cell}} = 1 \text{ (periphery cell)}, \quad 0 \text{ (center cell)}.$$

The Zhang model considers the regional difference of sinoatrial node, and the parameter values vary between periphery and center cells. Table 6.1 compares these parameter values of the two types of cells.

Table 6.1: Comparison of the parameter values between periphery and center cells of sinoatrial node.

Parameter	Periphery cell	Center cell
C	65 pF	20 pF
$\bar{g}_{\text{Na}}$	1.20×10^{-6} μS	0 μS
$\bar{g}_{\text{Ca,L}}$	6.59×10^{-2} μS	5.79×10^{-3} μS
$\bar{g}_{\text{Ca,T}}$	1.39×10^{-2} μS	4.28×10^{-3} μS
$\bar{g}_{\text{K,r}}$	1.60×10^{-2} μS	7.97×10^{-4} μS
$\bar{g}_{\text{K,s}}$	1.04×10^{-2} μS	3.45×10^{-4} μS
$\bar{g}_{\text{to}}$	3.65×10^{-2} μS	4.91×10^{-3} μS
$\bar{g}_{\text{sus}}$	1.14×10^{-2} μS	6.65×10^{-5} μS
$\bar{g}_{\text{f}}$	6.88×10^{-3} μS	5.47×10^{-4} μS
$\bar{g}_{\text{b,Na}}$	1.89×10^{-4} μS	5.82×10^{-5} μS
$\bar{g}_{\text{b,Ca}}$	4.30×10^{-5} μS	1.32×10^{-5} μS
$\bar{g}_{\text{b,K}}$	8.19×10^{-5} μS	2.52×10^{-5} μS
$\bar{I}_{\text{p}}$	155 pA	47.8 pA
k_{NaCa}	8.84×10^{-3} pA	2.72×10^{-3} pA

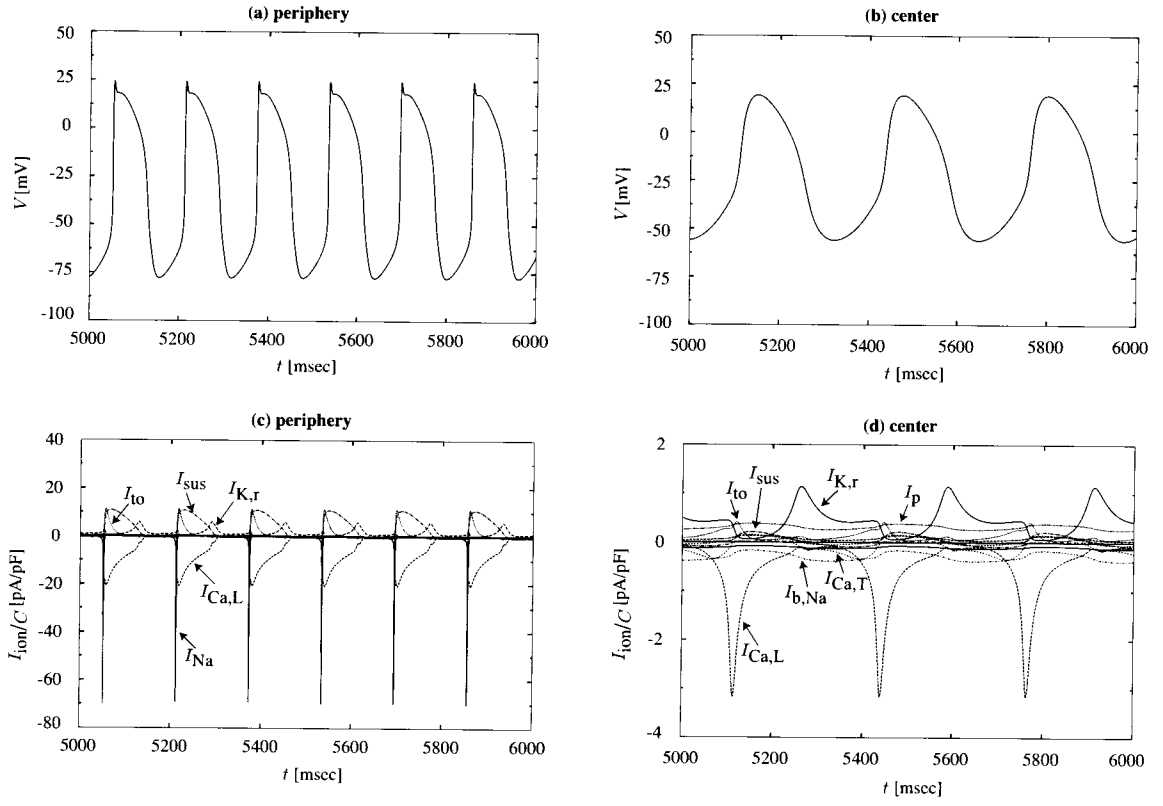

Figure 6.1: Temporal variations of (a) (b) membrane potential and (c) (d) membrane currents in normal condition ($I_{\text{ext}} = 0.0$ pA, $c_{\text{ion}} = 1.0$). In the panel (c) and (d), the inward currents and outward currents are denoted by negative and positive values, respectively.

Figure 6.1(a) and (b) shows temporal variations of membrane potential V in the normal condition ($I_{\text{ext}} = 0.0$ pA, $c_{\text{ion}} = 1.0$) of periphery and center cells, respectively. As a cardiac pacemaker, the sinoatrial node generates rhythmic action potentials spontaneously in both periphery and center cells without electrical stimuli ($I_{\text{ext}} = 0.0$ pA). However, the frequency and intensity of action potential generation vary with the region of sinoatrial node. The normal periods of periphery and center cells are about 161 msec and 325 msec, respectively, and the amplitude of the periphery cell is larger than that of the center cell. Figure 6.1(c) and (d) shows temporal variations of membrane currents which correspond to (a) and (b), respectively (only large membrane currents are labeled). The inward currents (flowing from the outside into the inside of cell membrane) and outward currents are denoted by negative and positive values, respectively. The inward currents cause membrane potential to

increase (depolarization), whereas the outward currents cause membrane potential to decrease (repolarization). It shows that, the very large sodium current I_{Na} is only present in the periphery cell, and the other currents in the periphery cell are quite larger than those in the center cell. Since I_{Na} is a fast inward current, the membrane potential depolarizes quickly in the periphery cell, whereas it depolarizes slowly in the center cell.

6.1 Effects of Changing Ion Channel Conductances on Pacemaker Rhythm

In this section, we analyze the Zhang model without the external current ($I_{\mathrm{ext}} = 0.0$ pA), which corresponds to the case of a single periphery/center cell. The global structure of the Zhang model is analyzed by using the bifurcation analysis software AUTO, where the conductance coefficients c_{ion} are varied as bifurcation parameters[1]. Based on the analysis results, the effects of changing ion channel conductances on pacemaker rhythm in the two types of cells are investigated.

6.1.1 One-parameter Bifurcation Analysis

Sodium Current I_{Na}

In the Zhang model, the major difference between the periphery and center cells is the presence or absence of the (very large) sodium current I_{Na} (which is only present in the periphery cell). At first, the one-parameter bifurcation diagram of the periphery cell model as for the sodium current I_{Na} is shown in Fig. 6.2(a), where c_{Na} is varied as bifurcation parameter. The solid and broken curves show the values of V of stable and unstable equilibrium points, respectively. The • and ○ circles show the maximum values of V of stable and unstable periodic orbits, respectively. The bifurcation points of Hopf, double-cycle bifurcations are denoted by HB, DC (with a number), respectively. Periods of several periodic orbits are also shown in the one-parameter diagram. Figure 6.2(b) shows the period of periodic orbits appeared in (a).

[1]Under physiological conditions, the conductance of each ion channel would not be negative or too large. However, in order to show the global bifurcation structure of the model, we compute for negative or very large conductance coefficients if necessary.

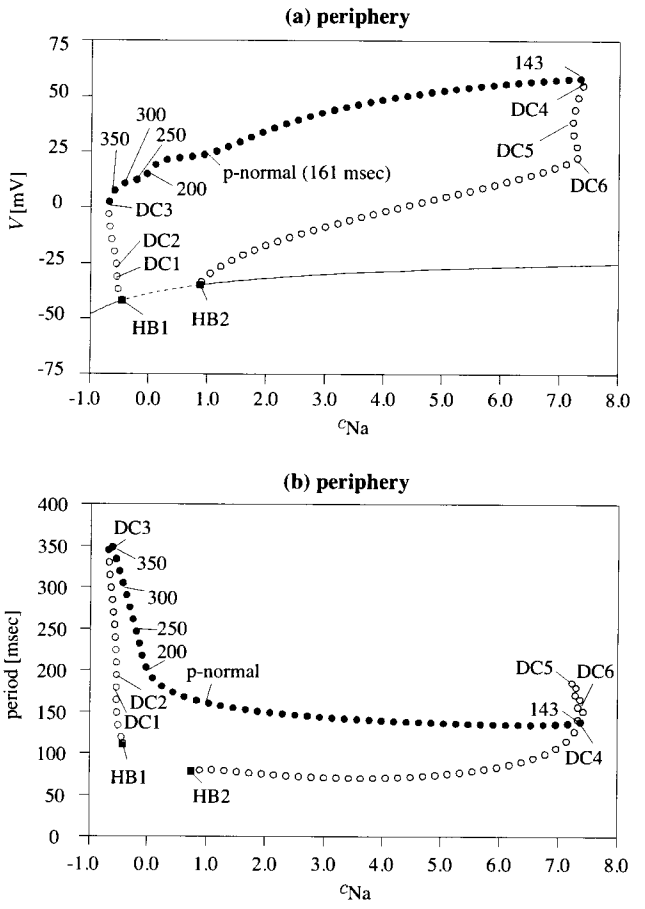

Figure 6.2: (a) One-parameter bifurcation diagram of the Zhang model as for the sodium current I_{Na} in the periphery cell, (b) periods of periodic orbits appeared in (a). The bifurcation points of Hopf and double-cycle bifurcations are denoted by HB and DC (with a number), respectively.

In the normal condition ($c_{\mathrm{Na}} = 1.0$), a stable periodic orbit whose period is about 161 msec (labeled with "p-normal"), coexists with a stable equilibrium point. Since the membrane potential V may converge to the stable equilibrium point for specific initial conditions, such a result is improper for a cardiac pacemaker cell model, and it is considered to be one limitation of the Zhang model [30].

For each value of c_{Na} between the double-cycle bifurcation points DC3 and DC4, a stable periodic orbit exists and rhythmic action potentials can be generated. When c_{Na} is increased, the periods decreases and the amplitude increases, which means that the action potential generation become more frequent and intensive. The variation

of period is large when c_{Na} is decreased from 1.0 (normal value), whereas that is small when c_{Na} is increased from 1.0. Thus, the parameter sensitivity of pacemaker rhythm of long period is higher than that of short period. In the left side of DC3 and in the right side of DC4, since only stable equilibrium points exist, the sinoatrial node (periphery) cell cannot generate rhythmic action potentials continuously and cannot fulfill the role of cardiac pacemaker.

The similar parameter sensitivity has also been found in the YNI model. That is, the pacemaker rhythm varies sensitively to the conductance change of I_{Na}, and the sodium channel plays an important role in the action potential generation. However, the variation range of period in the YNI model is larger than that in the Zhang model.

Next, Let's see the effect of the absence of I_{Na} on action potential generation in the periphery cell. Compared to the normal condition ($c_{\mathrm{Na}} = 1.0$), the case of the absence of I_{Na} ($c_{\mathrm{Na}} = 0.0$) generates rhythmic action potentials with a longer period and a smaller amplitude. Such a difference is also shown between the center and periphery cells (Fig. 6.1). However, the center cell (without I_{Na}) has a longer period than the case of $I_{\mathrm{Na}} = 0.0$ in the periphery cell (325 msec vs. 198 msec). Thus, not only the (presence or absence of) I_{Na}, but also the other currents are important in causing the regional difference.

L-type Calcium Current $I_{\mathrm{Ca,L}}$

Next, we vary the conductance coefficient of the L-type calcium current $I_{\mathrm{Ca,L}}$ (a large current in both periphery and center cells) as the bifurcation parameter. The one-parameter bifurcation diagrams are shown in Fig. 6.3 (a) (periphery cell) and (b) (center cell), and the period of periodic orbits are shown in (c) (periphery cell) and (d) (center cell).

Similar as the periphery cell, the center cell also has a stable periodic orbit whose period is about 325 msec (labeled with "c-normal"), and a coexisting stable equilibrium point in the normal condition ($c_{\mathrm{Ca,L}} = 1.0$).

The periphery cell generates rhythmic action potentials (which correspond to stable periodic orbits) for the values of $c_{\mathrm{Ca,L}}$ between double-cycle bifurcation points DC1 and DC2, DC3 and DC4. And the center cell generates rhythmic action potentials for the values of $c_{\mathrm{Ca,L}}$ between DC1 and DC2. The range of the value of $c_{\mathrm{Ca,L}}$ in which periodic action potentials can be generated is very different between the two cells (please note the different scale of abscissas between (a) (c) and (b) (d)). For

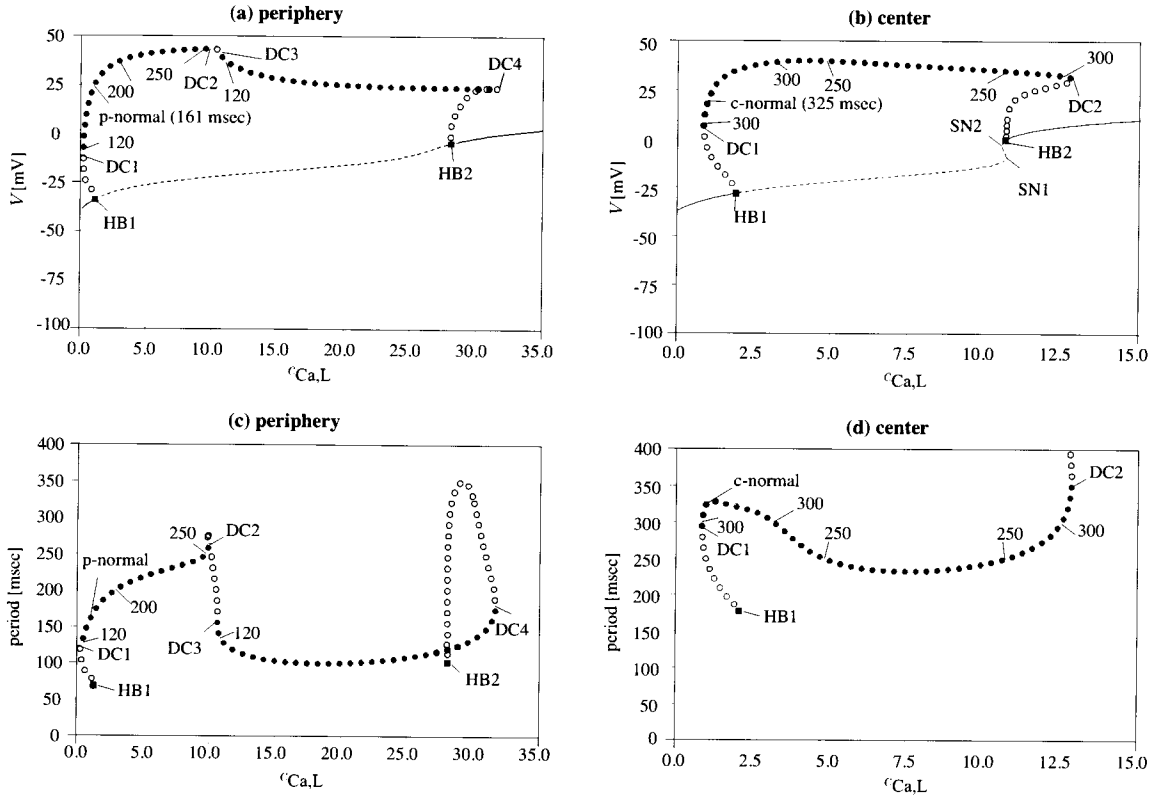

Figure 6.3: (a) (b) One-parameter bifurcation diagram of the Zhang model as for the L-type calcium current $I_{Ca,L}$, (c) (d) periods of periodic orbits appeared in (a) and (b).

both the periphery and center cells, the period decreases when $c_{Ca,L}$ is decreased from 1.0, whereas the period increases and decreases alternately when $c_{Ca,L}$ is increased from 1.0. It shows that the pacemaker rhythm is sensitive to the conductance change of $I_{Ca,L}$ in both periphery and center cells.

Between the double-cycle bifurcation points DC2 and DC3 in Fig. 6.3(a) and (c), since no stable equilibrium points and no stable periodic orbits were detected by AUTO, we also computed the one-parameter bifurcation diagram by numerical simulations for $9.7 \leq c_{Ca,L} \leq 10.7$ (Fig. 6.4). In this diagram, both the local maximum and minimum values of V for each value of $c_{Ca,L}$ were plotted. Many complicated variations of membrane potentials are generated between DC2 and DC3. The waveforms of membrane potential when $c_{Ca,L} = 10.0$ and 10.3 show abnormalities in action potential generation.

The L-type calcium current $I_{Ca,L}$ is one component of the slow inward current I_s of

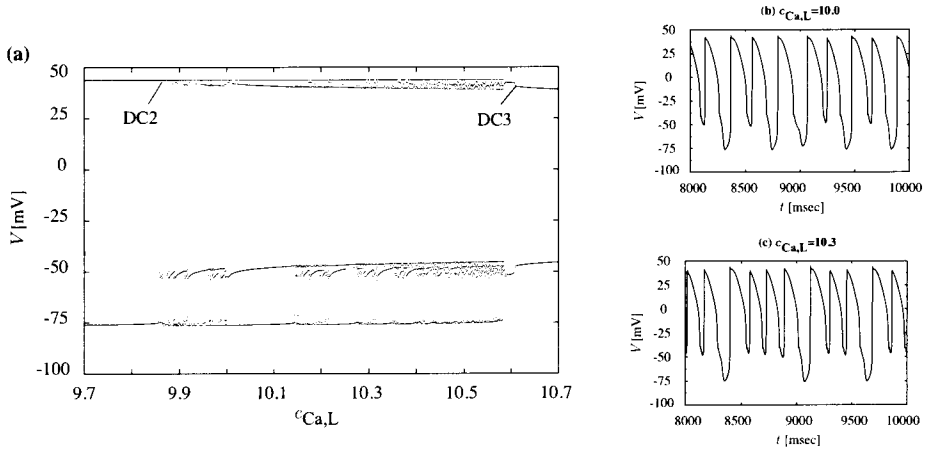

Figure 6.4: One-parameter bifurcation diagram of the Zhang model as for the L-type calcium current $I_{\mathrm{Ca,L}}$ by numerical simulations. (b) and (c) Abnormal waveforms of action potentials for two values of $c_{\mathrm{Ca,L}}$.

the YNI model (Eq. (3.3)). In the YNI model, the pacemaker rhythm also is sensitive to the conductance change of I_{s}. However, the period decreases monotonically with the increase of c_{s}. The abnormal action potentials have also been found in the YNI model.

6.1.2 Two-parameter Bifurcation Analysis

In the above subsection, we have analyzed the parameter sensitivity of pacemaker rhythm for each ion channel current solely. In this subsection, we analyze the parameter sensitivity on two ion channel currents simultaneously. The bifurcation curves and contour lines of various periods when two conductance coefficients are varied are plotted in the diagram to examine the pacemaker rhythm.

L-type Calcium Current $I_{\mathrm{Ca,L}}$ and Rapid Delayed Rectifying Potassium Current $I_{\mathrm{K,r}}$

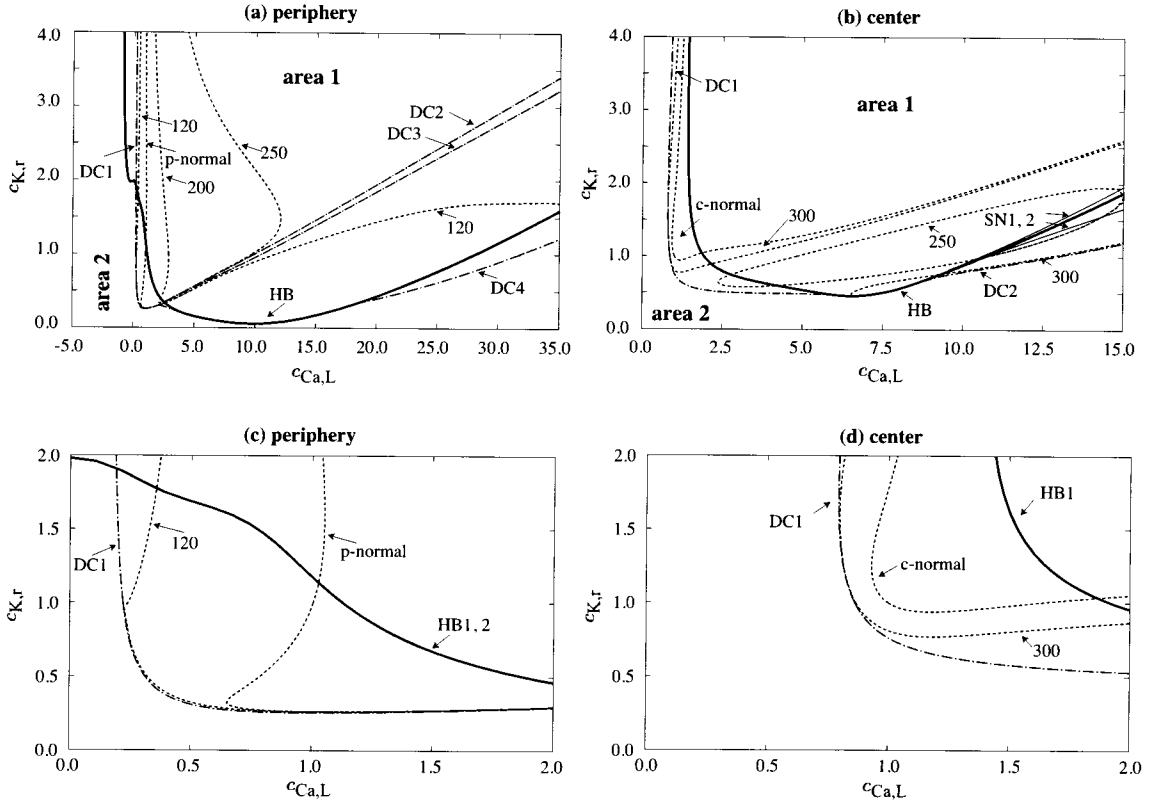

Figure 6.5: (a) (b) Two-parameter bifurcation diagram of the Zhang model as for the L-type calcium current $I_{\mathrm{Ca,L}}$ and the rapid delayed rectifying potassium current $I_{\mathrm{K,r}}$, (c) (d) magnifications of (a) and (b) near the normal value $c_{\mathrm{ion}} = 1.0$, respectively.

At first, the conductance coefficients of the L-type calcium current $I_{\mathrm{Ca,L}}$ and the rapid delayed rectifying potassium current $I_{\mathrm{K,r}}$ are varied simultaneously. Figure 6.5(a) and (b) shows the two-parameter bifurcation diagrams of periphery and

center cell models, respectively. When $c_{\mathrm{K,r}}$ is fixed to 1.0 and $c_{\mathrm{Ca,L}}$ is varied, the results correspond to the "one-parameter" bifurcation diagrams of Fig. 6.3(a) and (b), respectively. In each two-parameter bifurcation diagram, various periodic orbits exist in area 1 (surrounded by the Hopf bifurcation curve HB1, 2), which shows rhythmic action potentials can be generated in the area. However, the rhythmic action potentials cannot be generated in area 2, where no stable periodic orbit exists. In the case of small $c_{\mathrm{Ca,L}}$, the change of $c_{\mathrm{K,r}}$ affects the contour lines of periods little, which corresponds to a weak effect of changing $c_{\mathrm{K,r}}$ on pacemaker rhythm, whereas the effect is strong in the case of big $c_{\mathrm{Ca,L}}$. It shows that, there exists a strong interrelation between $I_{\mathrm{Ca,L}}$ and $I_{\mathrm{K,r}}$ in the case of big values of $c_{\mathrm{Ca,L}}$. In the case of strong interrelation, we can adjust one ion channel (by referring to the "normal" contour line) to correct the abnormal pacemaker rhythm caused by another ion channel.

L-type Calcium Current $I_{\mathrm{Ca,L}}$ and T-type Calcium Current $I_{\mathrm{Ca,T}}$

Next, the two-parameter bifurcation diagrams as for the L- and T-type calcium currents $I_{\mathrm{Ca,L}}$ and $I_{\mathrm{Ca,T}}$ are shown in Fig. 6.6. In the periphery cell, the bifurcation curves and contour lines of periods are almost vertical, which mean the conductance change of $I_{\mathrm{Ca,T}}$ affects the pacemaker rhythm little, and the parameter sensitivity is low. In the center cell, the conductance change of $I_{\mathrm{Ca,T}}$ affects the pacemaker rhythm much, and the parameter sensitivity is high. For another calcium current $I_{\mathrm{Ca,L}}$, its conductance change has a strong effect on pacemaker rhythm in both periphery and center cells. It shows that, the interrelation between $I_{\mathrm{Ca,L}}$ and $I_{\mathrm{Ca,T}}$ is weak in the periphery cell (because of the weak effect of $I_{\mathrm{Ca,T}}$ on pacemaker rhythm), whereas it is strong in the center cell.

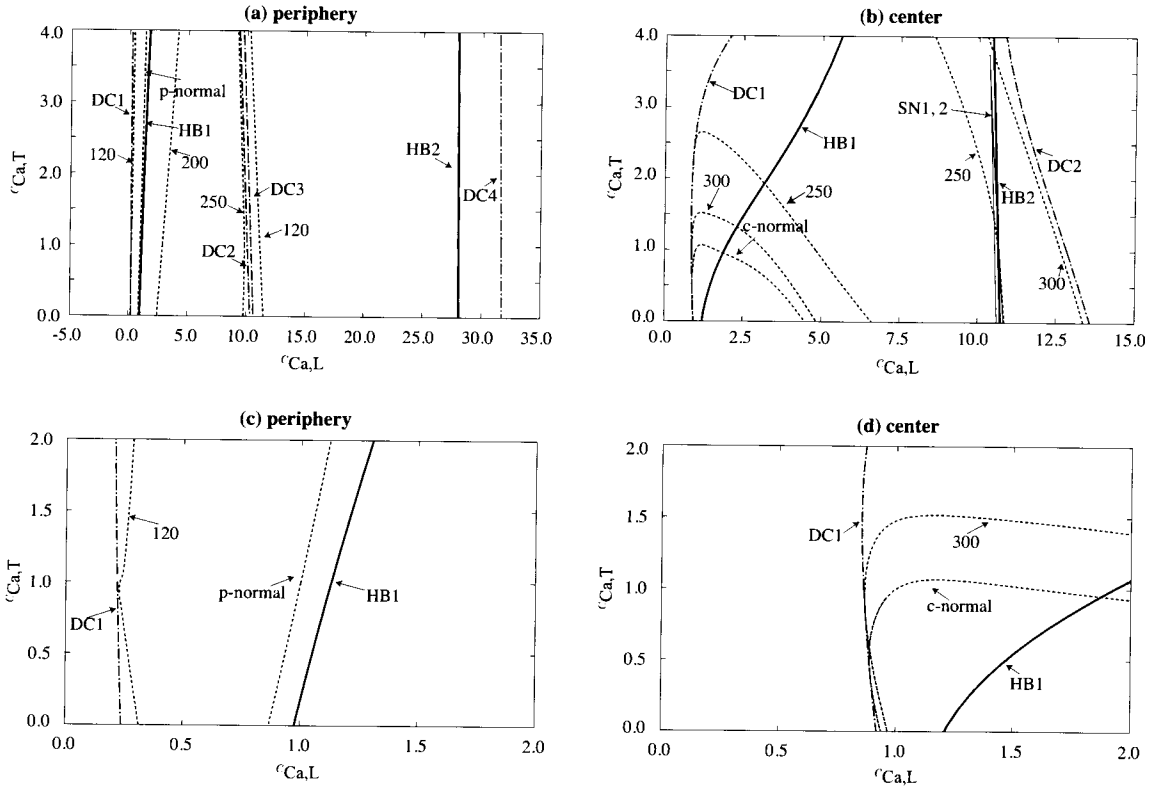

Figure 6.6: (a) (b) Two-parameter bifurcation diagram of the Zhang model as for the L-type calcium current $I_{Ca,L}$ and the T-type calcium current $I_{Ca,T}$, (c) (d) magnifications of (a) and (b) near the normal value $c_{ion} = 1.0$, respectively.

L-type Calcium Current $I_{\mathrm{Ca,L}}$ and Slow Delayed Rectifying Potassium Current $I_{\mathrm{K,s}}$

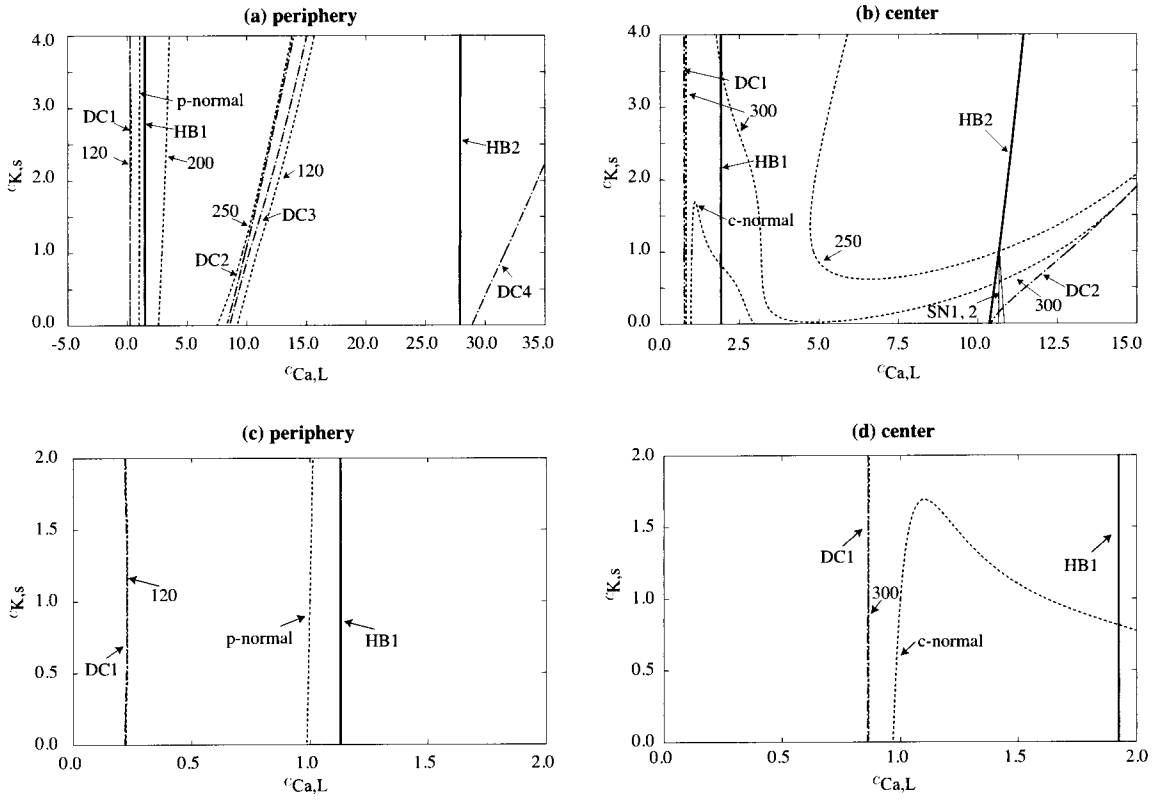

Figure 6.7: (a) (b) Two-parameter bifurcation diagram of the Zhang model as for the L-type calcium current $I_{\mathrm{Ca,L}}$ and the slow delayed rectifying potassium current $I_{\mathrm{K,s}}$, (c) (d) magnifications of (a) and (b) near the normal value $c_{\mathrm{ion}} = 1.0$, respectively.

Figure 6.7 shows the two-parameter bifurcation diagrams as for the L-type calcium currents $I_{\mathrm{Ca,L}}$ and the slow delayed rectifying potassium current $I_{\mathrm{K,s}}$. With respect to the conductance change of $I_{\mathrm{K,s}}$, the variation of pacemaker rhythm is little in the periphery cell, whereas that is large in the center cell. The sensitivities of the pacemaker rhythm to conductance change are quite different in the two types of cells.

Moreover, the two-parameter bifurcation diagrams as for $I_{\mathrm{Ca,L}}$ and I_{NaCa} (which are not shown in this thesis) show that the effect of I_{NaCa} on pacemaker rhythm is very weak in both periphery and center cells.

The above results show that the sensitivities of pacemaker rhythm on conductance

changes of $I_{Ca,L}$ and $I_{K,r}$ are high, whereas those of $I_{Ca,T}$, $I_{K,s}$, and I_{NaCa} are low. The above five currents are the components of I_s or I_K of the YNI model (Eqs. (3.3), (3.4)). The analysis of the YNI model has shown that I_s and I_K have strong effects on pacemaker rhythm. Moreover, the analysis of the Zhang model shows detailed information: the $I_{Ca,L}$ and $I_{K,r}$ play major roles in I_s and I_K, respectively.

L-type Calcium Current $I_{Ca,L}$ and Hyperpolarization-activated Current I_f (I_h)

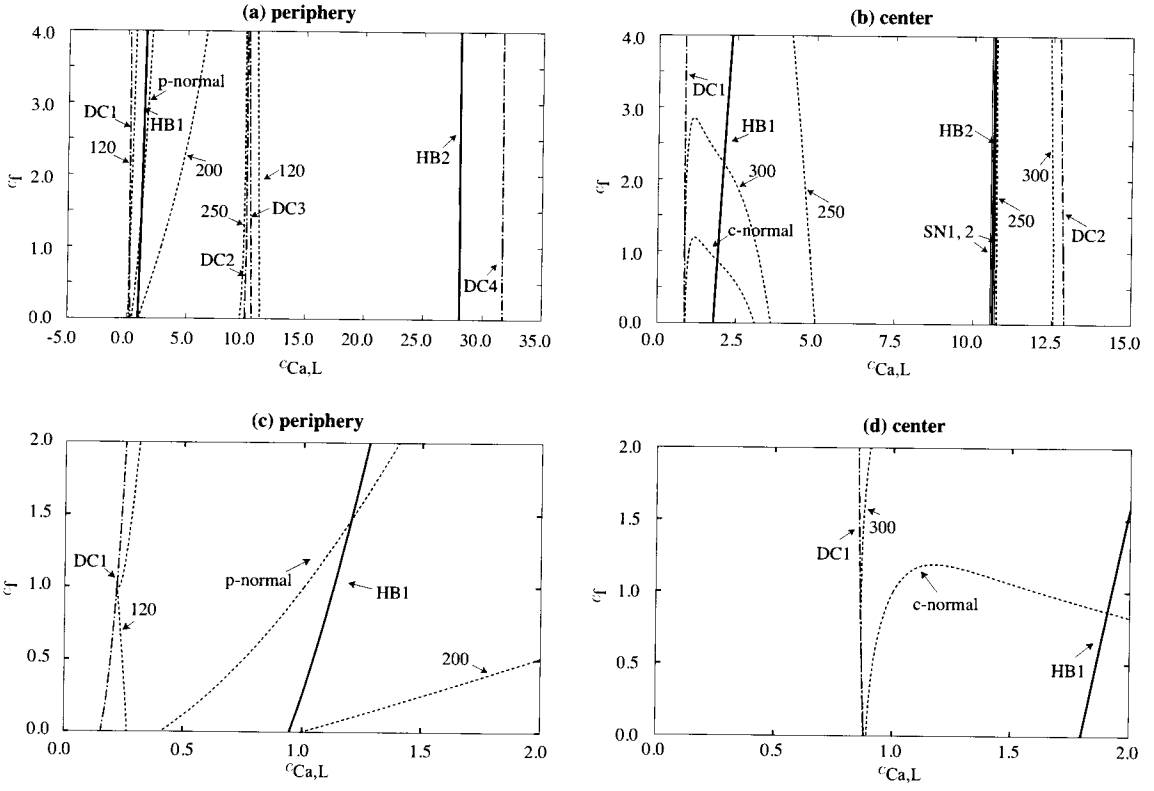

Figure 6.8: (a) (b)Two-parameter bifurcation diagram of the Zhang model as for the L-type calcium current $I_{Ca,L}$ and the hyperpolarization-activated current I_f, (c) (d) magnifications of (a) and (b) near the normal value $c_{ion} = 1.0$, respectively.

The two-parameter bifurcation diagrams (Fig. 6.8) as for the L-type calcium current $I_{Ca,L}$ and the hyperpolarization-activated current I_f show that, the bifurcation curves and contour lines of periods are almost vertical in both periphery and center cells. It means that the conductance change of I_f has a very weak effect on pacemaker rhythm. The similar results have also been found in the YNI model.

L-type Calcium Current $I_{Ca,L}$ and Background Currents

The two-parameter bifurcation diagrams as for the L-type calcium current $I_{Ca,L}$ and each background current are analyzed. Figures 6.9, 6.10, and 6.11 show the two-parameter bifurcation diagrams as for $I_{Ca,L}$ and $I_{b,Na}$, $I_{Ca,L}$ and $I_{b,Ca}$, $I_{Ca,L}$ and $I_{b,K}$, respectively. Based on these two-parameter bifurcation diagrams, we can see that the conductance changes of the three background currents have different effects between the periphery and center cells: there exist strong effects in the periphery cell, whereas there exist weak ones in the center cell. Especially for $I_{b,Na}$, the effects in center cell is very strong, it is due to that the $I_{b,Na}$ is very related to the depolarization in action potential generation [54].

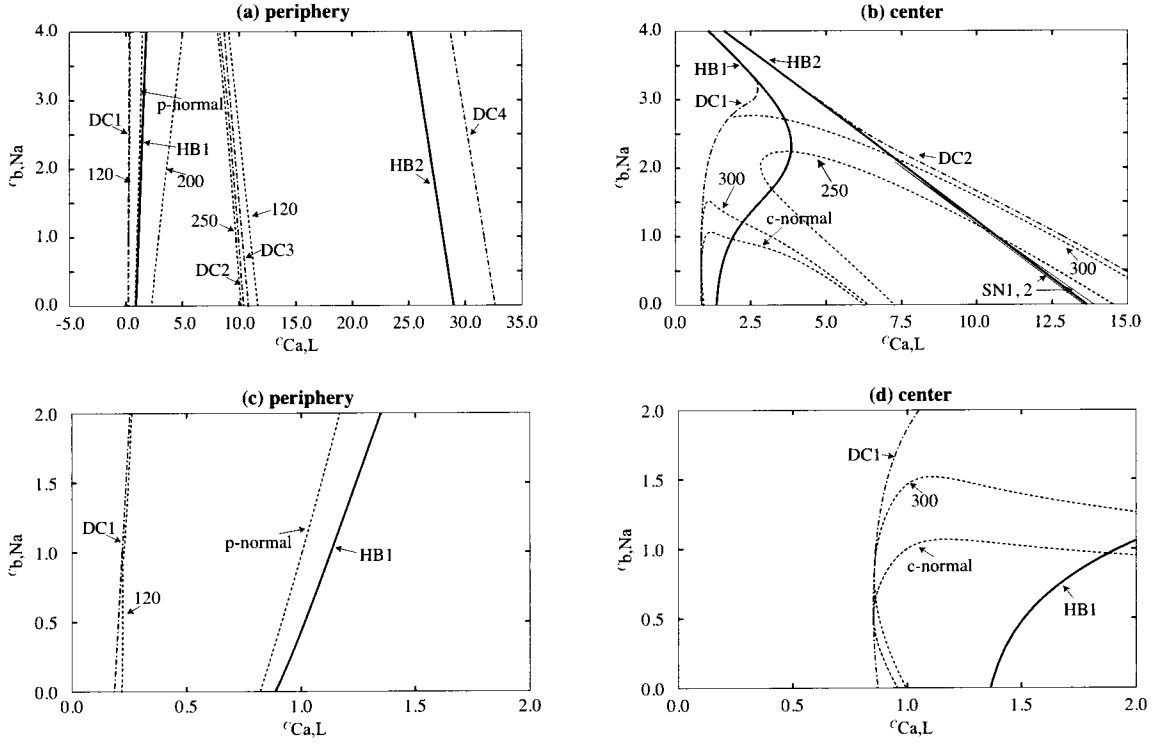

Figure 6.9: (a) (b)Two-parameter bifurcation diagram of the Zhang model as for the L-type calcium current $I_{Ca,L}$ and the background sodium current $I_{b,Na}$, (c) (d) magnifications of (a) and (b) near the normal value $c_{ion} = 1.0$, respectively.

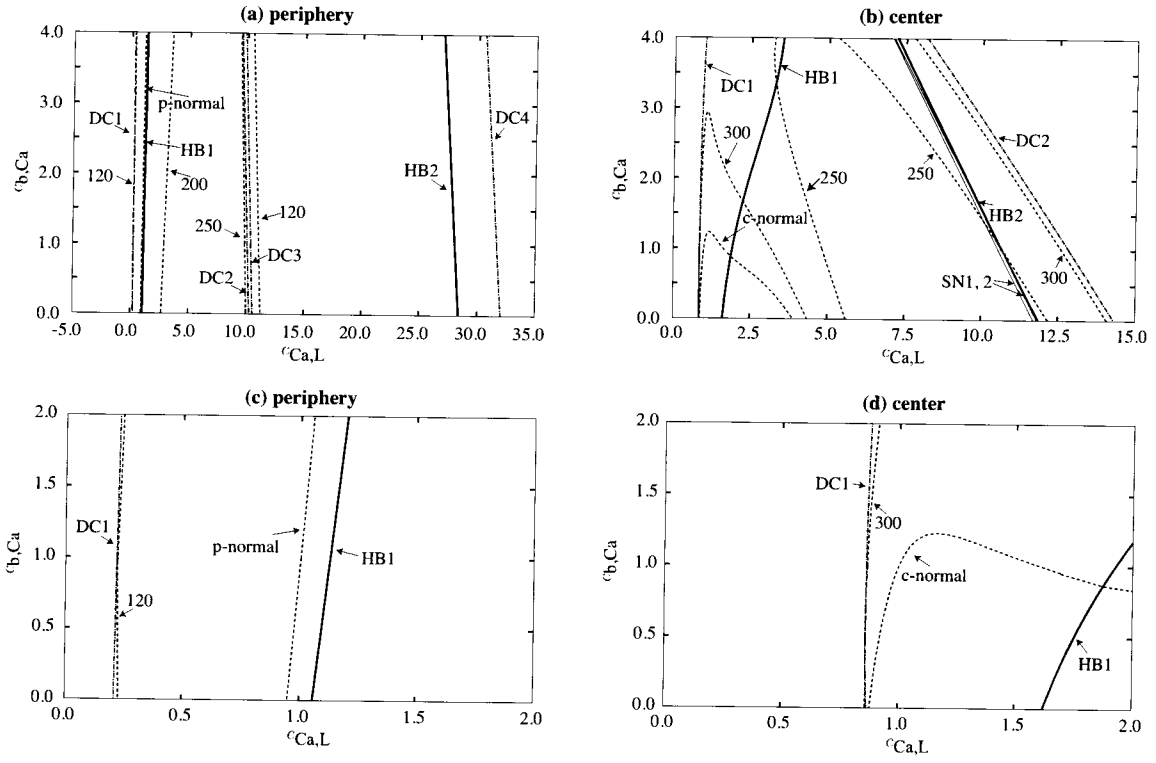

Figure 6.10: (a) (b) Two-parameter bifurcation diagram of the Zhang model as for the L-type calcium current $I_{\mathrm{Ca,L}}$ and the background calcium current $I_{\mathrm{b,Ca}}$, (c) (d) magnifications of (a) and (b) near the normal value $c_{\mathrm{ion}} = 1.0$, respectively.

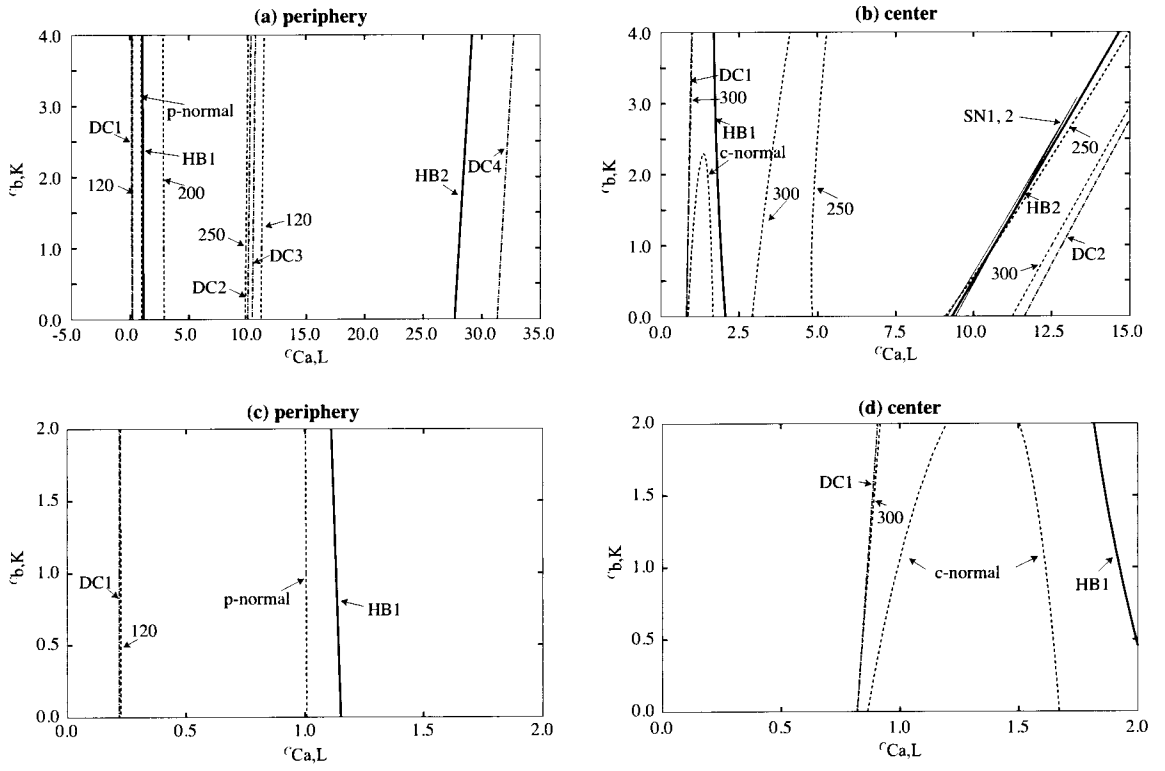

Figure 6.11: (a) (b)Two-parameter bifurcation diagram of the Zhang model as for the L-type calcium current $I_{\mathrm{Ca,L}}$ and the background potassium current $I_{\mathrm{b,K}}$, (c) (d) magnifications of (a) and (b) near the normal value $c_{\mathrm{ion}} = 1.0$, respectively.

6.2 Effect of Changing External Current on Pacemaker Rhythm

In above section, we have only examined the pacemaker rhythm of a single periphery/center cell. Here we consider the case of coupled cells, that is, the external current I_{ext} is varied to investigate the coupling effect on pacemaker rhythm approximately.

At first, we analyze the relations between the sodium current I_{Na} and the external current I_{ext} in periphery cell. The two-parameter bifurcation diagram is shown in Fig. 6.12. The bifurcation curves and contour lines of periods are almost vertical, which means the coupling effect on pacemaker rhythm is weak. Namely, whether in the case of a single cell or coupled cells, the parameter sensitivity of pacemaker rhythm to the conductance change of sodium channel is similar (a strong parameter sensitivity). Especially for the values of c_{Na} near 0, the parameter sensitivity is very strong.

Next, the relation between the L-type calcium current $I_{\text{Ca,L}}$ and the external current I_{ext} in periphery and center cells are investigated. Figure 6.13(a) and (b) shows the two-parameter bifurcation diagrams of periphery and center cells, respectively. As shown in Table 6.1 and Fig. 6.1, the membrane capacitance and the membrane currents are very different between the periphery and center cells. Thus, the scale of the ordinate in Fig. 6.13(a) and (b) are adjusted. In the periphery cell, the bifur-

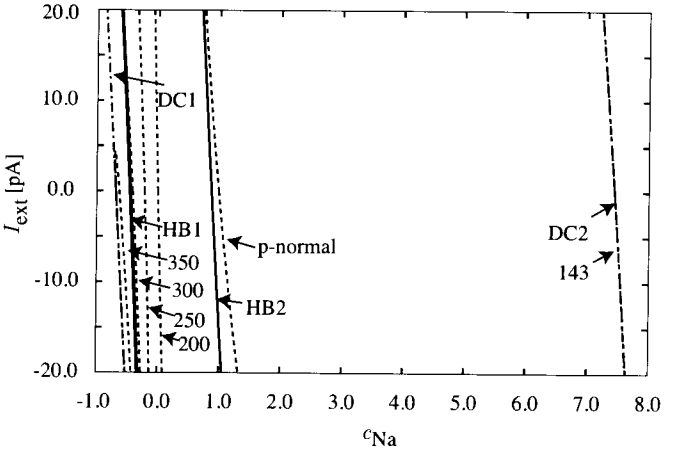

Figure 6.12: Two-parameter bifurcation diagram of the Zhang model (periphery cell) as for the sodium current I_{Na} and the external current I_{ext}.

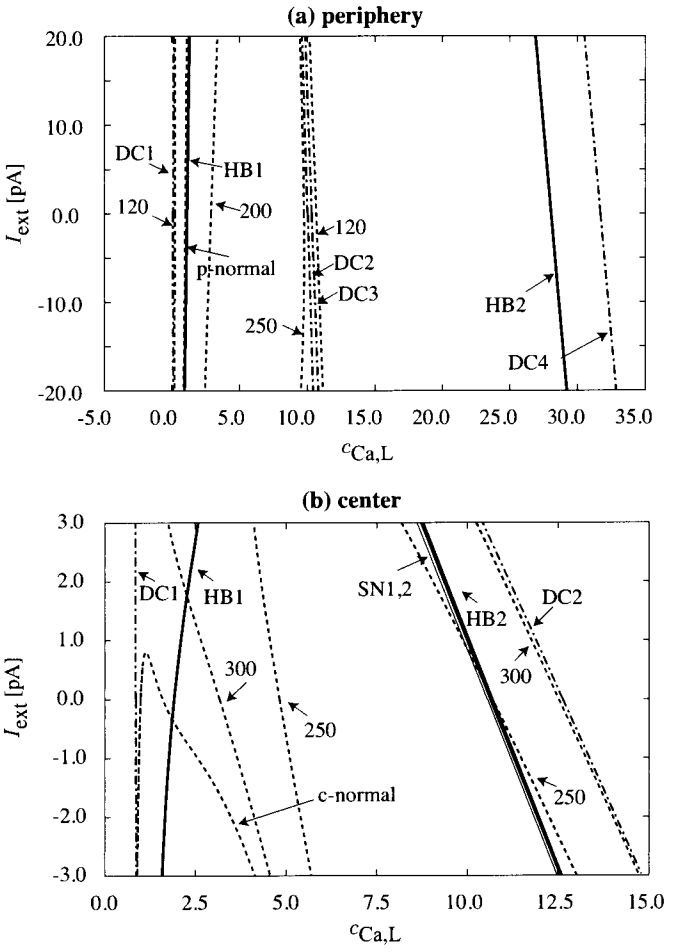

Figure 6.13: Two-parameter bifurcation diagram of the Zhang model as for the L-type calcium current $I_{\mathrm{Ca,L}}$ and the external current I_{ext}.

cation curves and contour lines are almost vertical, which mean that the pacemaker rhythm is insensitive to the change of I_{ext}. In the center cell, when I_{ext} is increased, the two Hopf bifurcation curves get close to each other, which means the range of $c_{\mathrm{Ca,L}}$ of rhythmic action potential generation becomes small. These results show that the coupling effect on pacemaker rhythm is weak in the periphery cell, whereas it is strong in the center cell.

Chapter 7

Conclusions

The sinoatrial node (cardiac pacemaker) cells generate rhythmic action potentials spontaneously to initiate the excitation conduction through the heart, and then to cause the cardiac activity regularly. The pacemaker rhythm in sinoatrial node cells decides the heart rate. Since the ion channels mainly control the action potential generation, their abnormalities disturb the pacemaker rhythm, and then the heart rate. As a result, sinus arrhythmias may be caused. The arrhythmias are usually treated by applying drugs which have effects on ion channels. Thus, the study on the relation between ion channels and pacemaker rhythm is necessary for arrhythmia treatment. In our study, we utilized two typical sinoatrial node cell models: the YNI model and the Zhang model to investigate the effects of conductance changes of various ion channels on pacemaker rhythm.

Both the YNI model and the Zhang model are HH-type models which are described by nonlinear ODEs with various parameters. We varied ion channel conductances as bifurcation parameters to analyze the global bifurcation structures of the two models and then investigated the variabilities of the pacemaker rhythm.

The YNI model is a simple but rather classic model. It considers five ion channel currents (which correspond to five different ion channels): sodium current I_{Na}, slow inward current I_{s}, potassium current I_{K}, hyperpolarization-activated current I_{h}, and leak current I_{l}. At first, we varied each ion channel conductance solely to investigate the one-parameter bifurcation structures and the variabilities of pacemaker rhythm. For I_{Na} and I_{s}, the increase of channel conductance accelerated the pacemaker rhythm, whereas for I_{K} and I_{l}, the increase of channel conductance decelerated the pacemaker rhythm. It was due to the fact that I_{Na} and I_{s} are inward currents, whereas I_{K} and I_{l} are outward currents. For the above four currents, the high pa-

rameter sensitivities showed that the conductance changes affected the pacemaker rhythm strongly. However, for I_{h}, the pacemaker rhythm changed little when varying its channel conductance (a low parameter sensitivity). Thus, the conductance change of I_{h} had a weak effect on pacemaker rhythm.

Next, we varied two ion channel conductances simultaneously to investigate the two-parameter bifurcation structures. Based on these analysis results, we examined the combined effects of changing two ion channel conductance on pacemaker rhythm. A strong combined effect corresponds to a strong interrelation between the two currents. It was found that, there were strong interrelations between I_{Na} and I_{K}, I_{s} and I_{K}, and a weak one between I_{Na} and I_{h} (since the conductance change of I_{h} affected the pacemaker rhythm little). When the two ion channels have a strong interrelation, we can adjust one ion channel to correct the abnormal pacemaker rhythm caused by the other one with reference to the two-parameter bifurcation structure.

Moreover, we varied the constant external current I_{ext} of the YNI model to analyze the coupling effect on pacemaker rhythm approximately. The one-parameter bifurcation diagram as for I_{ext} showed that, the pacemaker rhythm was sensitive to the change of I_{ext}, and was accelerated by a positive I_{ext}. In the two-parameter bifurcation diagrams as for each ion channel current I_{ion} and I_{ext}, it was shown that I_{Na} and I_{ext}, I_{s} and I_{ext}, I_{K} and I_{ext} had strong interrelations, whereas I_{h} and I_{ext} had a weak one. These results meant that the pacemaker rhythm varied sensitively to the conductance changes of I_{Na}, I_{s}, I_{K}, and varied insensitively to the conductance change of I_{h} in both a single cell and coupled cells.

The Zhang model is a detailed model. It considers eleven ion channel currents: sodium current I_{Na}, L- and T-type calcium currents $I_{\mathrm{Ca,L}}$ and $I_{\mathrm{Ca,T}}$, rapid and slow delayed rectifying potassium current $I_{\mathrm{K,r}}$ and $I_{\mathrm{K,s}}$, transient and sustained 4-aminopyridine-sensitive currents I_{to} and I_{sus}, hyperpolarization-activated current I_{f}, and background currents $I_{\mathrm{b,Na}}$, $I_{\mathrm{b,Ca}}$, and $I_{\mathrm{b,K}}$; one sodium-potassium pump current I_{p}; and one sodium-calcium exchanger curretn I_{NaCa}. Since the Zhang model considers the regional difference of sinoatrial node (the difference between the periphery and center cells of sinoatrial node), we analyzed the bifurcation structure of the Zhang model for periphery and center cells, respectively. The major difference between the periphery and center cells is the presence or absence of the (very large) I_{Na}, which is only present in the periphery cell. The sodium channel conductance of periphery cell was varied to investigate the parameter sensitivity of pacemaker rhythm. When the conductance was increased, the pacemaker rhythm accelerated

sensitively, which showed a strong effect. For the L-type calcium current $I_{Ca,L}$, which is a large current present in both periphery and center cells, the pacemaker rhythm was also sensitive to the conductance change. However, the ranges of channel conductance in which rhythmic action potentials can be generated were different between the periphery and center cells. The periphery cell has a wider range than the center cell. In both the two types of cells, the L-type calcium conductance changes had strong effects on the pacemaker rhythm.

Next, we varied two ion channel conductances simultaneously to analyze the two-parameter bifurcation structures, then to investigate the interrelations between two channel currents. In both periphery and center cells, $I_{Ca,L}$ and $I_{K,r}$ had a strong interrelation, whereas $I_{Ca,L}$ and I_f had a weak one (since the conductance change of I_f affected the pacemaker rhythm little). For $I_{Ca,L}$ and $I_{Ca,T}$, $I_{Ca,L}$ and $I_{K,s}$, $I_{Ca,L}$ and $I_{b,Na}$, $I_{Ca,L}$ and $I_{b,Ca}$, $I_{Ca,L}$ and $I_{b,K}$, the interrelations were weak in the periphery cell, whereas those were strong in the center cell. For the other membrane currents of the Zhang model, since I_{to} and I_{sus} are not consistently found in experiments [45], I_{NaCa}, I_p are not ion channel currents, their results are not analyzed in this thesis.

Moreover, we varied the constant external current I_{ext} of the Zhang model to analyze the coupling effect on pacemaker rhythm approximately. The two-parameter bifurcation diagrams as for I_{Na} and I_{ext} (periphery cell), as for $I_{Ca,L}$ and I_{ext} (periphery and center cells) showed that the coupling effect on pacemaker rhythm was small in the periphery cell, whereas that was big in the center cell.

The results on the two models were compared. For the two models, the pacemaker rhythm was sensitive to the conductance change of I_{Na} (although the Zhang model had a smaller variation of pacemaker rhythm than the YNI model), whereas it was insensitive to the conductance change of I_h or I_f. From the simple YNI model, it was shown that the conductance changes of I_s and I_K had strong effects on the pacemaker rhythm. Moreover, from the detailed Zhang model, it was shown that $I_{Ca,L}$ (one component of I_s) and $I_{K,r}$ (one component of I_K) played the major roles in I_s and I_K, respectively.

In conclusion, we analyzed the global bifurcation structures of two typical cardiac sinoatrial node cell models and investigated the effects of changing ion channel conductances and coupling effects on pacemaker rhythm. These results provided helpful suggestion on arrhythmia treatment, e.g., how to adjust a suitable ion channel to correct the abnormal pacemaker rhythm caused by another ion channel, although these suggestion should be confirmed experimentally before clinical application.

References

[1] Fink, M., Niederer, S.A., Cherry, E.M., Fenton, F.H., Koivumaki, J.T., Seemann, G., Thul, R., Zhang, H., Sachse, F.B., Beard, D., Crampin, E.J., Smith, N.P. (2011) Cardiac cell modelling: observations from the heart of the cardiac physiome project. Prog. Biophys. Mol. Biol. 104: 2–21.

[2] Sepulveda, N.G., Roth, B.J., Wikswo, J.P. (1989) Current injection into a two-dimensional anisotropic bidomain. Biophys. J. 55: 987–999.

[3] Roth, B.J., Wikswo, J.P. (1986) A bidomain model of the extracellular potential and magnetic field of cardiac tissue. IEEE Trans. Biomed. Eng. 3: 467–469.

[4] Roth, B.J. (1995) A mathematical model of make and break electrical stimulation of cardiac tissue by a unipolar anode or cathode. IEEE Trans. Biomed. Eng. 42: 1174–1184.

[5] Courtemanche, M., Winfree, A.T. (1991) Re–entrant rotating waves in a Beeler–Reuter based model of two-dimensional cardiac electrical activity. Int. J. Bifur. Chaos 1: 431–444.

[6] Holden, A.V., Panfilov, A.V. (1991) Spatiotemporal chaos in a model of cardiac electrical activity. Int. J. Bifur. Chaos 1: 219–225.

[7] Campbell, S.G., Flaim, S.N., Leem, C.H., McCulloch, A.D. (2008) Mechanisms of transmurally varying myocyte electromechanics in an integrated computational model. Phil. Trans. A Math. Phys. Eng. Sci. 366: 3361–3380.

[8] Hunter, P.J., Borg, T.K. (2003) Integration from proteins to organs: the physiome project. Nat. Rev. Mol. Cell Biol. 4: 237–243.

[9] Crampin, E. J., Halstead, M., Hunter, P., Nielsen, P., Noble, D., Smith, N., Tawhai, M. (2004) Computational physiology and the physiome project. Exp. Physiol. 89: 1–26.

[10] Christensen, D. (2002) In silico medicine: computer simulations aid drug development and medical care. Sci. News 162: 378–380.

[11] Noble, D. (2002) Modeling the heart - from genes to cells to the whole organ. Science 1: 1678–1682.

[12] Noble, D. (2006) Systems biology and the heart. BioSystems 83: 75–80.

[13] Smith, N.P., Crampin, E.J., Niederer, S.A., Bassingthwaighte, J.B., Beard, D.A. (2007) Computational biology of cardiac myocytes: Proposed standards for the physiome. J. Exp. Biol. 210: 1576–1583.

[14] Southern, J., Pitt-Francis, J., Whiteley, J., Stokeley, D., Kobashi, H., Nobes, R., Kadooka, Y., Gavaghan, D. (2008) Multi–scale computational modelling in biology and physiology. Prog. Biophys. Mol. Bio. 96: 60–89.

[15] Mangoni, M.E., Nargeot, J. (2008) Genesis and regulation of the heart automaticity. Physiol. Rev. 88: 919–982.

[16] Wahler, G.M. (2001) Cardiac action potentials. In: Sperelakis, N., Kurachi, Y., Terzic, A., Cohen, M. (Eds.), Heart Physiology and Pathophysiology. fourth edition. Academic Press, pp.199–211.

[17] Gessman, L.J., Trohman, R. (1992) Cardiac arrhythmias. In: Parrillo, J., Dellinger, R.P. (Eds.), Critical Care Medicine. third edition. Mosby, pp.647–675.

[18] Issa, Z.F., Miller, J.M., Zipes, D.P. (2009) Clinical Arrhythmology and Electrophysiology. Saunders.

[19] Ashcroft, F.M. (2000) Ion Channels and Disease : Channelopathies. Academic Press.

[20] Brown, H.F. (1982) Electrophysiology of the sinoatrial node. Physiol. Rev. 62: 505–530.

[21] Bowman, L.N., Jongsma, H.J. (1986) Structure and function of the sino-atrial node: a review. Eur. Heart J. 7: 94–104.

[22] Irisawa, H., Brown, H.F., Giles, W. (1993) Cardiac pacemaking in the sinoatrial node. Physiol. Rev. 73: 197–227.

[23] Hodgkin, L., Huxley, A.F. (1952) A quantitative description of membrane currents and its application to conduction and excitation in nerve. J. Physiol. 117: 500–544.

[24] Guckenheimer, J., Holmes, P. (2002) Nonlinear Oscillations, Dynamical Systems, and Bifurcations of Vector Fields. Springer.

[25] Kuznetsov, Y.A. (2004) Elements Of Applied Bifurcation Theory. Springer.

[26] Doi, S., Inoue, J., Pan, Z., Tsumoto, K. (2010) Computational Electrophysiology - Dynamical Systems and Bifurcations. Springer.

[27] Nagata, S., Takahashi, N., Doi, S., Kumagai, S. (2006) Analysis of stimulus response characteristics and drug sensitivity of ventricular myocardial cell using a nonlinear dynamic model. IEICE Trans. A J89-A: 1153–1167 (in Japanese).

[28] Takahashi, N., Doi, S., Kumagai, S. (2006) Parameter estimation of ventricular myocardial cell model using an on-line learning algorithm. Proc. of SICE–ICCAS International Joint Conference 2006, pp.2322–2327.

[29] Yamaguchi, R., Doi, S., Kumagai, S. (2007) Bifurcation analysis of a detailed cardiac cell model and drug sensitivity of ionic channels. Proc. of 15th IEEE International Workshop on Nonlinear Dynamics of Electronic Systems (NDES) 2007, pp. 205–208.

[30] Kurata, Y., Hisatome, I., Imanishi, S., Shibamoto, T. (2002) Dynamical description of sinoatrial node pacemaking: improved mathematical model for primary pacemaker cell. Am. J. Physiol. 283: H2074–H2101.

[31] Kurata, Y., Hisatome, I., Imanishi, S., Shibamoto, T. (2003) Roles of L-type Ca^{2+} and delayed-rectifier K^{+} currents in sinoatrial node pacemaking: Insights from stability and bifurcation analyses of a mathematical model. Am. J. Physiol. 285: H2804–H2819.

[32] Kurata, Y., Matsuda, H., Hisatome, I., Shibamoto, T. (2008) Regional difference in dynamical property of sinoatrial node pacemaking: Role of Na^{+} channel current. Biophys. J. 95: 951–977.

[33] Kurata, Y., Matsuda, H., Hisatome, I., Shibamoto, T. (2010) Roles of hyperpolarization-activated current If in sinoatrial node pacemaking: Insights

from bifurcation analysis of mathematical models. Am. J. Physiol. 298: H1748–H1760.

[34] Yanagihara, K., Noma, A., Irisawa, H. (1980) Reconstruction of sino-atrial node pacemaker potential based on the voltage clamp experiments. Jpn. J. Physiol. 30: 841–857.

[35] Zhang, H., Holden, A.V., Kodama, I., Honjo, H., Lei, M., Varghese, T., Boyett, M.R. (2000) Mathematical models of action potential in the periphery and center of the rabbit sinoatrial node. Am. J. Physiol. 279: H397–H421.

[36] Garny, A., Kohl, P., Hunter, P.J., Boyett, M.R., Noble, D. (2003) One-Dimensional Rabbit Sinoatrial Node Models: benefits and limitations. J. Cardiovasc. Electrophysiol. 14: S121–S132.

[37] Katz, A.M. (2005) Physiology of the Heart. fourth edition. Lippincott Williams & Wilkins.

[38] Zipes, D.P., Jalife, M. (2009) Cardiac Electrophysiology: From Cell to Bedside. Saunders

[39] Kleber, A.G., Rudy, Y. (2004) Basic Mechanisms of Cardiac Impulse Propagation and Associated Arrhythmias Physiol. Rev. 84: 431–488.

[40] Desplantez, T., Dupont, E., Severs, N.J., Weingart, R. (2007) Gap junction channels and cardiac impulse propagation J. Membrane Biol. 218: 13–28.

[41] Boyett, M.R., Honjo, H., Kodama, I. (2000) The sinoatrial node, a heterogeneous pacemaker structure. Cardiovasc. Res. 47: 658–687.

[42] Baruscotti, M., Barbuti, A., Bucchi, A. (2010) The cardiac pacemaker current. J. Mol. Cell. Cardiol. 48: 55–64.

[43] Cole, K. S. (1949). Dynamic electrical characteristics of the squid axon membrane. Arch. Sci. Physiol. 3: 253–258.

[44] Neher, E., SAKMANN, B. (1976). Single channel currents recorded from membrane of denervated frog muscle fibres. Nature, Lond. 260: 799–802.

[45] Wilders, R. (2007) Computer modelling of the sinoatrial node. Med. Bio. Eng. Comput. 45: 189–207.

[46] Models of cardiac cell: http://www.scholarpedia.org/article/Models_of_cardiac_cell

[47] CellML: http://models.cellml.org/exposure/listing/full-list

[48] Irisawa, H, Noma, A. (1982) Pacemaker mechanisms of rabbit sinoatrial node cells. In: Bouman, L.N., Jongsma, H.J (eds), Cardiac rate and rhythm: physiological, morphological, and developmental aspects. Martinus Nijhoff, pp.35–51.

[49] Bristow, D.G., Clark, J.W. (1982) A mathematical model of primary pacemaking cell in SA node of the heart. Am. J. Physiol. 243: H207–H218.

[50] Noble, D., Noble, S.J. (1984) A model of sino-atrial node electrical activity based on a modification of the DiFrancesco-Noble (1984) equations. Proc. R. Soc. Lond. B Biol. Sci. 222: 295–304.

[51] Noble, D., DiFrancesco, D., Denyer, J.C. (1989) Ionic mechanisms in normal and abnormal cardiac pacemaker activity. In: Jacklet JW (ed), Neuronal and cellular oscillators. Marcel Dekker, pp.59–85.

[52] Wilders, R., Jongsma, H.J., van Ginneken, A.C.G. (1991) Pacemaker activity of the rabbit sinoatrial node: a comparison of mathematical models. Biophys. J. 60: 1202–1216.

[53] Demir, S.S., Clark, J.W., Murphey, C.R., Giles, W.R. (1994) A mathematical model of a rabbit sinoatrial node cell. Am. J. Physiol. 266: C832–C852.

[54] Dokos, S, Celler, B.G., Lovell, N. (1996) Ion currents underlying sinoatrial node pacemaker activity: a new single cell mathematical model. J. Theor. Biol. 181: 245–272.

[55] Sarai, N., Matsuoka, S., Kuratomi, S., Ono, K., Noma, A. (2003) Role of individual ionic current systems in the SA node hypothesized by a model study. Jpn. J. Physiol. 53: 125–134.

[56] Lovell, N.H., Cloherty, S.L., Celler, B.G., Dokos, S. (2004) A gradient model of cardiac pacemaker myocytes. Prog. Biophys. Mol. Biol. 85: 301–323.

[57] Maltsev, V.A., Lakatta, E.G. (2009) Synergism of coupled subsarcolemmal Ca^{2+} clocks and sarcolemmal voltage clocks confers robust and flexible pacemaker function in a novel pacemaker cell model. Am. J. Physiol. Heart Circ. Physiol. 296: H594–H615.

[58] Rasmusson, R.L., Clark, J.W., Giles, W.R., Shibata, E.R., Campbell, D.L. (1990) A mathematical model of a bullfrog cardiac pacemaker cell. Am. J. Physiol. 259: H352–H369.

[59] Mangoni, M.E., Traboulsie, A., Leoni, A.L., Couette, B., Marger, L., Le Quang, K., Kupfer, E., Cohen-Solal, A., Vilar, J., Shin, H.S., Escande, D., Charpentier, F., Nargeot, J., Lory, P. (2006) Bradycardia and slowing of the atrioventricular conduction in mice lacking CaV3.1/alpha1G T–type calcium channels. Circ. Res. 98: 1422–1430.

[60] Kharche, S., Yu, J., Lei, M., Zhang, H. (2011) A mathematical model of action potentials of mouse sinoatrial node cells with molecular bases. Am. J. Physiol. Heart Circ. Physiol. 301: H945–H963.

[61] Hilgemann, D.W., Noble, D. (1987) Excitation-contraction coupling and extracellular calcium transients in rabbit atrium: reconstruction of basic cellular mechanisms. Proc. R. soc. Lond. B 230: 163–205.

[62] Earm, Y.E., Noble, D. (1990) A model of the single atrial cell: relation between calcium current and calcium release. Proc. R. Soc. Lond. B 240: 83–96.

[63] Lindblad, D.S., Murphy, C.R., Clark, J.W., Giles, W.R. (1996) A model of the action potential and underlying membrane currents in a rabbit atrial cell. Am. J. Physiol. 271: H1666–H1696.

[64] Nygren, A., Fiset, C., Firek, L., Clark, J.W., Lindblad, D.S., Clark, R.B., Giles, W.R. (1998) Mathematical model of an adult human atrial cell. The role of K currents in repolarization. Circ. Res. 82: 63–81.

[65] Courtemanche, M., Ramirez, R.J., Nattel, S. (1998) Ionic mechanisms underlying human atrial action potential properties: insights from a mathematical model. Am. J. Physiol. 275: H301–H321.

[66] Simitev, R.D., Biktashev, V.N. (2006) Conditions for propagation and block of excitation in an asymptotic model of atrial tissue. Biophys. J. 90: 2258–2269.

[67] Rasmusson, R.L., Clark, J.W., Giles, W.R., Robinson, K., Clark, R.B., Shibata, E.R., Campbell, D.L. (1990) A mathematical model of electrophysiological activity in a bullfrog atrial cell. Am. J. Physiol. 259: H370–H389.

[68] Ramirez, R.J., Nattel, S., Courtemanche, M. (2000) Mathematical analysis of canine atrial action potentials: rate, regional factors, and electrical remodeling. Am. J. Physiol. 279: H1767–H1785.

[69] Cherry, E.M., Ehrlich, J.R., Nattel, S., Fenton, F.H. (2007) Pulmonary vein reentry-properties and size matter: insights from a computational analysis. Heart Rhythm 4: 1553–1562.

[70] Liu, Y., Zeng, W., Delmar, M., Jalife, J. (1993) Ionic mechanisms of electronic inhibition and concealed conduction in rabbit atrioventricular nodal myocytes. Circul. 88: 1634–1646.

[71] Noble, D. (1962) A modification of the Hodgkin-Huxley equations applicable to Purkinje fibre action and pacemaker potential. J. Physiol. 160: 317–352.

[72] McAllister, R.E., Noble, D., Tsien, R.W. (1975) Reconstruction of the electrical activity of cardiac Purkinje fibres. J. Physiol. 251: 1–59.

[73] Di Francesco, D., Noble, D. (1985) A model of cardiac electrical activity incorporating ionic pumps and concentration changes. Phil. Trans. R. Soc. Lond. 307: 353–398.

[74] Stewart, P., Aslanidi, O.V.,Noble, D., Noble, J.P., Boyett, M.R., Zhang, H. (2009) Mathematical models of the electrical action potential of Purkinje fibre cells. Philos. T. R. Soc. A 367: 2225–2255.

[75] Sampson, K.J., Iyer, V., Marks, A.R., Kass, R.S. (2010) A computational model of Purkinje fibre single cell electrophysiology: implications for the long QT syndrome. J. Physiol. 588: 2643–2655.

[76] Beeler, G.W., Reuter, H. (1977) Reconstruction of the action potential of ventricular myocardial fibers. J. Physiol. 268: 177–210.

[77] Fenton, F.H., Karma, A. (1998) Vortex dynamics in three-dimensional continuous myocardium. Filament instability and fibrillation. Chaos 8: 20–47.

[78] Luo, C.H., Rudy Y. (1991) A model of the ventricular cardiac action potential, depolarization, repolarization and their interaction. Circ. Res. 68: 1501–1526.

[79] Nordin, C. (1993) Computer model of membrane current and intracellular Ca^{2+} flux in the isolated guinea pig ventricular myocytes. Am. J. Physiol. 265: H2117–H2136.

[80] Luo, C.H., Rudy, Y. (1994) A dynamic model of the cardiac ventricular action potential. I. Simulations of ionic currents and concentration changes. Circ. Res. 74: 1071–1096.

[81] Jafri, S., Rice, J.R., Winslow, RL (1998) Cardiac Ca^{2+} dynamics: the roles of ryanodine receptor adaptation and sarcoplasmic reticulum load. Biophys. J. 74: 1149–1168.

[82] Matsuoka, S., Sarai, N., Kuratomi, S., Ono, K., Noma, A. (2003) Role of individual ionic current systems in ventricular cells hypothesized by a model study. Jpn. J. Physiol. 53:105–123.

[83] Priebe, L., Beuckelmann, D.J. (1998) Simulation study of cellular electric properties in heart failure. Circ. Res. 82: 1206–1223.

[84] Bernus, O., Wilders, R., Zemlin, C.W., Verschelde, H., Panfilov, A.V. (2002) A computationally efficient electrophysiological model of human ventricular cells. Am. J. Physiol. 282: H2296–H2308.

[85] Ten Tusscher, K.H., Noble, D., Noble, P.J., Panfilov, A.V. (2004) A model for human ventricular tissue. Am. J. Physiol. 286: H1573–H1589.

[86] Ten Tusscher, K.H, Panfilov, A.V. (2006) Alternans and spiral breakup in a human ventricular tissue model. Am. J. Physiol. 291: H1088–H1100.

[87] Ten Tusscher, K.H, Panfilov, A.V. (2006) Cell model for efficient simulation of wave propagation in human ventricular tissue under normal and pathological conditions. Phys. Med. Biol. 51: 6141–6156.

[88] Iyer, V., Mazhari, R., Winslow, RL. (2004) A computational model of the human left-ventricular epicardial myocyte. Biophys. J. 87: 1507–1525.

[89] Bueno-Orovio, A., Cherry, E.M., Fenton, F.H. (2008) Minimal model for human ventricular action potentials in tissue. J. Theor. Biol. 253:544–560.

[90] Winslow, R.L., Rice, J., Jafri, S., Marban, E., O'Rourke, B. (1999) Mechanisms of altered excitation-contraction coupling in canine tachycardia-induced heart failure. II. Model studies. Circ. Res. 84: 571–586.

[91] Fox, J.J., McHarg, J.L., Gilmour, R.F. Jr. (2002) Ionic mechanism of electrical alternans. Am. J. Physiol. 282: H516–H530.

[92] Cabo, C., Boyden, P.A. (2003) Electrical remodeling of the epicardial border zone in the canine infracted heart: a computational analysis. Am. J. Physiol. 284: H372–H384.

[93] Hund, T.J., Rudy, Y. (2004) Rate dependence and regulation of action potential and calcium transient in a canine cardiac ventricular cell model. Circulation 110: 3168–3178.

[94] Greenstein, J.L., Winslow, R.L. (2002) An integrative model of the cardiac ventricular myocytes incorporating local control of Ca^{2+} release. Biophys. J. 83: H2918–H2945.

[95] Puglisi, J.L., Bers, D.M. (2001) LabHEART: an interactive computer model of rabbit ventricular myocytes ion channels and Ca transport. Am. J. Physiol. 281: C2049–C2060.

[96] Shannon, T.R., Wang, F., Puglisi, J., Weber, C., Bers, D.M. (2004) A mathematical treatment of integrated Ca dynamics within the ventricular myocytes. Biophys. J. 87: 3351–3371.

[97] Mahajan, A.,Shiferaw, Y., Sato, D., Baher, A., Olcese, R., Xie, L.H., Yan, M.J., Chen, P.S., Restrepo, J.G., Karma, A., Garfinkel, A., Qu, Z., Weiss, J.N. (2008) A rabbit ventricular action potential model replicating cardiac dynamics at rapid heart rates. Biophys. J. 94: 392–410.

[98] Pandit, S.V., Clark, R.B., Giles, W.R., Demir, S.S. (2001) A mathematical model of action potential heterogeneity in adult rat left ventricular myocytes. Biophys. J. 81: 3029–3051.

[99] Bondarenko, V.E., Szigeti, G.P., Bett, G.C., Kim, S.J., Rasmusson, R.L. (2004) Computer model of action potential of mouse ventricular myocytes. Am. J. Physiol. 287: H1378–H1403.

[100] Doedel, E.J., Champneys, A.R., Fairgrieve, T.F., Kuznetsov, Y.A., Sandstede, B., Wang, X.(1997) AUTO97: continuation and bifurcation software for ordinary differential equations (with HomCont). Technical Report. Concordia University.

[101] Lei, M., Brown, H.F. (1996) Two components of the delayed rectifier potassium current I_K in rabbit sino–atrial node cells Exp. Physiol. 81: 725–741.

Publications

• Journal Papers

J-1 Pan, Z., Doi, S. (2011) Global bifurcation structure and variability of pacemaker rhythm in a detailed model of cardiac sinoatrial node cells. IEEJ Trans. EIS 131: 2138–2147 (in Japanese).

J-2 Pan, Z., Yamaguchi, R., Doi, S. (2011) Bifurcation analysis and effects of changing ionic conductances on pacemaker rhythm in a sinoatrial node cell model. Biosystems 106: 9–18.

J-3 Pan, Z., Doi, S. (2011) Global bifurcation structure and parameter dependence of the Hodgkin-Huxley equations. IEEJ Trans. EIS 131: 514–520 (in Japanese).

• International Conferences

C-1 Pan, Z., Doi, S. (2011) Global bifurcation structure and effects of changing ion channel conductances on pacemaker rhythm in a coupled cardiac sinoatrial node cell model. Proc. of 4th Global COE International Symposium on Physiome and Systems Biology for Integrated Life Sciences and Predictive Medicine, p.68.

C-2 Pan, Z., Doi, S. (2010) Variability of pacemaker rhythm in a detailed model of cardiac sinoatrial node cells. Proc. of 2010 IEEE Region 10 Conference - TENCON 2010, pp.390–395.

C-3 Pan, Z., Yamaguchi, R., Doi, S. (2009) Analysis of bifurcations and variabilities of rhythm in a cardiac pacemaker cell model. Proc. of 2009 International Symposium on Nonlinear Theory and its Applications - NOLTA 2009, pp.360–363.

• Domestic Conferences

C-4 Pan, Z., Doi, S. (2010) Difference of variability of rhythm in periphery and center cells of cardiac pacemaker. Proc. of 20th Annual Meeting of JSMB, p.75 (in Japanese).

C-5 Pan, Z., Doi, S. (2010) Global bifurcation structure and variability of rhythm of a cardiac pacemaker cell model. Proc. of 22th JSME Bioengineering Conference, p.224 (in Japanese).

C-6 Pan, Z., Doi, S. (2009) On the pacemaker activities of cardiac sinoatrial node cells. IEICE Technical Report NLP2009-139, pp.71–76 (in Japanese).

C-7 Yamaguchi, R., Pan, Z., Senoo, M., Doi, S. (2009) Global bifurcation structures and parameter sensitivities of cardiac cell models. Proc. of 5th Theory of Bio-Mathematics and Its Applications, Kyoto University RIMS Kokyuroku1663, pp.182–187 (in Japanese).

C-8 Pan, Z., Doi, S. (2009) Pacemaker activities and variabilities of rhythm in sinoatrial node cells. Proc. of 2009 IEEJ Transactions on Electronics, Information and Systems, pp.73–76 (in Japanese).

C-9 Pan, Z., Yanaguchi, R., Senoo, M., Doi, S. (2009) Variability of rhythms in a cardiac pacemaker cell model. IEICE Technical Report NLP2008-160, pp. 53–58 (in Japanese).

• Book

Doi, S., Inoue, J., Pan, Z., Tsumoto, K. (2010) Computational Electrophysiology - Dynamical Systems and Bifurcations. Springer.

Other Publications

• International Conferences

C-10 Pan, Z., Senoo, M., Doi, S., Kumagai, S. (2007) A simple iterative algorithm for image interpolation by radial basis function networks. Proc. of 2007 Nonlinear Dynamics of Electronic Systems - NDES 2007, pp.221–224.

• Domestic Conferences

C-11 Pan, Z., Fujiwara, N., Doi, S., Kumagai, S. (2008) Image restoration and interpolation by radial basis function network. IEICE Technical Report NLP2007-152, pp.57–62 (in Japanese).

C-12 Pan, Z., Senoo, M., Doi, S., Kumagai, S. (2007) A very simple method for the image interpolation by radial basis function networks. IEICE Technical Report NLP2007-6, pp.17–22 (in Japanese).

C-13 Senoo, M., Pan, Z., Hiroyuki, K., Doi, S., Kumagai, S. (2007) Effects on random sampling on image interpolation by radial basis function networks. Proc. of 2007 IEICE General Conference, p.60 (in Japanese).